INFLUENCE OF ALKALI METAL PROMOTION ON THE PROPERTIES OF CO-PRECIPITATED Cu/Zn/Cr HIGHER ALCOHOL SYNTHESIS CATALYSTS

BY

MABOKA SYDNEY MABOKA

Submitted in fulfilment of the academic

requirements for the degree of

Master of Science

in the

Department of Chemistry and Chemical Technology,

University of Natal

Pietermaritzburg

1994

ABSTRACT

The effect of alkali metal doping on the catalytic and physico-chemical properties of our Cu/Zn/Cr methanol synthesis catalyst (ISO 63) was investigated. The prime objective was to convert ISO 63 to a high alcohol synthesis (HAS) catalyst. The physico-chemical tests were used to characterize the near-optimal HAS catalysts and to identify parameters (relevant to HAS) which needed further optimization. The catalyst, which was 38% Cu, 38% Zn and 24% Cr was prepared by the continuous co-precipitation method and impregnated with 2.26 $*10^{-4}$ moles alkali metal formates for per gram catalyst. The blank and alkali-impregnated catalyst batches were characterized by BET and BJH methods, XRD, H_2-TPD and XPS. In the study of the effect of alkali metal doping on the catalytic properties of the catalyst, HAS was used as the test reaction. It was established that alkali metal doping of ISO 63 resulted in both an increase of the catalyst selectivity towards HA and a decreased alkane selectivity. The catalyst's methanol activity and selectivity at 4000ml/Kg $_{cat.}$/h increased by alkali-doping. Decreasing the gas hourly space velocity (GHSV) of the synthesis gas increased the activity and selectivity of the alkali-impregnated ISO 63 catalyst towards both HA and alkanes. The Cs-doped catalyst batch showed the highest selectivity towards HA while the Li-doped batch showed the highest selectivity towards isobutanol. The Cs- and Li-impregnated catalytic systems also showed an industrially acceptable methanol / HA ratio of two. The activity and selectivity towards HAS were surprisingly high in both the Li- and Na-doped catalysts. It was shown by XPS that the catalyst had quantities of sodium chromate remaining in the parent catalyst. It was concluded that the performances of, not only the Na and Li batches but all batches, was influenced by the presence of sodium chromate. The physico-chemical properties of the catalyst were affected by alkali metal impregnation. Firstly, the process decreases the pore areas and volumes by deposition of alkali metal salts and some catalytic material on the inside walls of the pores thereby partially blocking them. Secondly, the alkali

doping processes resulted in the decrease of the external surface area of the Cs-, K- and Na-doped catalyst batches. This phenomenon was attributed to limited restructuring of the remnants of hydrotalcite precursor. In the case of the Rb- and Li-impregnated catalyst batches the impregnation process resulted in the increase of the catalyst surface area. This behaviour was attributed to the surface enrichment by Cu and Zn, a process which appeared to be related to the pH of the impregnating solution and the calcination temperature. Thirdly, the alkali metal impregnation process increased the CuO crystallite size. Characterization of our near-optimal alkali-impregnated HAS catalyst showed that it had moderate surface area and was mesoporous. The catalyst surface was dominated by the presence of Zn and the bulk had at least the phases CuO, ZnO and $CuCr_2O_4/ZnCr_2O_4$. The average CuO crystallite size for the HAS catalyst was 78 ± 6 Å. The above information in conjunction with the establishment of an optimal pH of the impregnating solution for optimum catalyst surface area, suitable calcination temperature, optimum quantities of sodium chromate and alkali metal of choice i.e. Cs or Li or both will be used to optimize this catalyst.

PREFACE

This research work was conducted at the Catalysis Technology Group laboratories in MATTEK Division at the CSIR in Pretoria. The time span for the research extended over the period January 1993 to December 1994. Prof. R. Haines from University of Natal, Pietermaritzburg was the supervisor and Dr A. Sofianos from the CSIR acted as the co-supervisor.

These studies represents original work by the author and have not otherwise been submitted in any form for any diploma or degree to any other University. Where use has been made of the work of others it is duly acknowledged in the text.

ACKNOWLEDGEMENTS

I wish to express my gratitude to the following:

(a) The Council for Scientific and Industrial Research for granting me this opportunity to study for my MSc.

(b) My supervisor Prof. R. Haines and my co-supervisor Dr A. Sofianos for their role in this project.

(c) Mrs R Dove for English editing this report.

CONTENTS

LIST OF FIGURES

LIST OF TABLES

LIST OF ABBREVIATIONS

AAS	Atomic Absorption Spectroscopy
BE's	Binding Energies
BET	Brunauer, Emmett and Teller
BJH	Barrett, Joyner and Halenda
BPR	Back-pressure-regulator
DME	Dimethyl ether
ETBE	Ethyl tert-butyl ether
FCC	Fluid catalytic cracking
FID	Flame ionization detector
GC	Gas chromatograph
GHSV	Gas hourly space velocity
HA	Higher alcohols
HAS	Higher alcohols synthesis
H_2 TPD	Hydrogen Temperature Programmed Desorption
MFC	Mass Flow Controller
MTBE	Methyl tert-butyl ether
ORR	Oxygen retention reversal
STY	Space-time-yield
TAME	Tert-amyl methyl ether
TBA	Tert-butyl alcohol
TCD	Thermal conductivity detector
TPD	Temperature programmed desorption
WGS	Water gas shift reaction
XPS	X-ray photoelectron spectroscopy
XRD	X-ray diffraction

1. LITERATURE REVIEW

1.1 INTRODUCTION

The carbon monoxide and photochemical smog pollution which is caused by the emissions from combustion engines led to the formulation, by US oil refineries of the concept of "reformulated gasoline" which was ultimately included in the US Clean Air Act of 1990. The act primarily set higher limits on oxygenates in gasoline used in areas where carbon monoxide pollution was serious and lower limits on compounds that promote the formation of photochemical smog (e.g. alkenes) where this kind of pollution was a major problem. In Comparison with the current formulation, reformulated gasoline will contain:

* Less hydrocarbons that evaporate at low temperatures.
* A lower amount of both light and heavy aromatics.
* Less photochemically reactive compounds, e.g. alkenes.
* An increased amount of oxygenates (ethers and alcohols) [Jones et. al. 1989].

Many other countries have already chosen to follow the above criteria in their own pollution-combating programmes. Controls on oxygenates and alkenes, coupled with the endeavour to remove lead and reduce the benzene content of gasoline, creates the problem of a decreased octane rating of gasoline. By blending gasoline with branched ethers, its octane rating can be improved and the requirement for increased oxygenates will be fulfilled. Ethers that can be used as gasoline additives are methyl tert-butyl ether (MTBE), tert-amyl methyl ether (TAME) and ethyl tert-butyl ether (ETBE). At the moment MTBE is the only ether used on a large scale as a gasoline additive and it is envisaged that its use will increase to address the demand for increased oxygenates in the gasoline mixture [Seddon 1992].

The one-step acid-catalyzed addition of methanol to isobutene (Reaction 1.1 below) is the method employed to produce MTBE. Normally, acidic cation exchange resins are used as catalysts in this synthesis, functioning at very mild reaction conditions.

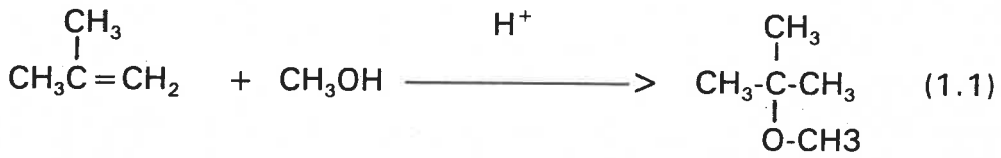

(1.1)

With the demand for MTBE increasing at approximately 15% per annum, isobutene is likely to be in short supply in the near future. It is currently obtained by fluid catalytic cracking (FCC) and sand cracking of crude oil fractions with a few additional possible processes open for exploration. The isomerization and subsequent dehydrogenation of n-butane in the STAR process of Phillips Petroleum, is also a possible route but, this technology is presently too expensive as it involves too many steps. Isobutanol produced in higher alcohol synthesis (HAS) has been considered by several authors including Keim and Falter [1989]; Seddon [1992] and Sofianos [1992], either as a source of isobutene (Reaction 1.2) or as a reaction component for the direct synthesis of MTBE as in Reaction (1.2a) below.

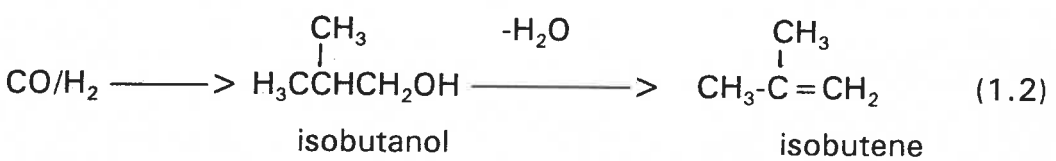

(1.2)

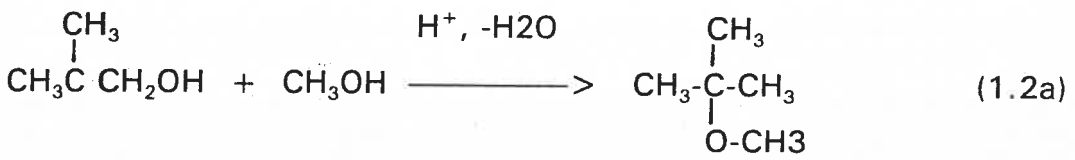

(1.2a)

Gasoline blending using mixtures of methanol and tert-butyl alcohol (TBA) or isobutanol can in addition address the requirement for increased oxygenates. When higher alcohols are added to the methanol component of the gasoline, the following advantages can be realized:

* The octane rating of the gasoline is increased.
* The water tolerance of the fuel in respect of phase separation is increased.
* The fuel volatility and its vapour-lock tendency decrease.
* High volumetric heating values are obtainable [Forzatti et al. 1991].
* This development takes the world a step closer towards a fuel which is totally dependent on coal, a natural resource which is at present abundant [Klier et al. 1991].

The above considerations demonstrate the need to develop the HAS process. In the following sections of this report, all the relevant aspects pertaining to optimization of the HAS process and the catalysts involved in it are discussed. The emphasis is on the formulation, optimization and characterization of the methanol synthesis catalysts, and the selectivity change effected by alkali metal doping of the catalyst. The catalysts' productivities as functions of preparation and structural features are discussed, as well as the present knowledge of the reaction mechanisms.

1.2 HIGHER ALCOHOL SYNTHESIS

1.2.1 Types of catalysts

According to their components, the HAS catalysts can be classified into four broad categories:

- modified methanol synthesis catalysts which produce both linear and branched alcohols [Forzatti et al. 1991],

- modified Fischer-Tropsch catalysts which produce linear alcohols following an Anderson-Schultz-Flory distribution pattern [Forzatti et al. 1991],
- Dow and Union Carbide-type catalysts whose key component is molybdenum sulphide, promoted by alkali metals and CoS [Kiennemann et al. 1992], and
- catalysts based mainly on noble metals of Group VIII elements, e.g. Pd, Pt and Rd [Kiennemann et al. 1992].

It is noted that, except for the methanol synthesis catalysts, other classes of catalysts show a tendency to form C_1-C_4 alkanes in large amounts. In addition to the above advantage, and as has already been mentioned, the modified methanol synthesis catalysts are capable of producing branched alcohols. Since isobutanol is of primary interest in this work, the focus will be on the modified methanol synthesis catalysts.

1.2.2 Modified methanol synthesis catalysts

A distinction can be made between the high- and low-temperature methanol synthesis catalysts. The former group consists of mixed oxide systems which have Zn/Cr,Mn/Cr and Zn/Mn/Cr in their composition and normally function at temperatures between 375 and 425 °C at pressures between 25 to 35MPa. The low-temperature and low pressure methanol synthesis catalysts are normally Cu-based systems and the maximum temperature under which they operate (when not suitably supported) is around 300 °C. At higher temperatures, the Cu component sinters with a concomitant loss of activity.

The number of components in the catalyst can be used to categorize the methanol synthesis catalysts. Copper-zinc oxide is a good example of a binary catalytic system. The Cu/ThO_2 catalysts belong to this group too [Klier 1982]. Industrially, $Cu/ ZnO/Al_2O_3$ is the most important ternary methanol synthesis

catalyst available. The alumina in the catalyst can be exchanged for chromia to afford the $Cu/Zn/Cr_2O_3$ catalyst, another member of the group. Systems consisting of Cu/Zn/Mn/Cr-oxide and Cu/Zn/Mn/Al-oxide were investigated by Xiaodong [1989]. These can be regarded as quaternary catalytic systems.

A knowledge of the function of individual catalyst components and additives is important in catalyst design. Copper in synergy with zinc oxide is regarded as the active component in the binary Cu/ZnO catalyst. The effect of other catalyst constituents on the activity of the primary Cu/ZnO catalytic system was studied by Stiles et al. [1991] and their findings supported the following conclusions, which are in agreement with those previously published by various research groups:

- **Manganese**: It increases the production of higher alcohols

- **Cobalt**: In small amounts, it increases the ethanol fraction of HA. It is noted that cobalt as a Fischer-Tropsch active metal produces C_1-C_4 alkanes, the undesirable products of HAS

- **Alkaline earth metals**: Except for barium, alkaline earth metals increase the thermal stability of the catalyst but catalytically are essentially inert. Barium carbonate shifts the product distribution towards the higher end of the higher alcohols product spectrum, i.e. to butanols and other alcohols with higher carbon numbers.

- **Lanthanides**: Cerium oxide has a positive effect on HA production but also increases methanation. It has been observed that cerium increases thermal stability and resistance to poisoning by halides and sulphides.

- **Refractory oxides**: If chromia is replaced by **silica**, dimethyl ether production is increased due to the acidic silanol groups of SiO_2 on

surface of the catalyst. **Titania** can be used as a stabilizer within a temperature range of 230-270 °C. **Zirconia** increases the productivity of the catalyst. It is also known to be an isosynthesis catalyst [Jackson and Ekerdt 1990].

- **Alkaline metals:** They are known to shift the catalyst selectivity towards higher alcohols [Mross 1983]. This process will be dealt with in detail in Chapter 2.

- **Alumina and chromia:** They act as structural promoters and help to disperse the active component, thus maximizing its surface area. Further, they stabilize the catalyst, thereby decreasing its deactivation rate [Klier 1988a]. Chromia is also known to be catalytically active since it possesses acidic centres on the surface.

1.2.3 Catalyst design

The design and preparation of an optimized methanol synthesis catalyst which is distinguished by both high activity and good thermal stability constitutes the first step in making a HAS catalyst. The second stage is optimal alkali impregnation of the catalyst so that an optimum HA product range at desired conditions can be achieved.

The following requirements could serve as a guide to the functions the methanol synthesis catalyst should have [Klier 1982]:

(i) It is important that the catalyst should not dissociate the CO molecule but rather activate it in such a way that it can be hydrogenated.

(ii) It must have a moderate hydrogenating function capable of CO hydrogenation.

The composition of the final HAS catalyst must meet at least the following requirements [Xiaodong 1989]:

(a) The catalyst must have a methanol-active component.

(b) There must be (a) promoter(s) which will change the selectivity of the catalyst towards HAS, e.g. alkali metals must be included.

(c) Since the activity is decreased by some alkali metals, in some cases the addition of group VIII, VIIB and VIB metals is recommended.

(d) Stabilizers against thermal deactivation are a requirement because for optimal productivity the catalysts are normally operated at temperatures and pressures higher than those of the methanol synthesis, in the presence of superheated steam. The following structural supports could be included: Al_2O_3, Cr_2O_3, alkali earths and some lanthanides.

1.2.4 Catalyst preparation and optimization

Industrial and laboratory catalysts can be prepared in many different ways. The copper-based methanol synthesis catalyst, which is a highly active and stable system with fine copper crystallites intimately intermixed with the other components, can only be achieved by the coprecipitation method of preparation. In this method, procedures similar to those employed in the preparation of catalysts having as precursors colloidal hydrous oxides, as shown in Figure 1.1, are used [Richardson 1989].

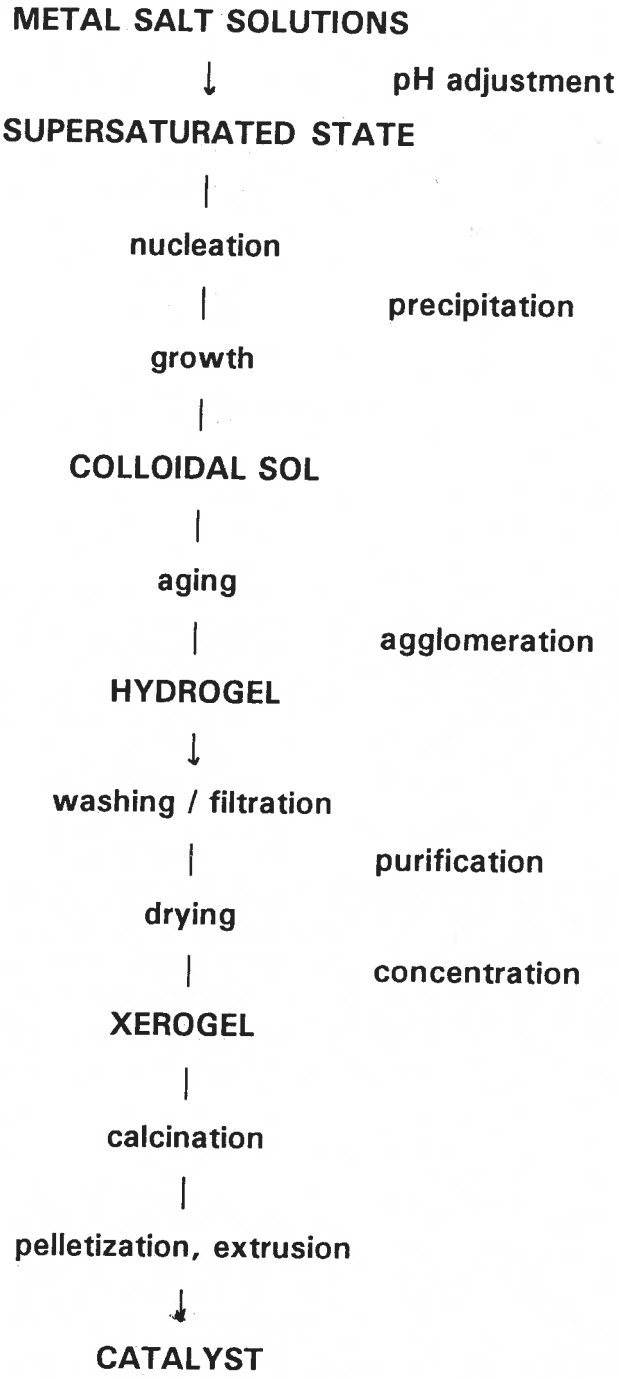

Figure 1.1: Simplified method of catalyst preparation similar to that of mixed oxide catalysts having as precursors colloidal hydrous oxides [Richardson 1989].

depending on the requirements of optimization [Klier et al. 1988a; Tronconi et al. 1989 and Stiles et al. 1991].

The catalyst preparation consists of various stages which are attained by the following unit operations: (1) coprecipitation, (2) filtration, (3) washing, (4) drying, (5) ion exchange separation of unwanted ions (if necessary), (6) calcination and (7) impregnation (if necessary).

Many forms of coprecipitation can be distinguished, i.e. normal coprecipitation, sequential precipitation, and reverse coprecipitation. The purity of the chemicals, the initial pH of the solutions used, the rate of addition of the reactants and the speed of stirring of the suspended precipitate are some of the variables considered in the catalyst-making process. However, the most important variables are the temperature of the coprecipitation, the pH and the level of supersaturation. The effect of changing the above variables on the properties of the catalyst and the nature of the optimized catalyst has been studied by various physico-chemical methods [Herman et al. 1979; Mehta et al.1979, and Klier et al. 1982, 1988a]. The above authors studied a series of preparation variables over their binary Cu/ZnO catalyst where the Cu/ZnO ratio was varied between 0/100 to 100/0 using XRD, XPS and Auger spectroscopy, BET surface area determinations and both scanning and transmission electron microscopy. The features of the optimized Cu/ZnO catalyst they were able to determine were as follows:

- The precipitate composition influenced the interdispersion of the Cu in Zn-oxide and hence, the copper crystallite size.
- The structure of the desired catalyst precursor was a copper-zinc hydroxy carbonate with a structure similar to that of aurichalcite i.e. $(Cu_{0.3}Zn_{0.75})(OH)_6(CO_3)_2$.
- The particle size and hence the surface area were related to the precursor composition and structure where small particles were

found in the composition range 0/100 to 30/100. The larger particles were found within the range 40/60 to 100/0.

- The morphology of the Zn-rich catalysts showed that the zinc oxide existed as a network of thin crystallites with their hexagonal crystal axis parallel to their major surface. In the Cu-rich catalysts ZnO was present as well-shaped hexagonal platelets which were thought to be induced by epitaxial growth of the oxide on $Cu_2(OH)_3NO_3$ at the calcination stage. Their hexagonal crystal axis were perpendicular to the platelet plane.

It has been shown that in order to change the selectivity of the methanol catalysts towards HAS, first, the catalyst has to be impregnated with a suitable alkali metal. Then, for maximum HA productivity, suitable operating conditions have to be established [Natta et al. 1957].

1.2.5 Effect of Operating Conditions

Another important aspect relating to HAS optimization is the determination of suitable operating conditions. The effect of reaction temperature, pressure, feed gas composition and contact time play an important role in HAS.

- **Temperature:** For both high- and low-temperature catalysts, a temperature increase results in an increase in the productivity of the higher alcohols at the expense of methanol. The explanation for this behaviour is found in the kinetics of HAS (see Section 1.3.5.). In the case of Cu-based catalysts, temperature increases need to be executed with care, because above 300 °C catalyst deactivation starts due to sintering of the copper. Methane and CO_2 formation were found to increase with rising temperature. The concentration of esters has been shown to decrease at high temperatures [Forzatti et al. 1991]. This behaviour will be explained in the

thermodynamics section (see Section 1.3.2.). For HAS, temperatures higher than those employed for methanol synthesis are preferred for high productivity.

- **Pressure:** The effect of total pressure on HAS was studied by Forzatti et al. [1991] on the Zn/CrO + 15 % Cs catalyst. Their results are shown in Figure 1.2 below. It is apparent that:

  * The yields of methanol and esters increase with reactor pressure.

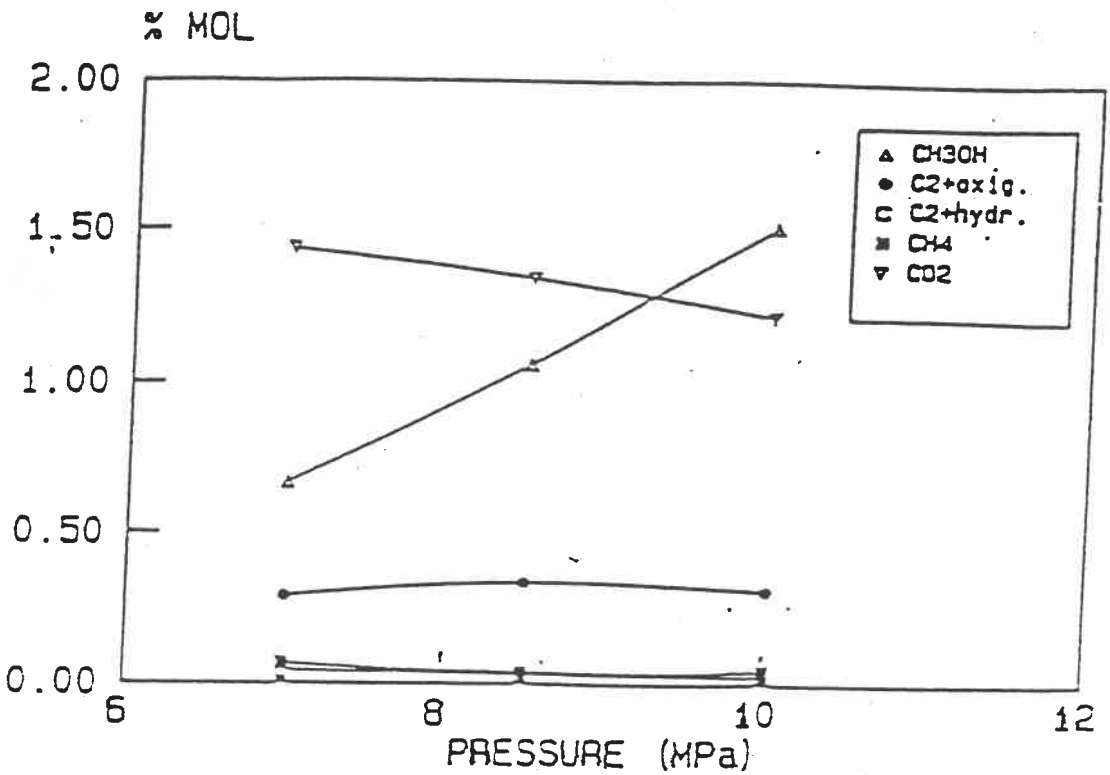

Figure 1.2: The effect of pressure on HAS product distribution over a Zn/CrO + 15% Cs catalyst at 405 °C, a H_2 : CO ratio of 1:1 and a GHSV = 8 000 ml/$g_{cat.}$h^{-1} [Forzatti et al. 1991].

* The formation of HA is only weakly pressure dependent.
* The yields of hydrocarbons decrease at high pressures.
* CO_2 formation decreases with the pressure due to the shifting to the right of the WGS reaction equilibrium (Reaction 1.7), in the presence of large amounts of water in the reaction mixture.

Operating reactors at pressures in the vicinity of 10 MPa leads effectively to a reduction in hydrocarbon formation, hence we have conducted many experiments at this pressure.

- **Gas composition:** The optimal H_2/CO ratio in synthesis gas for HAS using modified high-temperature methanol synthesis catalysts was found to be lower than that used for methanol synthesis. Forzatti et al. [1991], , found that 1 was the best ratio for optimal alcohol synthesis for their Zn/CrO catalyst while a value between 0.45 and 1 was determined by Klier et al. [1988a] in their Cu-based catalyst. A low content of CO_2 in the gas mixture seems to be desirable for the catalyst to retain its activity over time, but at high concentrations it appears to inhibit the catalyst performance [Slaa et al. 1992 and references therein].

- **Contact Time:** The selectivity towards higher alcohols as well as the total activity is increased by increasing the contact time for both high- and low-temperature modified methanol synthesis catalysts. It appears that HAS takes place consecutively with methanol synthesis [Natta et al.1957].

Modified methanol synthesis catalysts are suitable for HAS because in addition to being able to make branched alcohols, they show better selectivities towards higher alcohols than other groups of catalysts. The principles and procedures of

design and preparation of catalysts identified thus far provide pointers to the direction to be followed in making an optimized methanol synthesis catalyst. An understanding of the functions of the different chemical constituents helps the chemist to impart certain desirable functions to a primary Cu/ZnO catalyst. From the above analysis it can be seen that a wide variety of relevant methanol synthesis catalyst formulations are possible and, for a suitable formulation, optimal operating conditions will have to be established. Normally, the catalysts are tested at higher temperatures, medium-to-high reactor pressures, a syngas mixture with a CO/H_2 ratio around one and with or without CO_2. High contact time, i.e. higher than that required for methanol synthesis, is desirable.

1.2.6. Physico-chemical Properties of HAS Catalysts

Elucidation of the geometrical distribution of the alkali dopant on the catalyst surface can help to clarify the dependence of the HAS promotion effect on the dopant concentration. From X-ray diffraction data, XPS and scanning electron micrographs, Klier et al. [1992a] determined the location of Cs on the Cu/ZnO catalyst as shown in Figure 1.3. They demonstrated that the Cs in the form of CsOOCH was associated with the ZnO phase of the catalyst. It was further established that a CsOOCH molecular submonolayer was achievable on the $Cu/ZnO/M_2O_3$ catalyst (M = Al, Cr, Ga and Sc). The XPS data from a $Cu/ZnO/Al_2O_3$ catalyst promoted with K_2CO_3 indicated that potassium existed as K_2CO_3 [Boz 1992] on the surface of the catalyst. It was associated with oxides with a preference for alumina surfaces. The relevance of this geometrical distribution will be discussed later.

Vedage and co-workers [1983] established that the ratio of zinc-to-copper on the surface changes after alkali doping and believed that the zinc that dissolved during doping was redeposited on the surface of the catalyst. They further established from electron microscopy (STEM) and X-ray powder diffraction

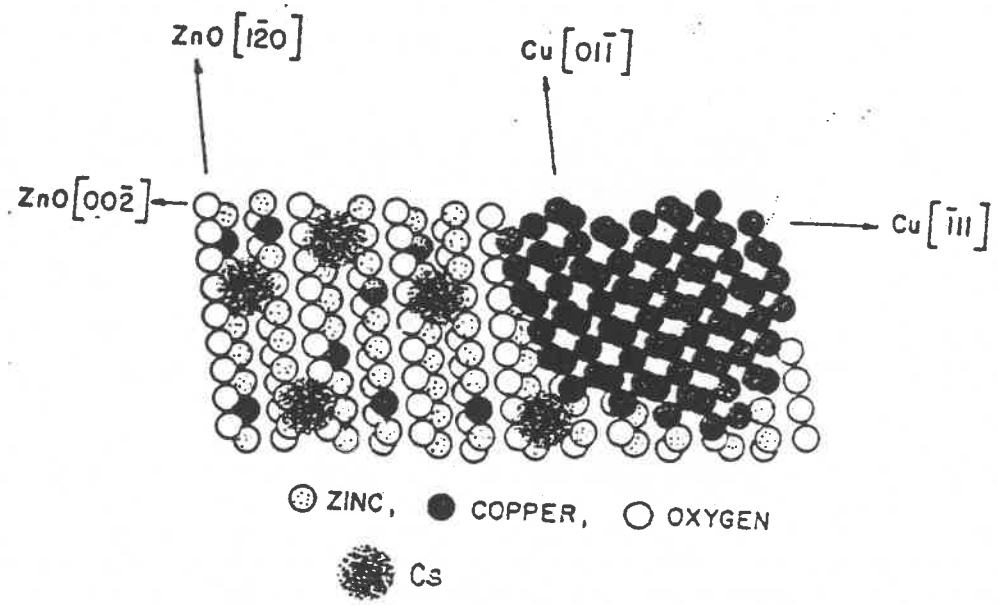

Figure 1.3: The model of 0.4 % CsOOCH on the Cu/ZnO catalyst (adopted from Klier et al. 1992a).

TABLE 1.1

The particle sizes of zinc oxide and copper oxide crystallites as determined by Vedage et al. [1983] on their catalyst.

Catalyst tested	Dimensions (nm)			
	ZnO[10$\bar{1}$0]	ZnO[0002]	ZnO[101$\bar{1}$]	Cu[111]
Cu/ZnO	15.1	17.9	14.6	10.7
Cu/ZnO/NaOH	22.0	23.0	19.5	19.8
Cu/ZnO/KOH	25.9	27.9	23.4	15.4
Cu/ZnO/RbOH	28.3	29.8	24.7	15.4
Cu/ZnO/CsOH	19.5	23.0	17.7	13.0

results (see Table 1.1) that the particle sizes of zinc oxide and copper oxide

crystallites in the alkali-doped catalyst were larger than in undoped catalysts. This phenomenon could be used to explain in part the changes induced by alkali doping in both the total surface area, the metal surface area and, indirectly, in the activity and selectivity of the catalytic system.

Alkali doping has been shown to influence the textural and surface properties of catalysts. A decrease in the total surface area and the specific metal surface area was reported when $Cu/ZnO/Al_2O_3$ catalysts were impregnated with a solution of K_2CO_3 [Slaa et al. 1992]. This effect was attributed to both partial coverage of the Cu metal by the salt and to surface restructuring of the catalyst due to the basicity of the impregnating solution [Slaa et al. 1992 and references therein]. Slaa and co-workers [1992] reviewed work by Nunan in which the same phenomenon was observed upon impregnating the $Cu/ZnO/Al_2O_3$ system with a Cs salt.

A change in catalyst surface area was also observed in the zinc-chromia catalyst studied by Di Conca et al. [1984]. This phenomenon, which was prominent in catalysts with excess ZnO, was attributed to (i) the formation of the surface compound $K_2Cr_2O_7$ for all air-calcined catalysts, (ii) the interaction of ZnO and K with a concomitant increase in ZnO crystal size and (iii) the detachment of a $Zn_xCr_{2/3(1-x)}O$ spinel-like phase from the ZnO crystallites.

Since there was a correlation between the amount of the spinel-like phase and the catalytic activity on their zinc-chrome catalyst, Di Conca et al. [1984] concluded that the $Zn_xCr_{2/3(1-x)}O$ was the active phase. Indications were that the octahedral sites of the spinel-like structure were occupied by Zn^{2+} ions. These ions, which were exposed to the surface, could be regarded as either the active centre or part of it where CO and H_2 could be coordinated to form methanol. It was concluded from TPD results that potassium impregnation resulted in a decrease in the number of active sites, although their nature did not change. The high selectivity of potassium-doped catalysts towards higher alcohols was

attributed to their basic character which increased the rate of base-catalyzed steps in the complex reaction process.

With regard to copper-containing catalysts, one theory states that the active centre is a Cu^+ ion which is in close contact with a promoter [Ponec 1992]. It is believed that there is an epitaxial relationship of Cu^+ on ZnO which is stabilised by incorporation in the ZnO matrix. This is given as the main reason for the advantage of the synergy between copper and zinc in methanol and related syntheses which is well documented in the literature. The desirable overall arrangement for optimal higher alcohol synthesis selectivity is close proximity between the hydrogenating function (the oxide) and the basic function (the alkali metal salt) on the catalyst surface [Klier 1992a]. This means that there is a certain optimal quantity of alkali metal able to fulfil the above requirement.

Normally, the alkali metal dopants are salts or hydroxides. The basicity of the counter-ions is thought to be controlled by the size of the cations, with heavier alkali metals showing superior performance to lighter ones in higher alcohol synthesis, methanol synthesis and the water-gas shift reaction [Klier 1992a].

The size of the alkali metal appears to have another important stereochemical function in certain reaction paths that are relevant to the synthesis of branched alcohols. The cis-trans isomerization of the postulated 1,3-ketoalkoxide intermediate which occurs over the alkali-doped Cu/ZnO catalyst is "more facile" with larger alkali metals than with smaller ones. The rate of chain growth and the selectivity towards products formed by the oxygen-retention pathway increase with the size of the alkali metal [Klier et al. 1992b]. The subsequent discussion of the overall reaction chemistry and mechanism will further clarify this point.

Elucidation of the structure-function relationships of modified methanol synthesis catalysts, by means of a series of physico-chemical methods, and an

attempt to determine either their active phases or their active sites, is central to the design of catalysts with certain specific desired functions. The physico-chemical investigations will be used to characterize the alkali impregnated catalyst batches in this work. Our attention is now turned to the chemistry of HAS.

1.3 HIGHER ALCOHOL SYNTHESIS CHEMISTRY

1.3.1 Types of reactions

The following reactions are possible in HAS:

$$CO + 2H_2 = CH_3OH \qquad (1.3)$$

$$nCO + 2nH_2 = C_nH_{2n+1}OH + (n-1)H_2O \qquad (1.4)$$

$$nCO + (2n+1)H_2 = C_nH_{2n+2} + nH_2O \qquad (1.5)$$

$$nCO + 2nH_2 = C_nH_{2n} + nH_2O \qquad (1.6)$$

$$CO + H_2O = CO_2 + H_2 \qquad (1.7)$$

$$CO_2 + 3H_2 = CH_3OH + H_2O \qquad (1.8)$$

$$nCO_2 + 3nH_2 = C_nH_{2n+1}OH + (2n-1)H_2O \qquad (1.9)$$

$$nCO_2 + (3n+1)\,H_2 = C_nH_{2n+2} + 2nH_2O \qquad (1.10)$$

$$nCO_2 + 3nH_2 = C_nH_{2n} + 2nH_2O \qquad (1.11)$$

$$CH_3(CH_2)_{n-2}CH_2OH = (CH_3)_2CH(CH_2)_{n-4}CH_2OH \qquad (1.12)$$

Hydrogenation of carbon oxides under HAS conditions involves the following four main classes of reactions: methanol synthesis, Fischer-Tropsch (F-T) reactions, HAS and the water-gas shift reaction (Equations 1.3 to 1.12). HAS is based primarily on reaction (1.4) with n varying from 1 to 8. Since the water-gas shift reaction (1.7) cannot be avoided on many HAS catalysts (especially the modified methanol synthesis catalysts), it influences the HAS reaction stoichiometry as shown in Equation 1.13 below. Thus, Equation 1.13 is the sum of Equations 1.4 and 1.7:

$$(2n\text{-}1)CO + (n+1)H_2 = C_nH_{2n+1}OH + (n\text{-}1)CO_2 \qquad (1.13)$$

Many other chemical reactions involving the reactants and products are possible but they are regarded as of little significance in the overall reaction network. The above reaction scheme offers a reasonable guide as to what occurs in the HAS process.

1.3.2 Thermodynamic considerations

"A priori" studies of the thermodynamics of HAS have been undertaken by a number of authors including Anderson [1956] and Natta et al. [1957]. Recently, results of studies on the thermodynamics of HAS was published by Anderson [1986]; Mawson et al. [1993]; Roberts et al. [1993] and Anderson [1956] showed that the WGS reaction has a more negative Gibbs free energy change (ΔG°) than both the HA and methanol syntheses under HAS conditions. WGSR is therefore more favourable than either of the latter. The situation is enhanced by the presence of water during the reaction as evidenced by reactions (1.4 to 1.11) above. The WGS reaction is known to be activated by the Cu-based HAS and methanol catalysts and the Fe-based F-T catalysts. However, it becomes less favourable as the reaction temperature is increased [Xiaoding et al. 1987]. It will be shown later that the reaction equilibrates at HAS conditions.
The F-T synthesis producing alkenes proceeds according to reactions (1.5) and

(1.10) and according to Xiaoding et al. [1987] the change in the Gibbs free energy ($\Delta G°$) for both reactions can be calculated using equations (1.14) and (1.15) respectively.

$$\Delta G° = -38.387n + 17.645 + (5.982n - 3.434)10^{-2}T \text{ (Kcal mol}^{-1}\text{)} \quad (1.14)$$

$$\Delta G° = -29.872n + 17.645 + (5.211n - 3.434)10^{-2}T \text{ (Kcal mol}^{-1}\text{)} \quad (1.15)$$

From the above two equations alkenes can be expected to be formed in appreciable amounts during HAS, but this is not the case. It seems they either get hydrogenated to alkanes or are incorporated into other reaction processes. Natta et al. [1957] calculated the $\Delta G°/n$ for alcohols, alkanes and alkenes using equations (1.4), (1.5) and (1.6). This was carried out over a temperature range of ΔT = 0 to 800 °C. The study showed that the $\Delta G°/n$ for methane was more negative than that for alcohols and other hydrocarbons at all temperatures in the specified temperature range. This explains the large quantities of methane associated with the HAS process. It follows from the above arguments that large quantities of methane might be detected in this work.

The heats of reaction are an important consideration in an industrial-scale operation because of the heat-removal implications of exothermic reactions. Excessive heat can cause deactivation of the catalyst by coking, sintering or disintegration [Anderson 1956]. Anderson [1956] studied the heats of reaction in the formation of hydrocarbons {reactions (1.5) and (1.6)} as functions of temperature. The change in the heats of reaction per carbon atom ($\Delta H°/n$) showed a weak dependence on temperature, with higher stability at higher temperatures. The length and the nature of the hydrocarbon influence the magnitude of $\Delta H°/n$ in the following way: for alkanes the $\Delta H°/n$ increases with an increase in carbon number, while for alkenes it decreases with increasing carbon number.

TABLE 1.2.

Heats of formation (ΔH) of alcohols according to Anderson [1956].

Alcohol	ΔH, (Kcal/mol)	ΔH/n, (Kcal/mol/carbon atom)
Methanol	-23.9	-23.9
Ethanol	-58.9	-29.5
1-Propanol	-98.0	-32.7

The heats of formation of three gaseous alcohols and water vapour at 18 °C, formed according to reaction (1.4), are shown in Table 1.2 above [Anderson 1956]. Since the heats of reaction do not show a strong dependence on the temperature, trends in the above data can be regarded as representative of the situation at HAS temperatures as well. It can be seen that ΔH/n becomes more negative with an increase in the carbon number of the alcohol.

Xiaoding and co-workers [1987] calculated the ΔG° of formation of the WGS reaction, alcohols, hydrocarbons and the temperatures (T°) at which their ΔG° became positive with a CO/H_2 gas mixture as the feed. Some results are shown in Table 1.3. The following deductions were made:

* Compounds of the same n value at the same temperature can be ranked according to the ease with which they are formed as shown below:

$$C_nH_{2n} > C_nH_{2n+1}OH > C_nH_{2n+2}$$

Natta et al. [1957] referred to a similar trend as above. This shows that the HAS catalysts need to be very selective.

* The ΔG° of formation for both hydrocarbons and alcohols increases with an increase in temperature. Therefore, they are thermodynamically unfavourable at higher temperatures, explaining why above 450 °C some oxygenates are said to decompose.
* Within a homologous series, the stability of a compound increases at lower temperatures with an increase in n. It is noted here that at 523.3 K (the typical methanol synthesis temperature), the selectivity of methanol on methanol synthesis catalysts is of the order of 98-99%, which implies that the reaction is kinetically controlled since it is thermodynamically less favourable. The data indicate that at high temperatures, the lower homologues seem to be thermodynamically favourable. The above three observations also hold for the synthesis of hydrocarbons and alcohols from a CO_2/H_2 gas mixture.

The ΔG° for the isomerization of alcohols as shown in reaction (1.12) can be calculated as follows [Xiaoding et al. 1987]:

$$\Delta G^\circ = -1.355 + 0.258 \times 10^{-2}T \text{ (Kcal mole}^{-1}\text{)} \qquad (1.16)$$

From equation (1.16) one expects reaction (1.12) to be less favourable with a temperature increase. The reaction could not be expected to be responsible for the formation of branched alcohols.

With the exception of reaction (1.7), reactions (1.3) to (1.11) involve a volume contraction, this being particularly so for those reactions where the value of n is large. Increasing the total reaction pressure will shift the equilibrium more to the right, especially for those reactions with a high n value.

Mawson et al. [1993] studied the thermodynamics of HAS in a system which had the following components: CO, H_2, CO_2, H_2O and C_1 - C_4 normal alcohols

and their isomers. The Gibbs free energy minimization module of the ASPEN PLUS process-simulation package was used in the calculations. The reactants and products were assumed to behave as ideal gases, an assumption that proved to be valid. They determined that the stoichiometric H_2/CO ratio varied from 2.0 to 0.5. They also established that for all temperatures up to 773 K, the equilibrium conversions for either CO or H_2 were above 90% and that the C_4 alcohols predominated. Tertiary butanol was found to be thermodynamically favoured at temperatures below 473 K, while isobutanol was preferably formed at higher temperatures, up to 773 K. The effect of total pressure on the reaction at equilibrium was not significant, while the recycling of an alcohol increased the yield of other alcohols up to a certain critical point above which no further increases were observed. It was again shown that at certain defined sets of temperatures and pressures multiple phases (i.e. be they liquids and gases) could exist in the reaction mixture and this resulted in a drastic change in the product distribution. The HAS reaction is normally far from equilibrium, therefore some of the observations above are not encountered in practice.

An "a posteriori" thermodynamic analysis of the oxygenate products of HAS has been reported [Tronconi et al. 1990]. These authors compared measured fugacity ratios with equilibrium constants at HAS conditions on Cs-doped Zn/Cr-oxide catalysts. It was established that the following reactions were all at equilibrium under the operating HAS conditions: (a) methanol synthesis, (b) WGS reaction, (c) formation of methyl formate and higher methyl esters, (d) hydrogenation of aldehydes to primary alcohols, (e) hydrogenation of ketones to secondary alcohols and (f) ketonization reactions. Secondly, the above reactions were related to the catalytic properties of the operating catalyst. The Zn/Cr-oxide system was shown to possess activity towards an aldol-type condensation, hydrogenation, hydrolysis and alcoholysis, dehydration, isomerization, dehydrogenation, decarboxylation as well as hydro-cracking functions. The first five reactions have been shown to be catalyzed under HAS conditions [Lietti et al. 1988]. The effect of operating conditions on the equilibria

TABLE 1.3

ΔG° of the WGS reaction, alcohols, alkanes, alkenes and the temperatures (T°) at which the ΔG° becomes positive [Xiaoding et al. 1987].

Compound	n	ΔG° (Kcal/mol)			T°
		523.3	600.0	673.3	
$C_2H_{2n+1}OH$	1	3.3	7.7	12.0	194
	2	-3.8	5.2	13.9	282
	3	-10.9	2.8	15.8	311
	4	-18.0	0.3	17.7	326
	5	-25.1	-2.2	19.6	334
	6	-32.1	-4.7	21.5	340
C_nH_{n+2}	1	27.5	32.0	36.3	55
	2	20.4	29.5	38.2	351
	3	13.3	27.0	40.1	449
	4	6.2	24.5	42.0	496
	5	-0.9	22.0	43.8	526
C_nH_{2n}	2	-14.5	-7.9	-1.7	420
	3	-21.6	-10.4	0.2	399
	4	-38.7	-22.9	-7.9	439
	5	-35.7	-15.4	4.0	385
	6	-42.8	-17.9	5.9	382
WGS reaction		-4.5	-4.1	-3.3	

mentioned above was demonstrated on the ketonization reactions. The following reactions were considered:

$$C_2H_5OH + n\text{-}C_3H_7OH = CH_3(CO)CH_2CH_3 + CO + 3H_2 \qquad (1.17)$$

$$n\text{-}C_3H_7OH + n\text{-}C_4H_9OH = CH_3(CH_2)_2(CO)CH_2CH_3 + CO + 3H_2 \quad (1.18)$$

$$n\text{-}C_3H_7OH + i\text{-}C_4H_9OH = (CH_3)_2CH(CO)CH_2CH_3 + CO + 3H_2 \quad (1.19)$$

$$2n\text{-}C_3H_7OH = CH_3CH_2(CO)CH_2CH_3 + CO + 3H_2 \quad (1.20)$$

Thermodynamic data showed that the above ketonization reactions were (i) at equilibrium at high temperatures and low GHSV, and (ii) far from equilibrium, thereby proceeding from right to left, at low temperatures, high GHSV, high H_2/CO ratio and gas feeds rich in CO_2. Further, it was shown (iii) that thermodynamics dictated the low concentrations of ketones, and (iv) the above reactions were proved to be thermodynamically reversible. The reactions were responsible for the consumption of ketones. Under **1.3.4 Reaction mechanisms**, the reverse ketonization reactions will be shown to be one of the routes responsible for the formation of higher alcohols.

From thermodynamics, the types of reaction products likely to be encountered under HAS can be predicted, i.e. alcohols, hydrocarbons, water, CO_2, etc. The HAS thermodynamic studies have highlighted the importance of controlling the reaction heat and the need to design highly selective catalysts. The abundance of C_4 oxygenates has at least in part been explained thermodynamically. Finally, the ketonization reactions showed the extent to which the reaction conditions can influence the reaction products for all those reactions which equilibrate under HAS conditions.

1.3.3 Mechanistic aspects

1.3.3.1 Reaction intermediates

Various mechanisms proposed previously for HAS were based on reaction intermediates, whose existence under conditions resembling those of HAS, could

not be verified experimentally [Slaa et al. 1992 and references therein]. These mechanisms were merely suggestions of a set of possible routes that the HAS reaction could follow from the reactants to the products stage. However, of late considerable research has been carried out in identifying possible reaction intermediates and chain-growth steps. Hindermann et al. [1993] reviewed reactions in which ethanol was shown to be formed from either methanol, formaldehyde or ethylene glycol, and in which either a formyl surface species existed or a correlation could be established between a formate species and catalytic activity. Klier et al. [1988b], from their experiments on Cs/Cu/ZnO, concluded that an aldehydic intermediate which they believed could be formaldehyde, dioxymethylene or a hydroxycarbene was involved in the reaction mechanism.

On a Zn/Cr catalyst system at 653 K, methanol or formaldehyde were converted to higher oxygenates with isobutanol predominating [Lietti et al. 1992]. It seems that an oxygenated C_1 plays a significant role in some HAS reaction mechanisms. Methyl formate has been related to the intermediate either as its precursor or as the actual intermediate since it can rearrange to acetic acid which can be hydrogenated to ethanol [Slaa and co-workers 1992].

1.3.3.2 The C-C bond formation

The aldol condensation with the so-called Oxygen Retention Reversal (ORR) has been shown to be the major chain-growth path for catalysts of the type Cu/ZnO/Cs [Nunan et al. 1989]. This aldol type reaction was claimed to be unique for the Cs-promoted catalysts. The ORR reaction path shown in Figure 1.4 was established using ^{13}C labelling. Although aldol coupling with ORR has been associated with Cs-doped catalysts, it has also been shown to occur for K-doped Zn/CrO catalysts where C_{2n} ketones are formed from C_n aldehydes [Lietti and co-workers 1992]. The condensation of a lower alcohol with methanol to form a higher alcohol, which was shown to proceed through dehydrogenation,

Classic Aldol Condensation

$$RCH_2{}^{13}CHO + H_2C{=}O \xrightarrow{-H_2O/+H_2} RC(CH_3)H^{13}C\underline{H}O$$

$$RC(CH_3)H^{13}C\underline{H}O \xrightarrow{+H_2} RC(CH_3)H^{13}CH_2\underline{O}H$$

Aldol Condensation with Oxygen Retention Reversal

$$RCH_2{}^{13}CHO + \overset{M}{HC{=}O} \xrightarrow{-MHO/+H_2} RCH(C\underline{H}O)^{13}CH_3$$

$$RCH(C\underline{H}O)^{13}CH_3 \xrightarrow{+H_2} RCH(CH_2\underline{O}H)^{13}CH_3$$

Figure 1.4: The difference between normal aldol coupling and coupling with oxygen retention reversal is shown with the retained oxygens underlined. M = metal atom or H in adsorbed formaldehyde [Nunan et al. 1989].

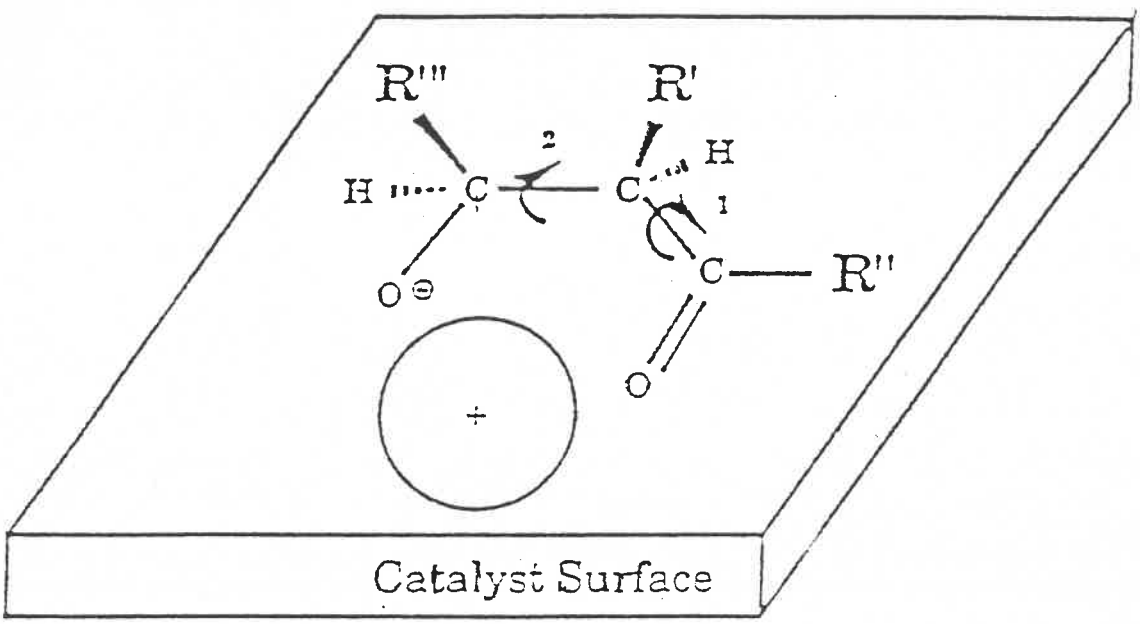

Figure 1.5: The C-C bond rotations in the 1,3-ketoalkoxide intermediate (adopted from Klier 1992b).

condensation, dehydration and hydrogenation on basic catalysts at 653 K [Ueda et al. 1992] can be regarded as evidence for the existence of a classic aldol condensation in HAS reactions. The formation of unsaturated C_{2n} aldehydes over a K-doped Zn/CrO catalyst from C_n aldehydes points to the occurrence of an aldol-type condensation for this catalyst [Lietti et al. 1992].

Both the classical Aldol condensation and Aldol condensation with ORR are β-additions on the growing carbon chain. The C_1 addition was shown to be preferable to C_{2+} (compounds which consist of two and more carbon atoms) on both ketones and primary alcohols, while coupling of two C_1 aldehydic species was shown to be responsible for the formation of C_2 oxygenates [Klier 1988b]. The C_{2+} oxygenates could result from aldol condensation with ORR between C_1 and C_n oxygenated species with branched C_4 oxygenates as the terminal species. The reaction intermediate is thought to be a 1,3-ketoalkoxide species attached to the alkali metal through its two oxygen atoms, as shown in Figure 1.5.

The C-C bond formation can also proceed by insertion of the C_1 species in a growing C_n intermediate to produce a linear alcohol. This would take place according to the mechanism suggested by Fox et al. [1984] or by means of an S_N2 reaction between the formaldehyde and an alcohol, where OH acts as a leaving group [Smith et al. 1991].

Various suggestions have been put forward to explain the high selectivity of some HAS catalysts towards the formation of branched alcohols, especially isobutanol. The stereochemical effects which affect the reaction intermediate were discussed by Klier and co-workers [1992b]. In the β-aldol condensation with ORR, the intermediate undergoes a cis-trans isomerization by rotation of the bonds numbered 1 and 2 in Figure 1.5. Significantly the sizes of the groups R'and R" determine whether isomerization takes place as well as influencing the extent thereof. Bulky groups (CH_3, C_2H_5) experience steric hindrance in their

interaction with the catalyst surface and the alkali metal, thereby limiting the rotations of the above-mentioned bonds. The overall process is completed by hydrogenation and dehydration of the ketonic group, followed by hydrolysis to release the 2-methyl alcohol [Klier et al. 1992b]. This implies that for isobutanol, both R′ and R" would be bulky groups, thereby hindering further reactivity.

Branched oxygenated C_4 molecules showed a low reactivity in the condensation reaction to form higher ketones in the case of K-doped Zn / Cr catalytic system described by Tronconi et al. [1990]. These researchers established that the ketonization reaction of isobutanol to form 2,4-dimethyl-3-pentanone was far from reaching equilibrium. It was suggested that this explained the high quantities of isobutanol in the HAS reaction product.

1.3.3.3 The C-O bond formation

It has been suggested that in HAS esters and ketones are derived from alcohols with aldehydes as intermediates [Hindermann 1993 and references therein]. Klier and co-workers [1988b] suggested the following reactions to account for methyl ester formation:

(i) The Cannizzaro reaction between a C_1 aldehyde and a C_n aldehyde.

(ii) A Tishchenko reaction between a methoxide and a C_n aldehyde.

(iii) A methoxide addition to CO to form methyl formate. The last route was confirmed by ^{13}C labelling.

In view of the above considerations, two relevant reaction mechanisms from the literature are discussed below.

1.3.4 Reaction mechanisms

In step (a) of Mechanism (1) below (see Figure 1.6), the linear growth of a C_1 to

Reaction Mechanism 1

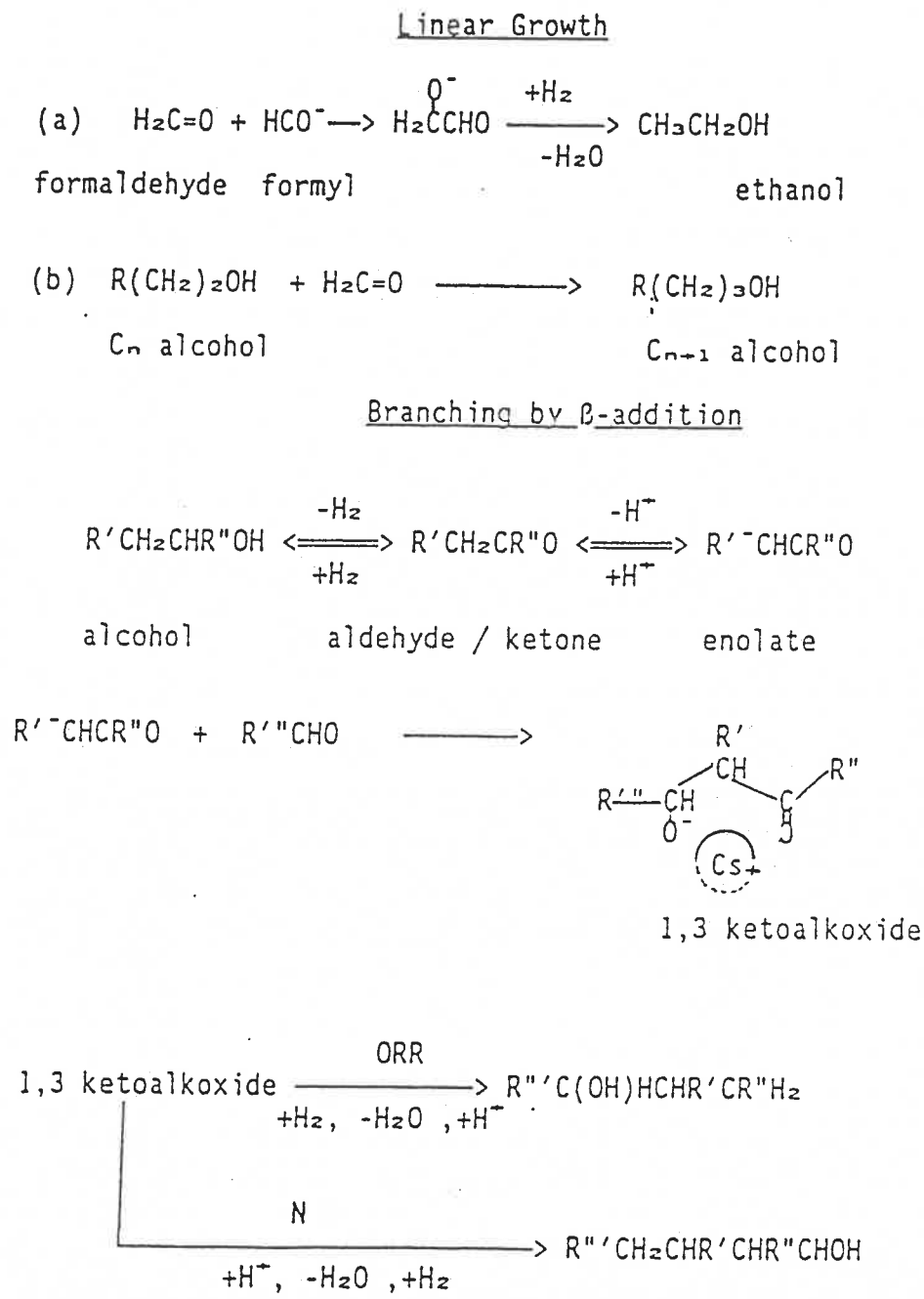

Figure 1.6: Reaction mechanism for HAS over a Cu/ZnO/Cs catalyst [adopted from Nunan et al. 1989; Smith et al. 1991 and Klier et al. 1992b]

C_2 species proceeds by condensation of formaldehyde with an adsorbed formyl species. Hydrogenation of the intermediate, followed by its dehydration, results

in the formation of ethanol. The condensation of a C_n alcohol with formaldehyde { step (b) } to form a C_{n+1} alcohol is regarded as one of the chain-growth steps. As mentioned earlier, the reaction follows either an S_N2 mechanism with the OH of the alcohol functioning as the leaving group or the mechanism proposed by Fox et al. [1984]. This mechanism explains the chain growth via the condensation of two adsorbed aldehyde molecules in the presence of a strongly basic alkali compound forming an adsorbed aldehyde with an increased carbon number. The β-additions in ORR and N modes result in chain branching and chain growth respectively.

In reaction Mechanism (2), below, (see Figure 1.7), the gas phase concentrations of oxygenates are related by the following equilibria:

- methanol synthesis,
- the WGS reaction,
- the hydrogenation of primary alcohols to aldehydes and secondary alcohols to ketones,
- methyl esters formation from primary alcohols and methanol and, finally,
- the equilibrium between primary alcohols and ketones [Forzatti et al. [1991].

The aldol-type condensation (β) and the carbonyl carbon addition (α) comprise the central routes for chain growth in this mechanism. The β-condensation in the normal (β_N) mode results in higher aldehydes which can either react further or be hydrogenated to alcohols. In the oxygen retention reversal mode (β_{ORR}), higher ketones are formed. Hydrogenation of the carbonyl group with its subsequent dehydration results in the formation of branched alcohols. The effect of reverse ketonization reactions (Γ) is to produce alcohols from ketones, as shown in the reaction scheme. The C_1 addition on the carbonyl carbon, both in the normal mode (α_N) and in the oxygen retention mode (α_{ORR}), is recognized in this mechanism. With formaldehyde as the starting compound, this route is

responsible for the formation of a C_2 alcohol.

Reaction mechanism 2

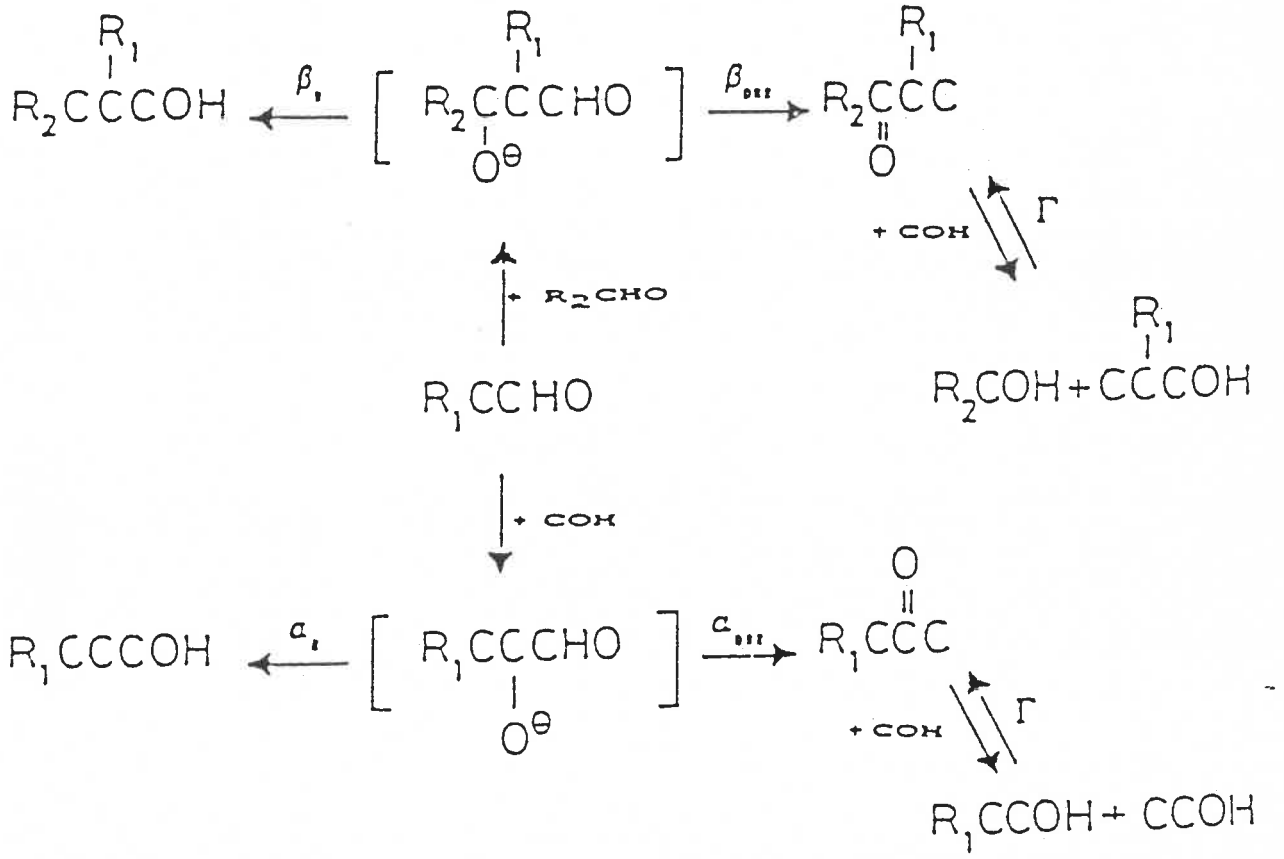

Figure 1.7: Reaction mechanism for HAS on Zn/Cr + Cs_2O catalysts according to Forzatti et al. [1991].

In the above mechanisms, different reaction routes are followed for two different catalysts. This could be attributed to differences in the composition of the

catalysts in question and probably different reaction conditions. The activation of the aldol-type condensation reaction by both catalytic systems is due to the presence of the basic function in the catalysts. This highlights the seemingly important role the basic function of the catalyst plays in HAS. The relative importance of different steps in the reaction mechanisms is demonstrated in section 1.3.5.

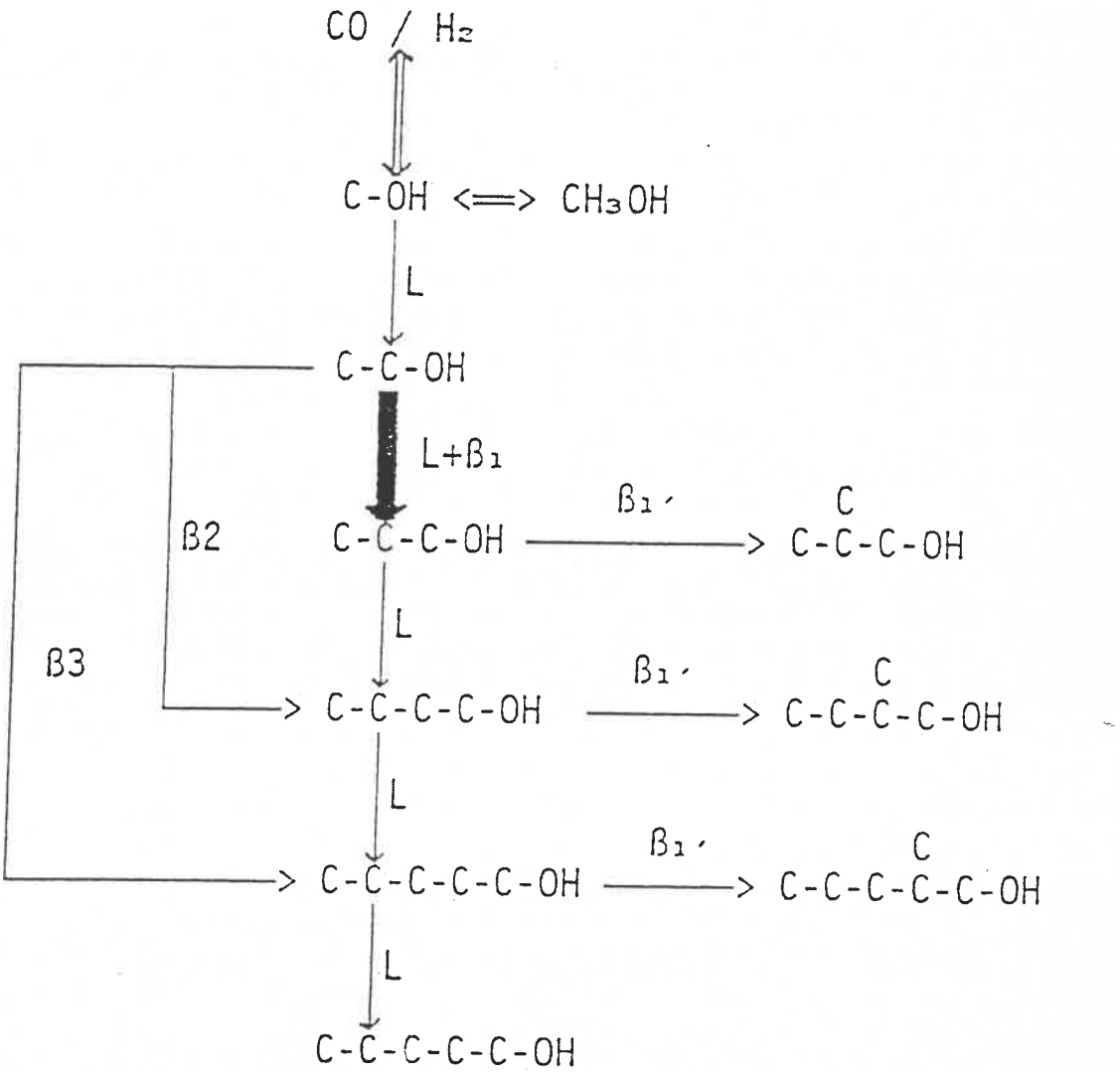

Figure 1.8: **The alcohol formation network, where linear growth of alcohols by C_1 addition is designated by L while C_2 and C_3 linear growth by $\beta 2$ and $\beta 3$, respectively. Chain branching by C_1 addition is represented by the route marked β_1' [Smith et al. 1991].**

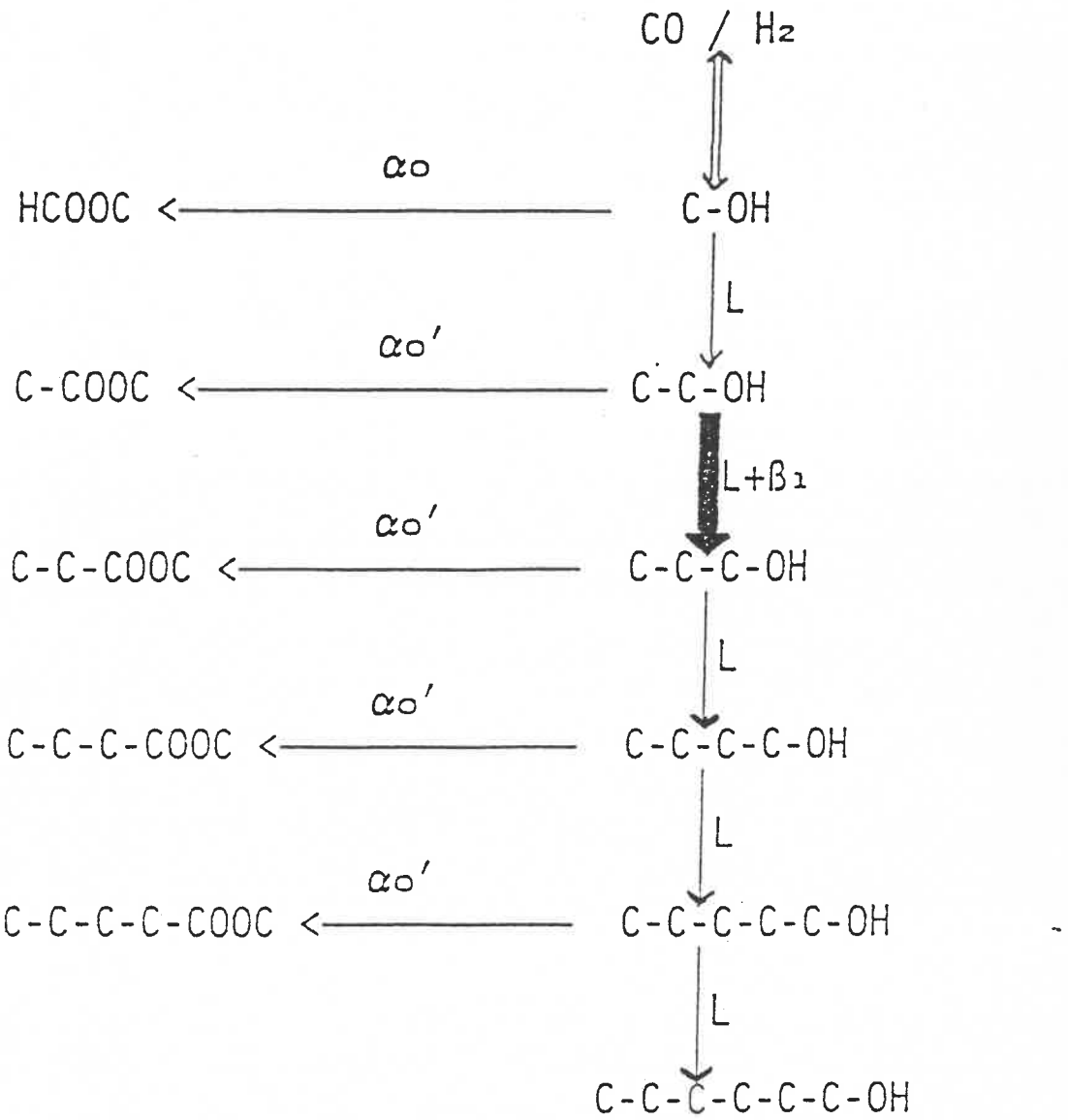

Figure 1.9: The ester formation network, where methyl formate is represented by the path α_o, while other methyl esters are shown by the paths α_o'. α_o = rate constant of formation of methyl formate and α_o' = rate constant of formation of other methyl esters [Smith et al. 1991].

1.3.5 Kinetics

A kinetic model for HAS was published by Vedage et al. [1985]. It was based on a reaction scheme proposed by Smith and Anderson [1984]. This Smith-Vedage model attempted to predict the selectivities of oxygenates in the reaction involving the CsOOCH/Cu/ZnO catalytic system. The key element of the model was that the reaction steps used in the calculations were based on a proposed reaction mechanism. This is the criterion used in this work to establish kinetic models relevant to the catalysts reviewed. The Smith-Vedage model revealed a serious discrepancy between measured and predicted values for certain products.

Recent work by Smith et al. [1991] lead to improvements being suggested for this model. They adopted the reaction schemes in Figures 1.8 and 1.9 for the formation of alcohols and methyl esters respectively. To the previous Smith-Vedage model, the following modifications were added:

(i) Methyl formate was formed by methanol carbonylation with a rate constant (α_o) different from that of methyl esters (α_o').

(ii) A distinction was made between the β-addition rate constant for C_2 intermediates (β_1) in the C_2 to C_3 step and the rate constant for intermediates with higher carbon numbers (β_1'). The former rate constant was regarded as larger in magnitude and the step was said to be specifically promoted by Cs.

(iii) Although the two-carbon addition (β_2) and three-carbon addition (β_3) could help to explain the formation of secondary alcohols, the main reason for their inclusion was to facilitate the prediction of the formation of alcohols such as 1-butanol, 1-pentanol, etc. which were present in small quantities.

(iv) Since the linear growth of branched intermediates was assumed to be negligible, these were ignored in the kinetic model.

In this model the mass balance of the -CCCOH intermediate was written as follows:

$$(k_L + k_\beta)A_{C_2}A_{C_1} = k_tA_{C_3} + (k_L + k_\beta' + k_A)A_{C_3}A_{C_1} + k_{\beta 2}A_{C_3}A_{C_2} + k_{\beta 3}A_{C_3}A_{C_3}$$

which was simplified to:

$$(L + \beta_1)A_{C_2} = (1 + L + \beta_1, + \alpha_o' + \beta_2 + \beta_3)A_{C_3}$$

where:

$$\beta_1 = k_\beta A_{C_1} / k_t$$

$$\beta_1' = k_\beta' A_{C_1} / k_t$$

$$\beta_2 = k_{\beta 2} A_{C_1} / k_t$$

$$L = k_l C_1$$

and A_{Cn} is the surface concentration of the C_n oxygenate. The rate constant for the termination step is designated by k_t. Assuming that $k_{\beta 2} = k_{\beta 3}$ one finds that β_3 is equal to $\beta_2 A_{C_3} / A_{C_2}$. By assuming differential reactor conditions, Smith et al. [1991] were able to reasonably predict the product distribution of oxygenates using five rate parameters with an error as low as 2-carbon atom percentage units. The model was shown to be valid for many different reaction conditions. It emphasizes the step-wise addition of C_1 to C_n in such a way that β-addition is dominant over linear growth, with its effect at C_2 being more pronounced than at C_n where n is greater than three. The C_2 formation, which is the rate determining step, is catalyzed by alkali metals. High temperatures increase rate constant of the C_2 formation step. The relative magnitudes of L and α_o' varied with temperature in the following manner:

$$L > \alpha_o' \text{ at } T > 300\ ^\circ C$$

$$L \approx \alpha_o' \text{ at } T = 300\ ^\circ C$$

$$L < \alpha_o' \text{ at } T < 300\ ^\circ C$$

Although the model was successful in predicting the reaction product distribution, its main weakness was that it was based on the assumption of a differential reactor regime. A further weakness was that it assumed that the growth and termination steps were irreversible, assumptions which have recently been shown not to be valid [Forzatti et al. 1991 and references therein].

A model for oxygenate product distribution involving a Cs-doped Zn/Cr catalyst based on the reaction scheme shown in Figure 1.7 was proposed by Forzatti et al. [1991] and Tronconi et al. [1992]. In the model an adsorption equilibrium for the species which were participating in the chain growth was assumed. Again, it was assumed that the C_1 intermediates formed were at equilibrium with CO/H_2 and that water competed for adsorption on the active sites. The following rate expressions for C_1 additions, normal aldol condensation and condensation with ORR were used.

$$\text{Normal mode: } r_{ij} = k_{ij}K_{ad}C_iC_j$$

$$\text{ORR mode: } r_{ij} = \frac{k_{ij}K_{ad}C_iC_j}{1 + K_wC_{H_2O}}$$

For ketonization kinetics the following expression was used:

$$r_{ij,ket} = \frac{k_TK_{ad}C_1P_{H_2}\{C_{ket}-(C_iC_j)/(P_{H_2}C_1K_{ket,ij})\}}{1 + K_wC_{H_2O}}$$

where k_{ij} is the aldol condensation rate between aldehydes i and j, K_{ad} is the adsorption equilibrium constant used for all species, and K_w is the adsorption equilibrium constant for water. $K_{ket,ij}$ is the constant for the ketonization reaction

where the reaction of methanol and a ketone resulted in the formation of alcohols i and j, and P_{H_2} was the partial pressure of H_2 gas. In the model nine rate parameters were used because each reacting species had a unique reactivity depending on its molecular structure. It was claimed that the model predicted accurately the distribution of 20 ketones and alcohols at different GHSVs, temperatures, pressures and different feed compositions. Again, the authors claimed that the formation of 50 other compounds that could not be detected in HAS could be predicted by the model.

The model highlighted the following aspects of the reaction mechanism: (i) aldol condensation is faster than C_1 additions on the carbonyl carbon by an order of magnitude; (ii) aldehydes are more reactive than ketones; (iii) apart from aldol condensation, reverse ketonization plays an important role in chain growth; and (iv) the ketonization reaction and aldol condensation with ORR were shown to be specifically inhibited by water.

The problem associated with this model is that, in its present form, it cannot be used to study the effects of the variations of the CO/H_2 ratio and total pressure on product distribution. The performance of the model on related catalyst formulations still has to be determined.

1.4 CONCLUDING REMARKS

Since HAS has not reached the stage where it can supply the motor industry with the necessary fuel, it appears that a lot of research still has to be carried out to bring the technology to the present state of the methanol synthesis process. The crucial area of research is development of a method for synthesis of a unique and active methanol catalyst and its conversion to a HAS system with fine-tuning of its structural properties so that it functions optimally. In this review it was shown that there are many different kinds of HAS catalytic systems. Much attention was focused on the modified methanol synthesis

catalytic systems because our research is based on them. Many different methods of preparation of these systems were highlighted. In this work a methanol synthesis catalyst is prepared by continuous co-precipitation method and then, impregnated with different alkali metal salt solutions in order to make it a HAS catalytic system. Information about the different functions of catalyst constituents shows that their addition results in incorporation of desirable features in the methanol synthesis catalysts. The physico-chemical tests have been shown to be crucial in catalyst optimization. Therefore, structure-function considerations are an important component of the optimization process and will be looked into in this work.

The importance of suitable test conditions for the HAS process were discussed. Higher temperatures and pressures with lower GHSVs, as compared with the conditions in the methanol synthesis reaction process, were shown to be desirable for HAS. These are the conditions which were used in our research. Thermodynamics and kinetics provide some answers to the behaviour of this process. Thermodynamic analysis of HAS showed that reasonable conversions could be obtained at temperatures that would not pose a problem in industry. Again, highlighted the fact that reaction heat was likely to be a problem in industrial scale HAS plants. We learnt that since formation of alcohols was less favourable thermodynamically than hydrocarbons, it was important that the HAS catalyst be very selective towards the desired products.

From the review, it was shown that an oxygenated C_1 species could be an important intermediate of the reaction mechanism of HAS. It has been established that the C-C bond formation proceeds by Aldol condensation with ORR in the Cs/Cu/Zn/Cr and K/Zn/Cr catalysts. Classical Aldol condensation is one of the alcohol chain-growth steps in the K/Zn/Cr catalysts. The above condensations result in both chain growth and chain-branching. The C_1 addition according to Fox et al. [1984] was suggested as another possible way chain elongation proceeds.

The reaction kinetics section has highlighted the importance of the formation of C_2 oxygenates in the case of the catalysts considered. Increasing the rate of this step is vital to the success of the process. The reaction schemes considered so far indicate that the mechanisms differ with different catalysts. But, catalysts with certain similar functions activate similar reaction-growth steps. The different Aldol condensations which are catalyzed by the basic function of the catalyst fall in this category. For successful optimization the new HAS catalysts reaction mechanisms should be determined. Again, it is important to determine a kinetic model for HAS in a new catalyst formulation as relevant information is learnt from such models. The HAS reaction kinetic model of Fozatti et al. [1991] for their Cs/Zn/Cr catalyst, highlighted the importance of ketonization and Aldol-type condensations in the reaction scheme.

1.5 AIMS AND SCOPE OF THE PROJECT

The aims and objectives of the project were as follows:

1) To study the effect of alkali salt doping on:

(i) The catalytic properties of the Cu/Zn/Cr catalyst using HAS as the test reaction. This entailed:

- Investigating the influence of GHSV and alkali doping on the activity of the catalysts
- Studying the effect of GHSV on the selectivity of these catalysts
- Determining alkali metal dopants that showed the highest selectivity towards HA, especially isobutanol, the lowest methanol/HA ratio and the lowest methanol / isobutanol ratio.

- Determining the optimal doping quantity of the best performing alkali dopant.

(ii) The physico-chemical properties of the said catalyst.

2) To characterize the catalyst by:

- identifying suitable features for optimal catalytic activity and the preparation parameters that influence them or
- alternatively identifying any features that need to be optimized and suggesting suitable ways in which they could be achieved.

The study was limited to a basic Cu/Zn/Cr catalyst which is 38% in Cu, 38% in Zn and 24% in Cr, prepared by the CSIR continuous co-precipitation technique.

1.6. REFERENCES

Anderson, R.B., The Thermodynamics of the Hydrogenation of Carbon Monoxide and Related Reactions. In: Catalysis, Emmett, P.H., Ed., Vol. 4, Chapter 1, pp 1-27, Reinhold, New York, **1956**.

Anderson, R.B., Thermodynamics of the Hydrogenation of Oxides of Carbon. J. Phys. Chem, **1986**, 90, 4806-4810.

Boz, I., Chadwick, D., Metcalfe, I.S. and Zheng, K., Potassium Promotion of Cu-ZnO-Al_2O_3 Catalysts for High Alcohol Synthesis. Proc. 10th Int. Congr. Catal., **1992**, 2785.

Di Conca, M., Riva, A., Trifiro, F., and Vaccari, A., The Zinc-Chromium Oxide Potassium Promoted Catalysts for Methanol and High Alcohol Synthesis. Proc. 8th Int. Congr. Catal., **1984**, II-173.

Forzatti, P., Tronconi, E. and Pasquon, I., Higher Alcohol Synthesis. Catal.Rev.-Sci.Eng., **1991**, 33 (1&2), 109-168.

Fox, J.R., Pesa, F.A. and Curatolo, B.S., Formation of Higher Alcohols from Methanol in the Presence of Metal Acetylides. J. Catal., **1984**, 90, 127-138.

Herman, R.G., Klier, K., Simmons, G.W., Finn, B.P., Bulko J.B. and Kobylinski, T.P., Catalytic Synthesis of Methanol from CO/H_2. I. Phases Composition, Electronic Properties, and Activities of the $Cu/ZnO/M_2O_3$ Catalysts. J. Catal., **1979**, 56, 407-429.

Hindermann, J.P., Hutchings, G.J. and Kiennemann, A., Mechanistic Aspects of the Formation of Hydrocarbons and Alcohols from CO Hydrogenation. Catal . Rev.- Sci. Eng., **1993**, 35(1), 1-127.

Jackson, N.B. and Ekerdt, J.G., Isotope Studies of the Effect of Acid Sites on the Reactions of C_3 Intermediates during Isosynthesis over Zirconium Dioxide. J. Catal, **1990**, 126, 46-56.

Jones, J.R., Ludlo, W.I., Miller, K.D. and Acosta, T.A., MTBE - A Practical Private Sector Route to Clean Fuels. Published discussion paper No. 89e in the Annual Meeting of the American Institute of Chemical Engineers, November **1989**.

Keim, W. and Falter, W., Isobutanol from Synthesis Gas. Catal. Lett., **1989**, 3, 59-64.

Kiennemann, A., Boujanna, S., Diagne, C. and Chaumette, P., Development of New Catalyst Formulations for Higher Alcohols Synthesis. Characterization, Reactivity, Mechanistic Studies and Predictive Correlations. Proc. 10th Int. Congr. Catal., **1992**, 1479.

Klier, K., Methanol Synthesis. Adv. Catal., **1982**, 31, 243-313.

Klier, K., Herman, R.G., Simmons, G.W., Nunan, J.G., Bogdan, C.E. and Himelfarb, P.B., Direct Synthesis of 2-methyl-1-propanol / Methanol Fuels and Feedstocks. Final Technical Report, DOE # DE-AC22-84PC70021. **1988a.**

Klier, K., Herman, R.G., Nunan, J.G., Smith, K.J., Bogdan, C.E., Young, C.-W. and Santiesteban, J.G., Mechanism of Methanol and Higher Oxygenate Synthesis. In: Methane Conversion, Bibby, D.M., Chang, C.D., Howe, R.F. and Yurchak, S., Eds., 109, Elsievier, Amsterdam, **1988b.**

Klier, K., Herman, R.G. and Vedage, G., (Lehigh University) U.S 4,843,101 **(1989)**

Klier, K., Herman, R.G., Bastian, R.D., DeTavernier, S., Johansson, M., Kieke, M. and Feeley, O.C., High Octane Ethers From Synthesis-Gas-Derived Alcohols. DOE Indirect Liquefaction Contractors' Review Meeting, Pittsburgh, September **1991**.

Klier, K., Preparation of Bifunctional Catalysts. Catal. Today, **1992a**, 15, 361-382.

Klier, K., Herman, R.G., Himelfarb, P.B., Young, C.-W., Hou, S., and Marcos, J.A., C-C Bond Formation via β-Addition with Oxygen Retention Reversal in Oxygenate Synthesis. Proc. 10th Int. Congr. Catal. **1992b**, 1441.

Lietti, L., Botta, D., Forzatti, P., Mantica, E., Tronconi, E. and Pasquon, I., Synthesis of Alcohols from Carbon Oxides and Hydrogen VIII. A Temperature-Programmed Reaction Study of n-Butanal on a Zn-Cr-O Catalyst. J. Catal., **1988**, 111, 360-373.

Lietti, L., Tronconi, E. and Forzatti, P., Identifying the Reaction Network of the Higher Alcohol Synthesis over Alkali-Promoted ZnCrO Catalysts. Proc. 10th Int. Congr. Catal., **1992**, 2765.

Mawson, S., McCutchen, M.S., Lim, P.K. and Roberts, G.W., Thermodynamics of Higher Alcohol Synthesis. Energy and Fuels, **1993**, 7, 257-267.

Mehta, S., Simmons, G.W., Klier, K. and Herman, R.G., Catalytic Synthesis of Methanol from CO/H_2. II. Electron Microscopy (TEM, STEM, Microdiffraction, and Energy Dispersive Analysis) of the $Cu/ZnO/Cr_2O_3$ Catalysts. J. Catal., **1979**, 57, 339-360.

Mross, W. -D., Alkali Doping in Heterogeneous Catalysis. Catal.Rev.-Sci.Eng., **1983**, 25(4), 591-637.

Natta, G., Colombo, U., and Pasquon, I., Higher Alcohols. In: Catalysis, Emmett, P.H., Ed., Vol. 5, Chapter 3, pp 131-174, Reinhold, New York, **1957**.

Nunan, J.G., Bogdan, C.E., Herman, R.G. and Klier, K., Efficient Carbon-Carbon Bond Formation in Ethanol Homologation by CO/H_2 with Specific C_1 Oxygen - Retention over Cs/Cu/ ZnO Catalysts. Catal. Lett., **1989**, 2, 49-56.

Ponec, V., Active Centres for Synthesis Gas Reactions. Catal. Today, **1992**, 12, 227-254.

Richardson, J.T., Catalyst Preparation: How they are Made. In: Principles of Catalyst Development, Chapter 6, pp 95-134, Plenum Press, New York, **1989**.

Roberts, G.W., Lim, P.K., McCutchen, M.S. and Mawson, S., The Thermodynamics of Higher Alcohol Synthesis. DOE Indirect Liquefaction

Contractors' Review Meeting, Pittsburgh, September **1991**.

Seddon, D., Reformulated Gasoline, Opportunities for New Catalyst Technology. Catal. Today, **1992**, 15, 1-21.

Slaa, J.C., van Ommen, J.G. and Ross, J.R.H., The Synthesis of Higher Alcohols using Modified $Cu/ZnO/Al_2O_3$ Catalysts. Catal. Today, **1992**, 15, 129-148.

Smith, K.J. and Anderson, R.B., The High Alcohol Synthesis Over Promoted Copper/Zinc Oxide Catalysts. Can. J. Chem. Eng., **1983**, 61, 40-45.

Smith, K.J. and Anderson, R.B., A Chain Growth Scheme for the Higher Alcohols Synthesis. J. Catal., **1984**, 85, 428-436.

Smith, K.J., Young, C.-W., Herman, R.G. and Klier, K., Development of a Kinetic Model for Alcohol Synthesis over a Cesium-Promoted Cu/ZnO Catalyst. Ind. Eng. Chem. Res. **1991**, 30, 61-71.

Sofianos, A., Production of Branched-Chain Hydrocarbons via Isosynthesis. Catal. Today, **1992**, 15, 149-175.

Stiles, A.B., Chen, F., Harryson, J.B., Xiaodong, Hu., Storm, D.A., and Yang, H.X., Catalytic Conversion of Synthesis Gas to Methanol and Other Oxygenated Products. Ind. Eng. Chem. Res., **1991**, 30, 811-821.

Tronconi, E., Lietti, L., Forzatti, P. and Pasquon, I., Higher Alcohol Synthesis over Alkali-Promoted Higher-Temperature Methanol Catalysts. Appl. Catal., **1989**, 47, 317-333.

Tronconi, E., Forzatti, P. and Pasquon, I., An Investigation of the Thermodynamic Constraints in Higher Alcohol Synthesis over Cs-Promoted

ZnCr-Oxide Catalyst. J. Catal., **1990**, 124, 376-390.

Tronconi, E., Lietti, L., Groppi, G., Forzatti, P. and Pasquon, I., Mechanistic Kinetic Treatment of the Chain Growth Process in Higher Alcohol Synthesis over a Cs-Promoted Zn-Cr-O Catalyst. J. Catal., **1992**, 135, 99-114.

Ueda, W., Ohshida, T., Kuwabara, T. and Morikawa, Y., Condensation of Alcohol over Solid-Base Catalyst to Form Higher Alcohols. Catal. Lett., **1992**, 12, 97-104.

Vedage, G.A., Himelfarb, P., Simmons, G.W. and Klier, K., Alkali Promoted Cu/ZnO Catalysts for Low Alcohol Synthesis. Symposium on the Role of Solid State Chemistry in Catalysis, presented before the Division of Petroleum Chemistry, American Chemical Society, Washington, **1983**.

Vedage, G.A., Himelfarb, P., Simmons, G.W. and Klier, K., Alkali-Promoted Copper-Zinc Oxide Catalysts for Low Alcohol Synthesis. ACS Symp. Ser., **1985**, 279, 295-312.

Xiaodong, Hu., Scientific Basis for Design of Heterogeneous Catalysts . A Study of Alcohol Synthesis Catalysts. PhD Thesis, Department of Chemical Engineering, University of Delaware, Delaware, USA, **1989**.

Xiaoding, Xu., Doesburg, E.B.M. and Scholten, J.J.F., Synthesis of Higher Alcohols from Syngas. Recently Patented Catalysts and Tentative Ideas on the Mechanism. Catal. Today, **1987**, 2, 125-170.

2: STUDY OF THE EFFECT OF ALKALI METAL DOPING ON THE CATALYTIC PROPERTIES OF Cu/Zn/Cr CATALYST USING HAS AS THE TEST REACTION

2.1 INTRODUCTION

As described in Chapter 1 it has been established that alkali doping of methanol synthesis catalysts changes their overall activity and shifts their selectivity towards the synthesis of other oxygenates. Studies by Vedage et al. [1983], in which a binary Cu/Zn catalyst was impregnated with hydroxides of different alkali metals, demonstrated several important effects. Firstly, methanol activity decreased for both Li- and Na-doped catalyst batches while it increased for K-, Rb- and Cs-doped catalyst batches. Secondly, it was established that selectivity towards higher alcohols (C_2-C_4) and esters increased, an observation which has been confirmed by other authors [Tronconi et al.1992]. In his review, Mross [1983] stated that for Cu-based catalysts, catalytic activity decreased with an increase in the amount of alkali dopant.

It was shown by Boz and co-workers [1992] that potassium doping of a $Cu/ZnO/Al_2O_3$ catalyst reduces the selectivity towards hydrocarbons at low potassium loading. The same alkali metal reduces the CO hydrogenation activity of the zinc-chromium oxide catalyst tested by Di Conca et al. [1984]. Li and Na doping result in the decline of catalytic activity of the zinc-chromia catalyst whereas Rb and Cs do not [Mross 1983].

The promotion effect towards higher alcohols has been found to increase in the order:

$$Li < Na < K < Rb < Cs$$

in an H_2/CO stream for both the Cu/ZnO and the zinc-chromia catalysts [Vedage 1983]. Xiaodong [1989] investigated the effect of alkali doping by the individual alkali metals on a Cu/Zn/Mn/Co/Cr catalyst. He found that the selectivity

towards higher alcohols in his catalyst decreased in the order:

K > Rb > Cs > unpromoted catalyst.

TABLE 2.1

The effect of the weight per cent of alkali metal salts on HAS selectivity on a Cu/ZnO catalyst (from Smith and Anderson (1983)). Reaction conditions: Pressure = 13.2 MPa, Temperature = 285 °C.

Wt. % K_2CO_3	0.0	0.5	1.0	2.0	3.0	10.0
GHSV (h^{-1})	4300	3300	3800	4300	4600	2900
H_2:CO in feed	0.44	0.47	0.52	0.49	0.48	0.44
Alcohol selectivity %						
methanol	65.8	48.6	61.4	75.7	82.4	81.8
ethanol	6.4	4.8	4.8	3.7	2.6	1.6
2-propanol	1.7	0.8	1.8	1.4	1.4	0.3
1-propanol	5.3	6.7	9.2	8.1	7.0	5.2
1-butanol	2.1	4.0	2.5	1.3	1.1	2.2
2-butanol	0.8	1.5	1.7	1.0	1.3	0.9
2-Methyl-1-propanol	10.1	18.8	13.8	7.1	3.8	4.6
pentanols	8.0	14.8	4.8	1.2	0.5	3.4
consumption:						
H2 [$mmol.g^{-1}.h^{-1}$]	50.5	58.5	68.5	41.5	54.3	16.0
CO [$mmol.m^{-1}.h^{-1}$]	1.19	1.61	1.76	1.18	1.66	0.89

It appears that the promotion effect of individual alkali metals may depend on the

nature of the catalyst. For every individual alkali metal, the promoting effect varies with the quantity of the metal dopant present. In Table 2.1 above, the variation of the higher alcohol selectivity over the Cu/ZnO catalyst with percentage weight of the K_2CO_3 dopant is shown. Higher alcohol selectivity varies with the level of alkali doping. With the exception of ethanol, the selectivity of each higher alcohol goes through a maximum with increasing quantity of alkali doping. For propanols, butanols and pentanols, the maxima lie between 0.5 and 1.0 %. It appears that for an optimal HAS system, there is a limit to the amount of alkali metal that can be added to the catalyst. Klier et al. [1988] reported an optimum HAS selectivity at about 3 mass-% Cs loading on their ternary $Cu/ZnO/Cr_2O_3$ catalyst, whereas in the case of Smith and Anderson [1983] a loading of 0.4 wt % K_2CO_3 was used.

It appears that the promotion effect of alkali doping of methanol synthesis catalysts towards higher alcohols could be different for different catalyst formulations. Therefore, the subject has to be studied (experimentally) for every new catalyst formulation designed.

In this chapter extensive reporting on catalyst preparation, testing and data analysis for HAS is documented. The effect of alkali doping on the performance of our Cu/Zn/Cr catalyst was studied using HAS as the test reaction. The effect of changing gas hourly space velocity (GHSV) on catalyst productivities was investigated. This was done for two reasons. Firstly, there was a need to have a crude idea of suitable GHSVs for the catalyst. Secondly, it was desirable to experiment at low GHSV in order to save on the costs of the gas. This means one had to know whether results at low GHSV would be a valid reflection of the effect of alkali doping on this methanol synthesis catalyst or not. As an optimization step, the optimal quantities of the highest performing alkali metal dopants were determined.

2.2. EXPERIMENTAL

2.2.1. CATALYST PREPARATION

2.2.1.1. Co-precipitation

The catalyst was prepared by continuous co-precipitation of 1M nitrate solutions of copper, zinc and chromium with sodium carbonate at constant pH. The precipitate was filtered, washed and dried at 80 °C. The material was then calcined at 350 °C for three hours, after which it was ready for methanol synthesis. The catalyst precursor was a homogeneous and highly crystalline hydroxycarbonate of the hydrotalcite type with the following general chemical formula:

$$(Me^{II})_6(Me^{III})_2(OH)_{16}.CO_3.4H_2O$$

The process variables of co-precipitation were strictly controlled as they influence the extent of crystallization in the catalyst precursor. The precipitation was effected under the preferred conditions of supersaturation. The chemical composition of the nitrates was 38% Cu, 38% Zn and 24% Cr. That catalyst batch was named ISO 63. Analytical-grade chemicals from Merck were used in all preparations.

2.2.1.2 Impregnation

The alkali metal doping of ISO 63 was achieved by using a formate salt of the metal in question. A bicarbonate or carbonate solution of the alkali metal was neutralized with sufficient formic acid to form the required salt according to either reaction (2.1) or (2.2) below:

$$2HCOOH + M_2CO_3 \longrightarrow 2HCOOM + H_2O + CO_2 \quad (2.1)$$

$$HCOOH + M'HCO_3 \longrightarrow HCOOM' + H_2O + CO_2 \quad (2.2)$$

where M = Li, Na, K and M' = Cs.

In the case of rubidium formate, a ready-made salt from Sigma was used. The cesium bicarbonate used in the preparation of the formate salt was also obtained from Sigma. The carbonates of both Li and K were obtained from Merck Chemicals while sodium formate was prepared using BDH AnalaR sodium carbonate.

For alkali metal doping, the incipient wetness method was employed. The procedure involved two basic steps, i.e. preparation of the formate salt and impregnation of the different catalyst batches. A known quantity of alkali metal carbonate / bicarbonate was dissolved in water, sufficient to completely wet a specified mass of the catalyst. The dissolved carbonate / bicarbonate was reacted with formic acid as explained above to form a formate salt. The solution was added to the catalyst, which had initially been pressed at a pressure of 3 tonnes / 7" dia. ram., and then ground to granules of diameters varying between 300 and 500 μm. The catalyst was then ready to be dried and calcined.

Air-drying of the catalyst was carried out in a fume cupboard over a period of 24 h. Further drying, when necessary, was effected in a conventional oven at 110 °C. The catalyst was calcined under N_2 gas flowing at 200 ml/min. It was heated to 350 °C, using a temperature programme, at a rate of 1.5°C per minute and then held at that temperature for 1h. At the end of that period, it was allowed to cool down rapidly to room temperature under flowing N_2 gas.

2.2.2 CATALYST TESTING

The testing of the catalyst under conditions of the HA synthesis was carried out in a high-temperature, high-pressure experimental rig, shown in Figure 2.1. Three

distinct components of the rig can be distinguished, i.e. the gas and liquid flow-control systems, the reactors and the condensers.

- **The flow-control system:** The tubing material for the liquids and all the gases, i.e. H_2, N_2, and the CO/H_2 synthesis gas mixture, was stainless steel. Swagelok and Cajon fittings and Nupro valves were used at the connection and flow-control points, respectively. The gas flow rates were controlled by mass-flow controllers from Brooks Instruments B.V. To avoid condensation of reaction products in the tubing, the lines from the reactors to the back-pressure regulator (BPR) were heated to 145 °C and from the BPR to the gas chromatograph to 200 °C . The temperatures were controlled by RKC controllers. It was envisaged that a liquid-feed system, which consisted of a liquid reservoir and a pump, would be used at an advanced stage of the work.

- **The microreactor:** A diagram of the fixed-bed microreactor used is shown in Figure 2.2. It was made of stainless steel type 316. Running through the centre of the reactor was a narrow casing for a thermocouple. The reactor was designed to withstand temperatures and pressures of up to 450 °C and 12 500 kPa respectively. A bench-scale reactor was meant for research on scaling-up tests.

- **The solid-liquid separation (condenser section):** The hot condenser (M) was designed to trap any waxy product from the reactor which could block the tubing of the gas chromatograph downstream. A cold trap, whose coolant was ethanol, was used occasionally to collect a liquid sample for the purpose of identifying the product mixture on the GC-MS. The lowest temperature at which the cooling system was capable of operating was -25 °C.

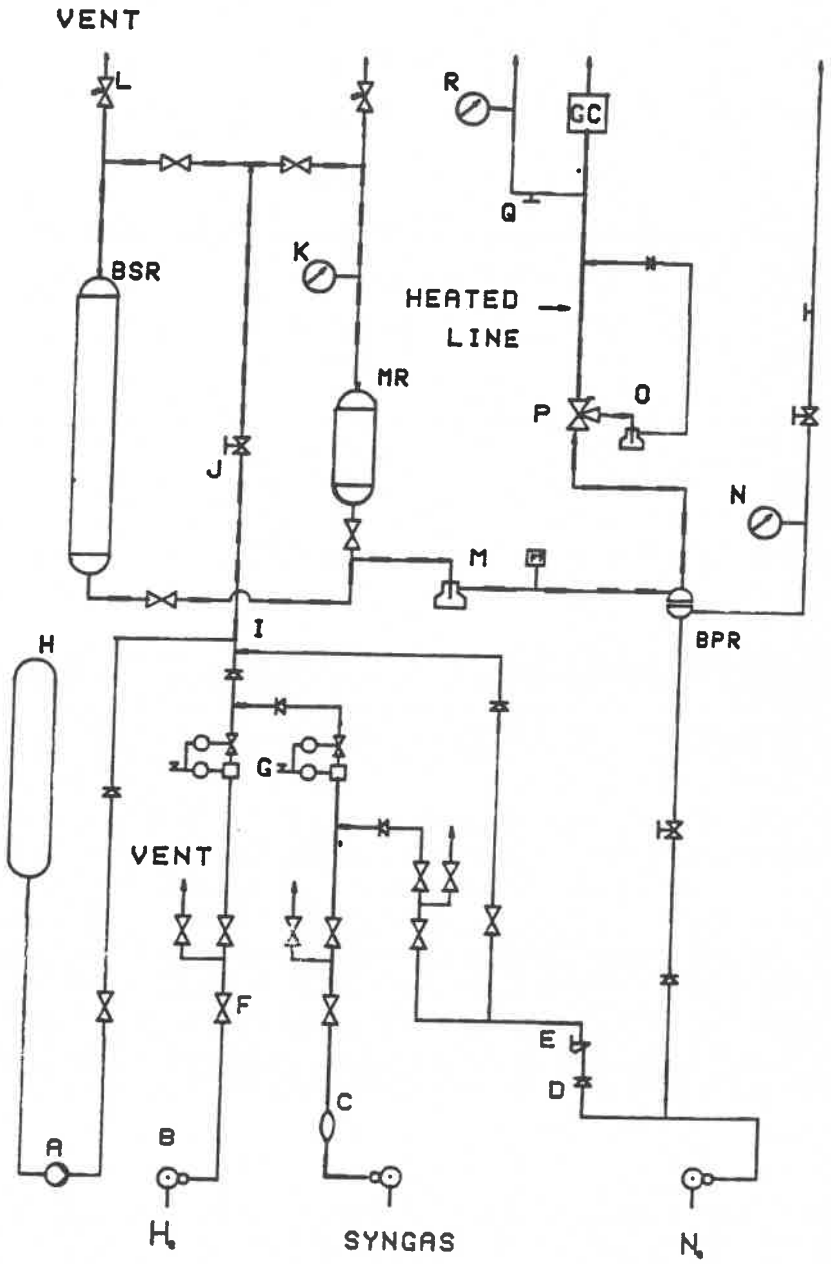

Figure 2.1: The catalyst-testing unit in which the different parts have been labelled thus: (A) pump for liquids; (B) gas regulator; (C) filter; (D) one-way valve; (E) Bellows metering valve; (F) solenoid valve; (G) mass-flow controller; (H) liquid reservoir; (I) preheater; (J) manually operated needle valve; (K) pressure gauge; (L) pressure-relief valve; (M) hot condenser; (N) pressure gauge; (O) cold condenser; (P) ball and plug valve (3-way); (Q) metering valve; (R) wet gas flowmeter; (BSR) bench-scale reactor; (BPR) back-pressure regulator; (GC) gas chromatograph; (PT) pressure transducer; (MR) microreactor.

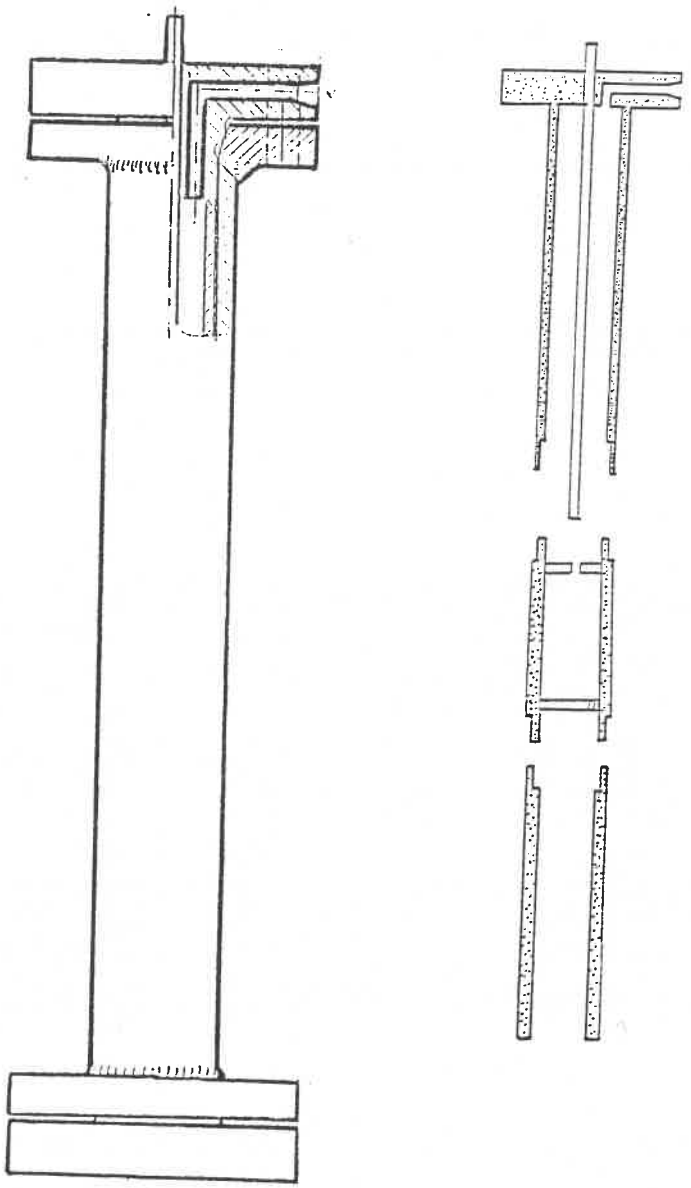

(a) (b)

Figure 2.2. **The microreactor system which shows the reactor metal casing (a) and the three distinct componets of the reactor (b).**

2.2.2.1 Activation of the catalyst

A modified ICI method of activation for methanol synthesis catalysts was used

to activate the catalysts. In order to avoid hot spots in the catalyst bed, 4g of quartz (with the same particle size as the catalyst) was added to each 1g of the catalyst and the mixture was loaded into the reactor. Nitrogen gas was allowed to pass through the reactor at a flow rate of 300 ml/min. After one hour, heating of the reactor using a temperature programme, was initiated. The heater was programmed to increase the temperature of the reactor to 130 °C over a period of two hours. The reactor temperature was then increased to 200 °C over a period of three-and-a-half hours at 8 bars reactor pressure. At the same time the gas flow was changed to 300 ml/min of 2 % hydrogen gas in argon. The reactor was held under these conditions overnight. Reactor temperature was then increased to 240 °C over a period of one hour at a flow rate of 300 ml/min of 12 % H_2 gas in N_2 gas. At this stage the catalyst was ready for HAS testing conditions.

The reactor was set to the required HAS testing conditions. The reactor temperature and pressure were set to increase to 325 °C (in 3 h) and 100 bars, respectively. The pressurizing of the reactor and the testing of the catalyst were effected using synthesis gas of composition 47 % CO, 47 % H_2, 5 % Ar and 1 % CO_2 at a suitable gas hourly space velocity (GHSV) in the range 4 000 to 8 000 ml/g_{cat}/h. When the desired conditions were attained a suitable induction period (usually 24h) was allowed for, before samples were taken from the product stream.

2.2.2.2 Identification of reaction products

The products of the reaction were separated using an on-line Varian 3400 gas chromatograph (GC). The GC was equipped with a capillary column connected to a flame ionization detector (FID) and a packed carbosieve column with a thermal conductivity detector (TCD). The capillary column, which was 60 m long and had an internal diameter of 0.32 mm, was coated with SPB-1 bonded phase with a thickness of 1.0 micron. The capillary column was used to separate all

reaction products except Ar, CO and CO_2. These gases were separated on a steel packed column which was 3.225m long, had an internal diameter of 2.2 mm and was packed with carbosieve of mesh range 60/80. The GC was equipped with two Valco valves which simultaneously injected known and reproducible amounts of samples into the two columns. Its operating conditions are summarized in Table 2.2 below.

TABLE 2.2.

Operating conditions of the gas chromatograph

Column	Carrier Gas Inlet pressure (psi)	Temperature Programme
capillary	14	53°C for 8 min, 8°C/min to 200°C, held for 50 min.
packed	20	same as above

Notes: (1) In both columns helium was the carrier gas.

(2) Injector temperature = 150 °C

Detector temperature = 220 °C

The data from the chromatograph were collected and analyzed by a 2600 Series Chromatography Data System from Nelson Analytical, Inc. The system, which was based on the IBM family of personal computers (and compatibles), had two channels for sampling data from both the TCD and the FID. Joining the computer, through an interface card, and the gas chromatograph was a Nelson

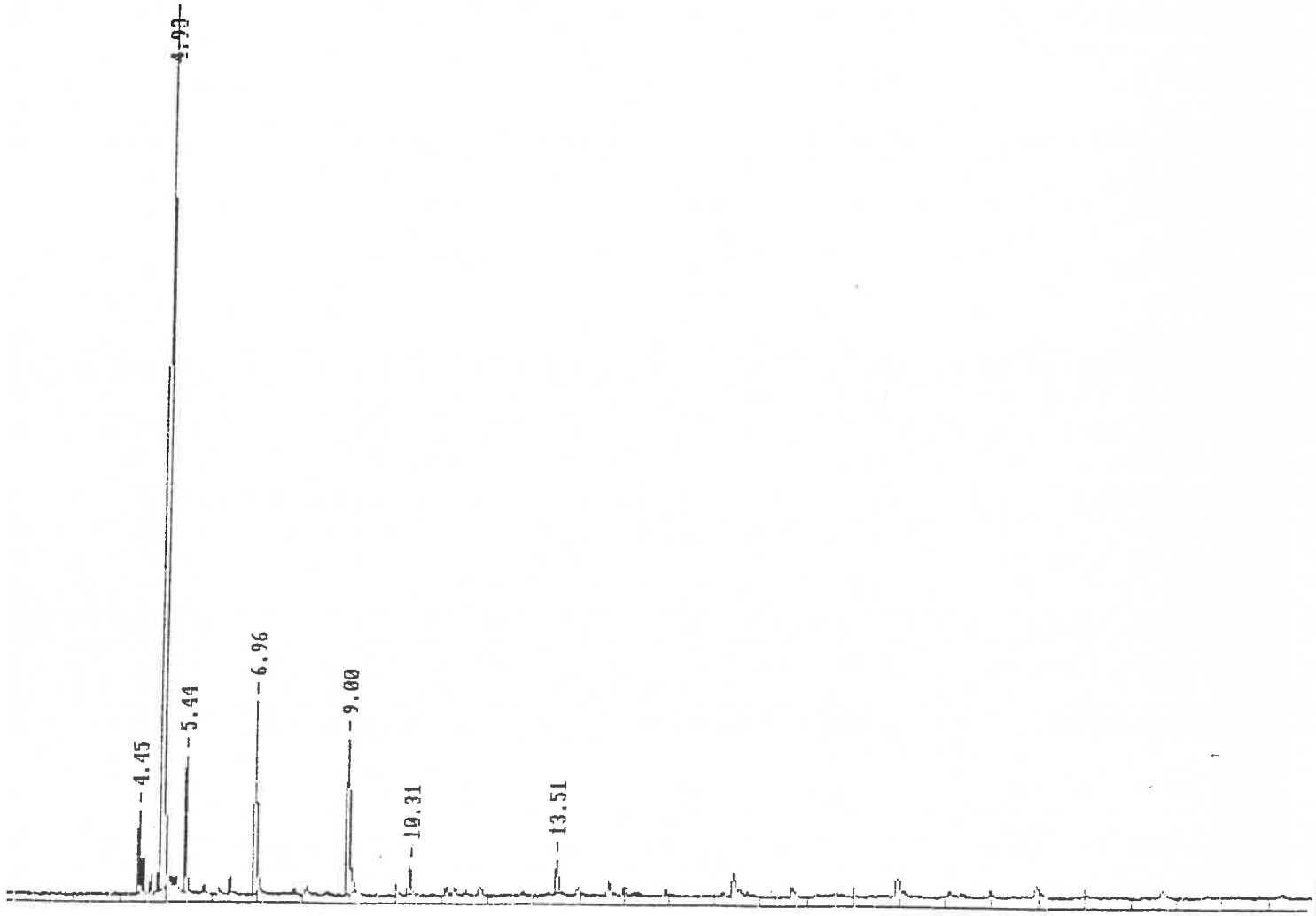

Figure 2.3. A chromatogram showing the separation of reaction products by the capillary column where the following retention times correspond to the compounds identified: (4.45) methane, (4.93) methanol, (5.44) ethanol (6.96) 1-propanol, (9) isobutanol, (10.31) 1-butanol and (13.51) 2-Methyl-1-Butanol.

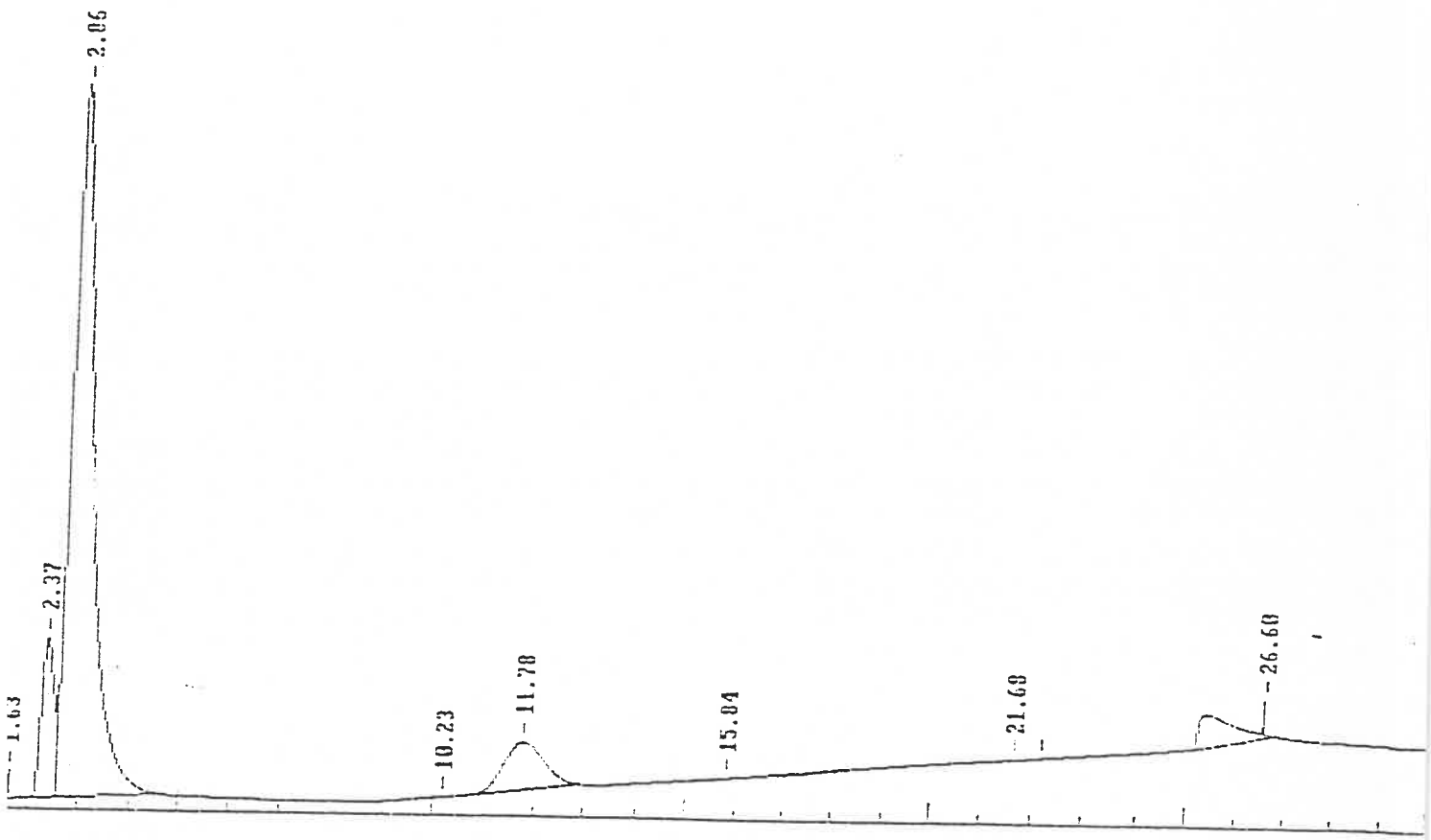

Figure 2.4. A chromatogram obtained via a packed column-TCD set-up where the retention times correspond to the compounds shown: (2.37) argon, (2.86) CO, (11.78) CO_2 and (26.00) methanol.

760 Series Interface. Once initiated, the chromatograph was programmed to take samples automatically every one-and-a-half hours until it was manually stopped. The chromatograms in Figures 2.3 and 2.4 show the quality of separation that could be achieved from both the capillary and the packed columns, respectively. Products were identified by matching retention times of unknown compounds to those of pure known substances and by GC-MS.

2.3 DATA ANALYSIS

The quantities of the different compounds were calculated using the following relationship:

Amount (μmoles) = Response Factor (μmoles/area) X Area

where **Area** was defined as the area of a peak corresponding to the compound in question and the **Response Factor** was obtained by calibration. The calibration procedure involved injecting known quantities of the compounds in question into the column and determining the peak areas represented by that compound. This procedure was repeated several times in order to improve accuracy of the response factor. In this analysis the main focus was on the total carbon oxides conversion, selectivities and yields of both methanol and HA (including isobutanol) and on the space time yields (STY) of all products. These parameters are defined below.

Analysis of the reaction products is achieved by concentrating on all the reactions the carbon atoms undergo. In a catalytic reaction where hydrogen, carbon dioxide (CO_2) and carbon monoxide (CO) react to form known concentrations of methane, ethane, ethene, propane, propene, methanol (MeOH), unreacted CO_2 and CO, etc., the following parameters were defined thus:

- **Conversion of carbon oxides:**

$$\text{Conversion [\%]} = \frac{\{[CH_4] + 2[C_2 + C_{2=}] + 3[C_3 + C_{3=}] + [MeOH] + .\} * 100}{\{[CH_4] + 2[C_2 + C_{2=}] + 3[C_3 + C_{3=}] + [MeOH] + ..[CO] + [CO_2]\}}$$

- **Methanol yield:**

$$\text{Yield [\%]} = \frac{[MeOH] * 100}{\{[CH_4] + 2[C_2 + C_{2=}] + 3[C_3 + C_{3=}] + [MeOH] + ..[CO] + [CO_2]\}}$$

- **Methanol selectivity:**

$$\text{Selectivity [\%]} = \frac{[MeOH] * 100}{\{[CH_4] + 2[C_2 + C_{2=}] + 3[C_3 + C_{3=}] + [MeOH] + ..\}}$$

- **Methanol space-time-yield:**

$$\text{Space-Time-Yield [\%]} = \text{Yield} * \{\text{molar GHSV}\} * M_{MeOH} * 10^{-5} = \ldots \text{kg/kg/h}$$

where M_{MeOH} was the molecular mass of methanol and 10^{-5} was the conversion factor used to convert the answer to $kg/kg_{cat}/h$ units. Similar formulae applied to calculations concerning other reaction products. An in-house computer program was developed to execute these calculations.

The above parameters could also be calculated using the internal standard method. In such a case argon gas of known concentration [Ar] was added to the feed stream and in the calculations that followed, the concentrations of all other substances were taken relative to that of argon. This method was employed to calculate the conversion which was defined as:

$$\text{CONVERSION [\%]} = \frac{\{[CO]^0 + [CO_2]^0\}/[Ar] - \{[CO]^1 + [CO_2]^1\}/[Ar] \ * \ 100}{\{[CO]^0 + [CO_2]^0\}/[Ar]}$$

where $[CO]^0$ was the concentration of carbon monoxide in the feed stream and $[CO]^1$ was its concentration in the product stream. The same notation was applied to CO_2 as well. This is the conversion that is used in all the results analyzed in this report and it is referred to as the "total conversion".

2.4. RESULTS

TABLE 2.3.

STY for an undoped Cu /Zn / Cr catalyst operating at T = 325 °C, P = 10.0 MPa, H_2/CO = 1 and GHSV = 4 000 ml / g cat. / h.

COMPOUND	STY [g /Kg $_{cat.}$ / h]
	20.60
Alkanes	12.91
Methane	11.70
Ethane	9.74
Propane	3.62
n-Butane	1.21
n-Pentane	2.85
n-Hexane	
n-Heptane	421.24
	258.88
	4.52
	11.60
Primary Alcohols	13.10
Methanol	3.29
Ethanol	
1-Propanol	
1-Butanol	32.04
	9.29
Branched Alcohols	6.76
2-Methyl-1-Propanol	2.15
2-Methyl-1-Butanol	
2-Methyl-1-Pentanol	
2-Methyl-1-Hexanol	
Carbon Dioxide	
Ethers	
DME	

TABLE 2.4a

The STY of products formed by the Cu/Zn/Cr catalyst impregnated with $2.26*10^{-4}$ moles/$g_{cat.}$ of CsOOCH at GHSV = 4 000 - 8 000ml/$g_{cat.}$/h, T = 325 °C, P = 10.0 MPa and H_2 / CO = 1.

PRODUCTS		STY (g/kg_{cat}/h) at GHSV		
		4 000	6 000	8 000
Alkanes				
	Methane	19.15	20.98	10.27
	Ethane	3.23	3.98	-
	Propane	2.23	2.35	-
Straight-chain alcohols				
	Methanol	264.64	441.58	651.4
	Ethanol	12.76	22.21	26.03
	1-Propanol	28.58	42.34	36.07
	1-Butanol	4.88	6.90	5.43
Branched alcohols				
	2-Methyl-1-Propanol	46.89	53.34	25.79
	2-Methyl-1-Butanol	8.73	11.51	-
	2-Methyl-1-Pentanol	4.87	6.58	-
	2-Methyl-1-Hexanol	2.19	2.17	-
Carbon dioxide		422.75	586.38	504.0
Ethers				
	DME	4.10	4.61	-
MeOH / HA		2	3	7
MeOH / isobutanol		6	8	25

TABLE 2.4b

The STY of products formed by the Cu/Zn/Cr catalyst impregnated with $2.26*10^{-4}$ moles/$g_{cat.}$ of RbOOCH at GHSV = 4 000 - 8 000ml/$g_{cat.}$/h, T = 325 °C, P = 10.0 MPa and H_2 / CO = 1.

PRODUCTS		STY (g/kg_{cat}/h) at GHSV		
		4 000	6 000	8 000
Alkanes				
	Methane	10.25	10.89	11.42
	Ethane	1.57	-	-
	Propane	1.60	-	-
Straight-chain alcohols				
	Methanol	320.78	480.17	671.43
	Ethanol	14.33	22.75	25.50
	1-Propanol	21.64	31.90	32.54
	1-Butanol	3.78	5.70	5.92
Branched alcohols				
	2-Methyl-1-Propanol	30.90	39.79	38.56
	2-Methyl-1-Butanol	5.79	8.34	8.39
	2-Methyl-1-Pentanol	3.25	-	-
Carbon dioxide		289.06	409.67	474.68
Methanol / HA		4	4	6
Methanol / isobutanol		10	12	17

TABLE 2.4c

The STY of products formed by the Cu/Zn/Cr catalyst impregnated with $2.26*10^{-4}$ moles/$g_{cat.}$ of KOOCH at GHSV = 4 000 - 8 000ml/$g_{cat.}$/h, T = 325 °C, P = 10.0 MPa and H_2 / CO = 1.

PRODUCTS		STY (g/kg_{cat}/h) at GHSV		
		4 000	6 000	8 000
Alkanes				
	Methane	25.12	29.04	42.31
	Ethane	8.14	7.75	11.38
	Propane	5.96	8.75	6.81
	n-Butane	4.66	9.19	3.30
	n-Pentane	3.32	-	-
Straight-chain alcohols				
	Methanol	327.83	519.96	738.81
	Ethanol	13.07	20.97	19.63
	1-Propanol	20.72	31.40	21.54
	1-Butanol	3.54	4.90	-
Branched alcohols				
	2-Methyl-1-Propanol	35.51	47.95	23.00
	2-Methyl-1-Butanol	5.78	7.23	-
	2-Methyl-1-Pentanol	3.39	-	-
Carbon dioxide		406.49	497.37	412.68
Ethers				
	DME	5.63	-	-
Methanol / HA		4	5	12
Methanol / isobutanol		9	11	32

TABLE 2.4d

The STY of products formed by the Cu/Zn/Cr catalyst impregnated with $2.26*10^{-4}$ moles/$g_{cat.}$ of NaOOCH at GHSV = 4 000 - 8 000ml/$g_{cat.}$/h, T = 325 °C, P = 10.0 MPa and H_2 / CO = 1.

PRODUCTS		STY ($g/kg_{cat}/h$) at GHSV		
		4 000	6 000	8 000
Alkanes				
	Methane	21.62	26.56	14.97
	Ethane	7.67	4.97	3.99
	Propane	6.61	4.22	3.92
	n-Butane	3.18	2.75	-
Straight-chain alcohols				
	Methanol	338.26	557.81	722.81
	Ethanol	13.86	16.43	16.29
	1-Propanol	20.51	16.05	13.27
	1-Butanol	4.01	-	-
Branched alcohols				
	2-Methyl-1-Propanol	41.53	15.43	33.46
	2-Methyl-1-Butanol	10.39	-	7.28
	2-Methyl-1-Pentanol	6.16	-	-
	2-Methyl-1-Hexanol	1.60	-	-
Carbon dioxide		307.66	345.71	285.06
Ethers				
	DME	7.80	8.11	9.13
Methanol / HA		3	8	16
Methanol / isobutanol		8	21	48

TABLE 2.4e

The STY of products formed by the Cu/Zn/Cr catalyst impregnated with $2.26*10^{-4}$ moles/$g_{cat.}$ of LiOOCH at GHSV = 4 000 - 8 000ml/$g_{cat.}$/h, T = 325 °C, P = 10.0 MPa and H_2 / CO = 1.

PRODUCTS		STY (g/kg_{cat}/h) at GHSV		
		4 000	6 000	8 000
Alkanes				
	Methane	31.58	30.48	17.14
	Ethane	8.67	9.96	4.14
	Propane	5.62	5.30	-
	n-Butane	3.86	4.10	-
	n-Pentane	1.29	-	-
Straight-chain alcohols				
	Methanol	255.36	389.12	676.90
	Ethanol	9.09	14.60	22.04
	1-Propanol	16.15	24.65	23.53
	1-Butanol	2.75	4.37	-
Branched alcohols				
	2-Methyl-1-Propanol	57.67	76.57	33.46
	2-Methyl-1-Butanol	10.99	15.35	7.28
	2-Methyl-1-Pentanol	6.55	8.55	-
	2-Methyl-1-Hexanol	1.60	2.43	-
Secondary alcohols				
	2-Propanol	2.91	3.23	-
Carbon dioxide		613.14	751.12	404.56
Ethers				
	DME	10.21	9.24	9.93
Methanol / HA		2	3	6
Methanol / isobutanol		4	5	20

TABLE 2.5

The selectivities for various HAS products by the blank ISO 63 catalyst at GHSV = 4 000 - 8 000 ml/$g_{cat.}$/h, T = 325 °C, P = 10.0 MPa and H_2/CO = 1.

PRODUCT	SELECTIVITY (%)
Alkanes	15.49
HA	19.35
Methanol	64.03
Isobutanol	7.93

TABLE 2.6.

The carbon oxide conversion by an undoped and alkali doped Cu/Zn/Cr catalyst at GHSV = 4 000ml/$g_{cat.}$/h, T = 325 °C, P = 10.0 MPa and H_2 / CO = 1.

Catalyst treatment	Conversion (%)
undoped	18.58
Rb	17.33
Cs	17.81
Li	19.39
K	20.00
Na	21.13

TABLE 2.7

The variation of HAS STY with the quantity of Cs impregnated on the catalyst at GHSV = 4 000ml/$g_{cat.}$/h, T = 325 °C, P = 10.0 MPa and H_2 / CO = 1.

Cs Loading	HA STY (g/KG $_{cat.}$/h)
0.00	78.23
1.00	60.44
2.00	49.44
3.00	108.90
4.00	72.39

TABLE 2.8

The variation of STY of isobutanol with the quantity of Li impregnated on the Cu/Zn/Cr catalyst at GHSV = 4 000ml/$g_{cat.}$/h, T = 325 °C, P = 10.0 MPa and H_2 / CO = 1.

Li (moles/$g_{cat.}$) * 10^{-4}	HA STY (g/KG $_{cat.}$/h)
0.000	32.040
0.753	32.820
1.510	30.140
2.260	57.670
3.010	37.630

2.5. DISCUSSION

The space time yields (STY) of products obtained by passing syngas over blank Cu/Zn/Cr catalysts and alkali-doped Cu/Zn/Cr catalysts under similar conditions (T, P and GHSV) are shown in Tables 2.3 and 2.4, respectively. The reaction products of all catalysts impregnated with alkali metal salts consist of alkanes,

straight and branched-chain primary alcohols, secondary alcohols, DME and traces of aldehydes, ketones and esters. Water (although an analysis of its formation was not done) was present in the product stream as a product of the various HAS reactions (see reactions (1.3) to (1.12)). All the above products have already been shown to be thermodynamically stable to varying degrees under HAS conditions [Anderson 1956 and 1986; Natta et al. 1957; Roberts et al. 1991].

The presence of the 2-methyl alcohols as reaction products is an indication of the presence of basic sites which are responsible for the different aldol condensation reactions discussed in section 1.1.4.4. Although the catalyst is dominated by basic centres, it seems that there are few acidic centres which are responsible for DME formation in both the blank and alkali impregnated catalyst batches.

The alcohol product spectrum is dominated by 1-propanol for straight chain HA and isobutanol for 2-methyl branched HA. This shows that the rate constant of 1-propanol formation is high. This could be explained in terms of the reaction routes responsible for its formation. In reaction Mechanisms 1 and 2 it is clear that 1-propanol is formed via two parallel routes (see section 1.3.4). This would comprise C_n condensation with formaldehyde to form C_{n+1} species shown in Mechanism 1 in section 1.3.4. which happens simultaneously with the Aldol-type condensation. Alternatively, the routes could involve the Aldol-type condensation and carbonyl carbon addition route in Mechanism 2 (section 1.1.4.4). The $L+\beta$ rate constants in the Smith-Vedage model and the β_1 rate constant for the formation of C_3 intermediates in the Smith's model [1991] are high.

It is apparent from Tables 2.3 and 2.4 that of all the 2-methyl branched alcohols, isobutanol had the highest STY. It appears that the C_4 oxygenated isobutanol precursor is the terminal species because of its apparent low reactivity. Klier et

al. [1992b] suggested that stereochemical factors were responsible for the lack of reactivity of the isobutanol precursor. Tronconi et al.[1990] established that the ketonization reaction of isobutanol to 2,4-dimethyl-3-pentanone was far from reaching equilibrium. It is noted that traces of ketones could be identified. Ketonization reactions which result in the consumption of ketones in favour of the formation of alcohols [Lietti et al. 1988] might explain the low quantities of the former being detected. The above analysis of the product spectra shows that HAS over these catalysts has features which can be related to both reaction Mechanisms 1 and 2. But, the actual mechanism might be close to Reaction Mechanism 1 because ISO 63 and Smith's catalyst are close in composition.

The carbon oxide conversions involving the undoped Cu/Zn/Cr catalyst and the alkali metal-impregnated Cu/Zn/Cr catalysts are shown in Table 2.6 . The Li-, Na- and K-impregnated catalytic systems exhibit marginally higher carbon oxide conversions than the undoped methanol synthesis catalysts. Conversions of catalyst batches doped with both the Rb and Cs salts decreased slightly as a result of the doping treatment. The increase in overall catalytic activity by impregnation with some alkali metals agrees with work by Klier et al. [1989]. Results of the Li- and Na-doped catalyst batches contradict observations by both Vedage et al. [1983], over their binary Cu / Zn, and Mross' report [1983] on the effect of the above metals on activities and selectivities of the zinc-chrome catalyst. Apart from alkali doping, GHSV has an influence on catalytic conversions and other properties.

Graphs of the variation of carbon oxide conversions for alkali-impregnated Cu/Zn/Cr catalysts with GHSV are shown in Figure 2.5. The conversions are seen to decrease with an increase in the GHSV. This relationship indicates that at higher gas flow rates the residence time of the gas is not long enough for it to react sufficiently. Therefore, for high catalytic activity, lower GHSVs are essential. In the studies of the effect of Cs loading on the selectivity towards HA formation the catalyst batches were tested at low GHSV.

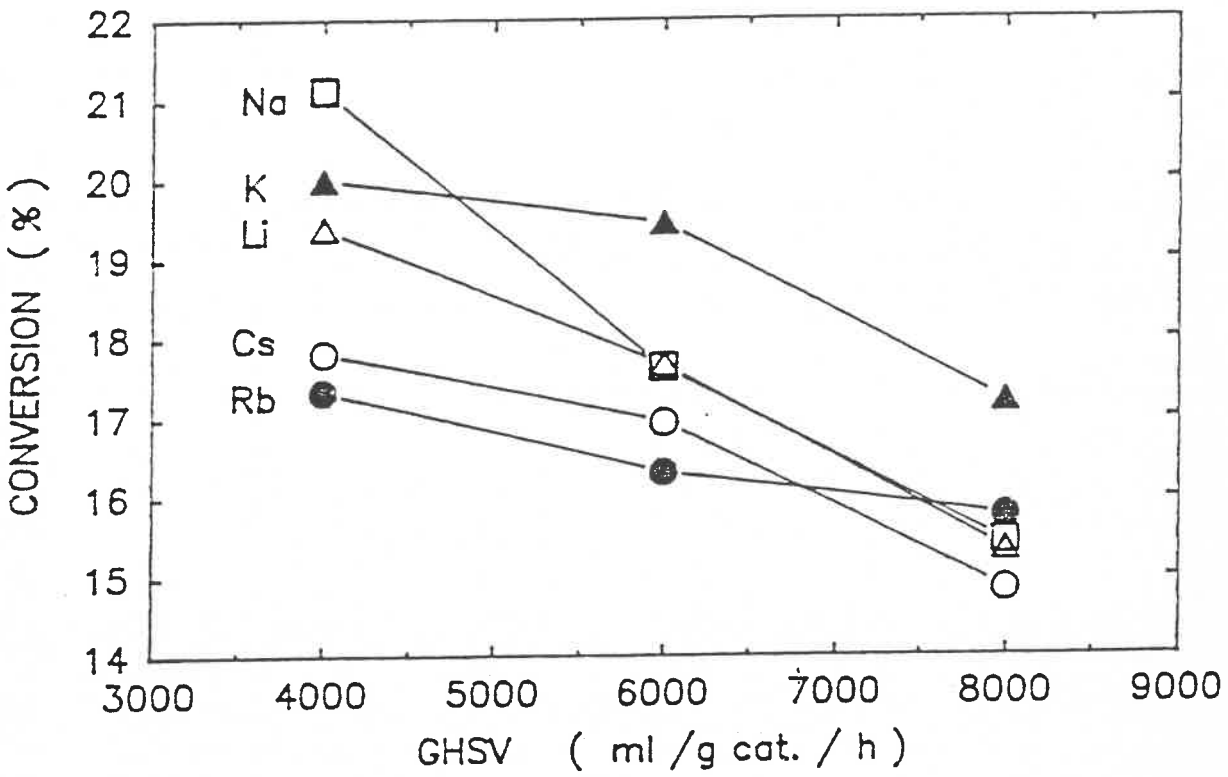

Figure 2.5: The dependence of the carbon oxide conversions on the GHSV of the Cu/Zn/Cr catalysts impregnated with the formates of Cs, Rb, K, Na and Li at T = 325 °C and P = 10 MPa.

The effect of GHSV on alkane selectivity for catalysts impregnated with different alkali metal formates is shown in Figure 2.6. It is apparent that the selectivities towards alkane formation increase with a decrease in the GHSV. Although it is beneficial to operate at lower GHSVs in the HAS reactions (because of increased carbon conversions), increased alkane selectivity at such flow rates is a serious problem. Furthermore, it is apparent that alkane selectivity (which is undesirable) varies from one alkali metal to the other. Both the desirable and undesirable properties of all alkali metal salts were considered when we had to recommend a suitable metal for HAS in our catalyst. From Tables 2.4 and 2.5 and Figure 2.6 it is noted that doping ISO 63 with alkali metal salts resulted in the decrease of the catalyst selectivity towards alkanes. This is a desirable situation since we are only interested in alcohols in this process.

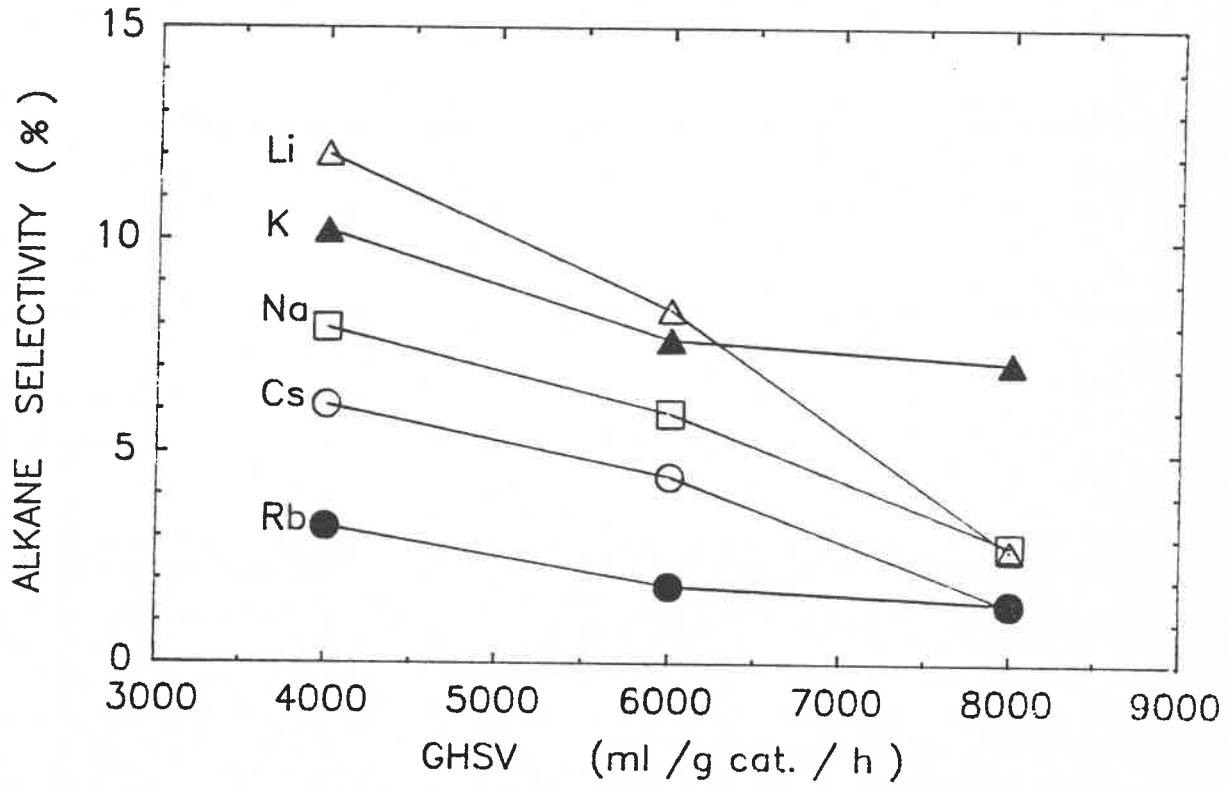

Figure 2.6: Graphs showing the influence of GHSV on alkane selectivity by the Cu/Zn/Cr catalysts impregnated with the formates of Cs, Rb, K, Na and Li at T = 325 °C and P = 10 MPa.

It is apparent from the results summarized in Tables 2.4 and 2.5 and Figure 2.7 that alkali doping of the blank ISO 63 catalyst changes the selectivity of the catalyst in favour of the formation of HA. The HA selectivities as functions of the GHSV for catalysts impregnated with different alkali metal formates are plotted in Figure 2.7. The graphs show that HA selectivities increase with a decrease in GHSV. This implies that the HAs are formed by a series of steps which have reasonable time to proceed when the gas residence time in the reactor is high. A large fraction of HAs consist of isobutanol, 1-propanol and ethanol. The other alcohols which are formed in significant quantities, especially at lower GHSVs, are 2-methyl-1-butanol, 2-methyl-1-pentanol and

2-methyl-1-hexanol. It appears that the rate constants of formation of the above 2-methyl alcohols are significant at lower GHSV.

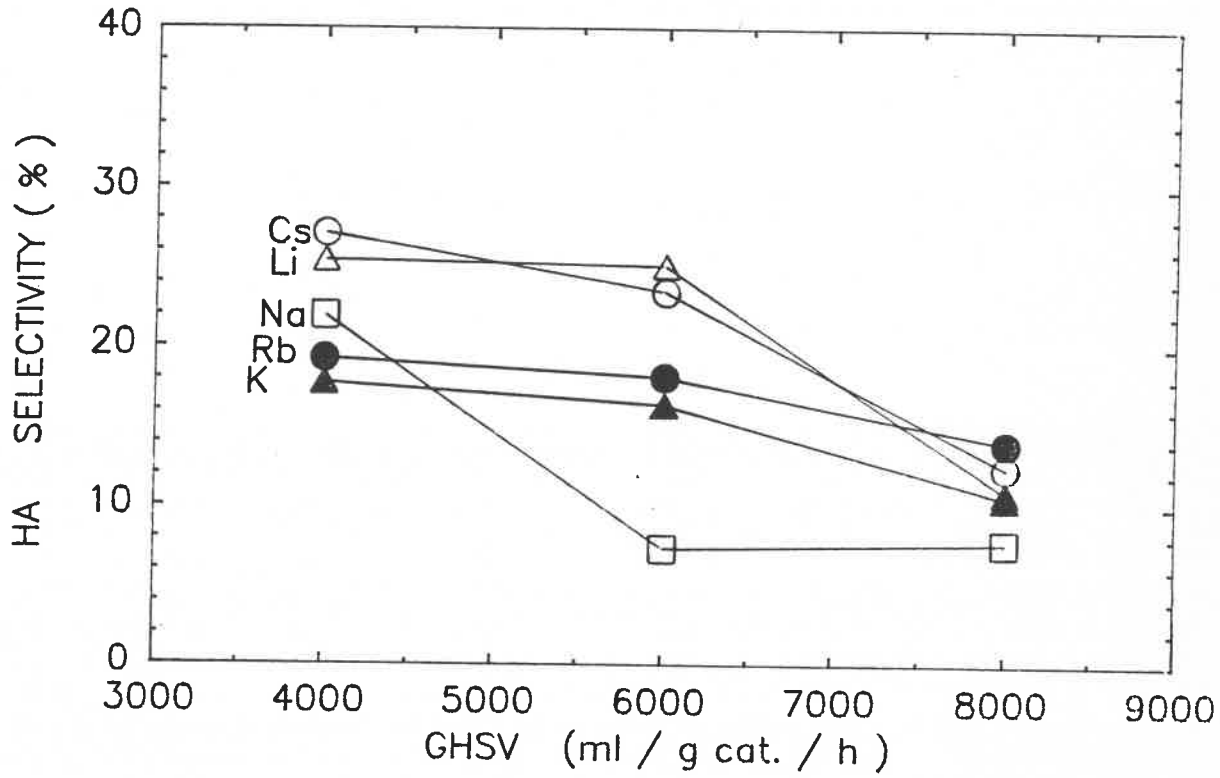

Figure 2.7: The dependence of HA selectivity on the GHSV of the Cu/Zn/Cr catalysts impregnated with the formates of Cs, Rb, K, Na and Li at T = 325 °C and P = 10 MPa.

At 4 000 ml/g_{cat}/h, 325 °C and 10 MPa, the Cs dopant shows the highest selectivity towards HA, i.e. about 28%. It is noted that the influence of GHSV on both HA and alkane selectivities is similar. Both selectivities decrease with an increase in GHSV.

The percentage selectivities of the formation of methanol and isobutanol as functions of GHSV are shown in Figures 2.8 (a) and (b) for catalysts doped with the formates of Cs, Rb, K, Na and Li. For isobutanol, selectivity decreases with

an increase in GHSV, but it increases with an increase in GHSV in the case of methanol selectivity. This shows that at a lower GHSV isobutanol and other higher alcohols are formed at the expense of methanol. The behaviour is well documented in the literature [Forzatti et al. 1991]. The selectivities for methanol at 4 000 ml/$g_{cat.}$/h for all the alkali-impregnated catalyst batches is higher than that for a blank catalyst batch. Except for Li, the methanol STYs of all the other alkali-doped catalyst batches were higher than that of the blank. This shows that, for this catalyst, activity towards methanol is promoted by alkali doping. The observation agrees with work by Klier et al.[1988a]. Doping of ISO 63 with Cs, Li and Na resulted in the catalyst's selectivity towards isobutanol increasing. For all alkali-impregnated ISO 63 batches the STY of the peak isobutanol production decreases as shown below:

$$Li > Cs > Na > Rb > K$$

The high isobutanol selectivity for the Li-doped catalysts has also been reported by Keim and Falter [1989]. This shows that the Li-impregnated catalyst has the potential to achieve a low methanol / isobutanol ratio after careful optimization.

The methanol/HA and methanol/isobutanol ratios are an important consideration in HAS research because of the need to reduce the production of methanol as much as possible. In Table 2.4 it is seen that the above ratios increase as the GHSV is increased. The dependence of HA and methanol selectivities on GHSV clearly explains the relationships. The industrial target for the methanol/HA ratio is between 1 and 2.33 [Forzatti et al. 1991]. The Cs-doped catalyst whose methanol/HA is about 2.40 % can be said to meet this requirement already. The same is true of the Li-doped catalyst. The high methanol/HA and Methanol/isobutanol ratios were drastically reduced in the new CSIR HAS catalyst formulation. This catalyst, which is to be patented was developed from ISO 63 by including other metal ions in the catalyst formulation procedure.

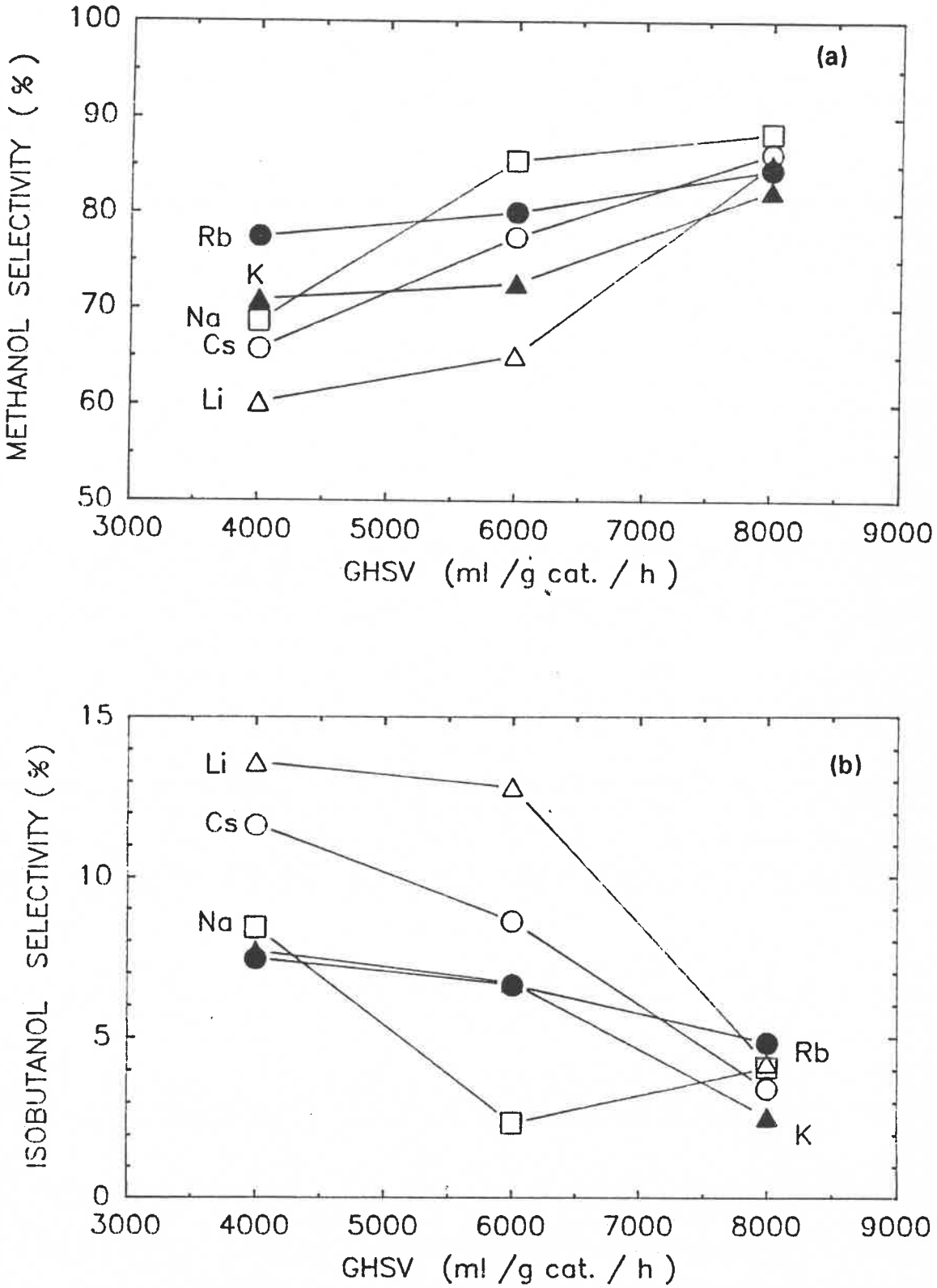

Figure 2.8: **The selectivities of methanol (a) and isobutanol (b) as functions of GHSV for catalysts doped with Cs, Rb, K, Na and Li formates at T = 325 °C and P = 10 MPa.**

The highest HA selectivities of the different alkali metal formates on this Cu/Zn/Cr catalyst decrease in the following order:

$$Cs > Li > Na > Rb > K$$

It is noted that the following order of HA selectivities has been established by other authors [Vedage et al. 1983]:

$$Cs > Rb > K > Na > Li$$

When our results are compared with those of Vedage et al. [1983], it can be seen that the two results share one similarity, namely the order of HA selectivity for Cs, Rb and K as dopants. The high catalytic activity and selectivity towards HA and isobutanol for both the Na- and Li-doped catalysts contradict the current understanding of the process. It will be shown later that the performances of the Li- and Na-doped catalyst batches are related to the presence of Na compounds in the original catalyst batch. The STY of isobutanol by both the Li- and Cs-impregnated catalysts indicates that the performance of this catalytic system is amongst the best of catalysts published in the literature [Sofianos 1992] which operate at relatively low conditions of temperature, pressure and GHSV.

The determination of the optimum quantities of Cs for optimal HAS by ISO 63 catalyst is shown in Figure 2.9(a). In Figure 2.9(b) results of a study of the dependence of isobutanol STY on the quantity of the Li dopant on the catalyst are presented. From the figure it can be seen that the optimum quantity of Cs for optimal HAS is 3.3% Cs (by mass). This is very close to the figure established by Klier et al. [1988] for their $Cu/Zn/Cr_2O_3$ catalysts. In the case of the Li-doped catalyst it seems that the optimal quantity of the dopant is close to $2.26*10^{-4}$ moles/$g_{cat.}$ The optimum quantities for the Cs and Li dopants are very close.

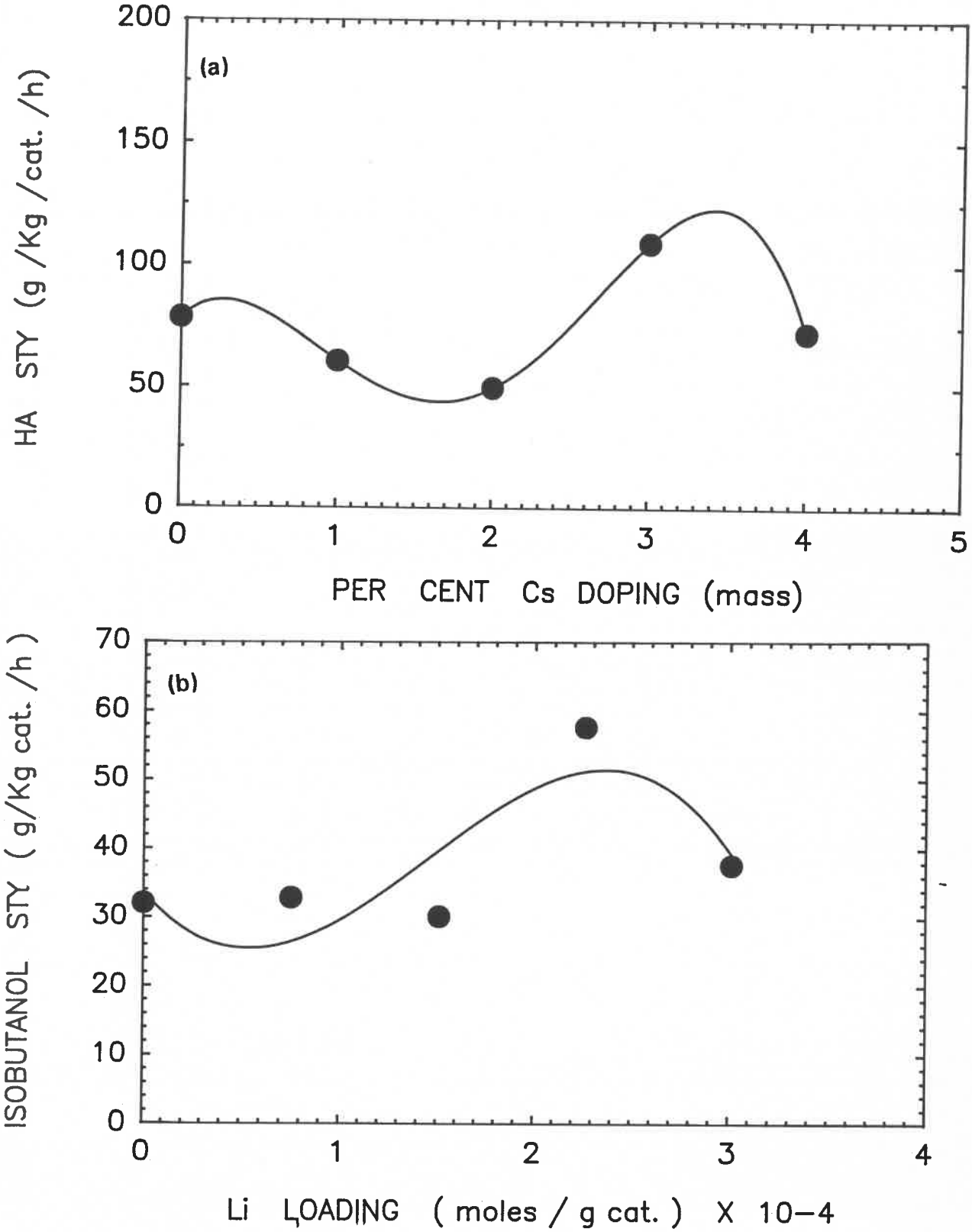

Figure 2.9: Effect of the variation of (a) Cs quantity on the HA STY and (b) Li dopant on the STY of isobutanol, for the Cu/Zn/Cr catalyst at GHSV = 4000ml/$g_{cat.}$/h, T = 325°C and P = 10MPa.

2.6. CONCLUSIONS

It is concluded that alkali doping of our Cu/Zn/Cr methanol synthesis catalyst increased its selectivity in favour of HAS. This is related to the basic functions of the alkali metal salts. Since the property is the same as that found in catalysts of Smith et al. [1991] and Forzatti et al. [1991] it is concluded that even in this case, base-catalyzed reaction steps were promoted. Doping ISO 63 with alkali metal salts resulted in the decrease of catalyst selectivity towards alkanes. This is a welcome development as alkanes are undesirable in this reaction. Impregnation with Li, Na and K alkali metal salts enhanced the catalytic activity. Catalytic activity, selectivity towards alkanes, HA selectivity and selectivity towards isobutanol, all decrease with an increase in GHSV. This is explained by the fact that many HAS are multi-step reactions and therefore conditions of high residence times are conducive for their formation. The methanol selectivity was increased by doping ISO 63 with Cs, Rb, K, and Na. The result is in good agreement with the work of Klier et al. [1988].

The Cs-doped catalyst is best suited for production of HA since it showed the highest HA selectivity. Both the Cs- and Li-doped catalysts have industrial potential in HAS because they achieved acceptable methanol/HA ratio of about two. The Li-impregnated catalyst is acceptable as the system of choice in the synthesis of isobutanol because of its high STY and selectivity towards this alcohol. Another favourable aspect of this system is that it has the lowest methanol/isobutanol ratio. The performances of the Li- and Cs-doped catalysts show that our systems are among the best of those operating at a relatively low temperature, pressure and GHSV. The high catalytic activity and HA selectivity of both Li- and Na-impregnated catalyst batches seemed to contradict the assertion that the performance of alkali metals in the HAS reaction was related to the basicity of the metal. This performances will be shown later to be related to the presence of Na compounds in the parent catalyst batch. This leads to the conclusion that the observed performances of the alkali metal-impregnated

batches are in fact a result of the combined performances of sodium compound and individual alkali metal salts in each case. The ISO 63 catalyst's highest HA selectivity was at about 3.3% Cs (mass %) loading while the highest isobutanol selectivity was at $2.26*10^{-4}$ moles Li/g_{cat}.

2.7. REFERENCES

Anderson, R.B., The Thermodynamics of the Hydrogenation of Carbon Monoxide and Related Reactions. In: Catalysis, Emmett, P.H., Ed.; Reinhold, New York, **1956**; Vol. 4, Chapter 1, pp 1-27.

Anderson, R.B., Thermodynamics of the Hydrogenation of Oxides of Carbon. J. Phys. Chem, **1986**, 90, 4806-4810.

Boz, I., Chadwick, D., Metcalfe, I.S. and Zheng, K., Potassium Promotion of Cu-ZnO-Al_2O_3 Catalysts for High Alcohol Synthesis. Proc. 10th Int. Congr. Catal., **1992**, 2785.

Di Conca, M., Riva, A., Trifiro, F., and Vaccari, A., The Zinc-Chromium Oxide Potassium Promoted Catalysts for Methanol and High Alcohol Synthesis. Proc. 8th Int. Congr. Catal., **1984**, II-173.

Forzatti, P., Tronconi, E. and Pasquon, I., Higher Alcohol Synthesis. Catal.Rev.-Sci.Eng., **1991**, 33 (1&2), 109-168.

Keim, W. and Falter, W., Isobutanol from Synthesis Gas. Catal. Lett., **1989**, 3, 59-64.

Klier, K., Herman, R.G., Simmons, G.W., Nunan, J.G., Bogdan, C.E. and Himelfarb, P.B., Direct Synthesis of 2-methyl-1-propanol / methanol Fuels and Feedstocks. Final Technical Report, DOE # DE-AC22-84PC70021. **1988.**

Klier, K., Herman, R.G. and Vedage, G., (Lehigh University) U.S 4,843,101 **(1989)**.

Klier, K., Herman, R.G., Himelfarb, P.B., Young, C.-W., Hou, S., and Marcos, J.A., C-C Bond Formation via β-Addition with Oxygen Retention Reversal in Oxygenate Synthesis. Proc. 10th Int. Congr. Catal. **1992**, 1441.

Mross, W., -D., Alkali Doping in Heterogeneous Catalysis. Catal.Rev.-Sci.Eng., **1983**, 25(4), 591-637.

Lietti, L., Botta, D., Forzatti, P., Mantica, E., Tronconi, E. and Pasquon, I., Synthesis of Alcohols from Carbon Oxides and Hydrogen VIII. A Temperature-Programmed Reaction Study of n-Butanal on a Zn-Cr-O Catalyst. J. Catal., **1988**, 111, 360-373.

Natta, G., Colombo, U., and Pasquon, I., Higher Alcohols. In: Catalysis, Emmett, P.H., Ed., Vol. 5, Chapter 3, pp 131-174, Reinhold, New York, **1957**.

Roberts, G.W., Lim, P.K., McCutchen, M.S. and Mawson, S., The Thermodynamics of Higher Alcohol Synthesis. DOE Indirect Liquefaction Contractors' Review Meeting, Pittsburgh, September **1991**.

Smith, K.J. and Anderson, R.B., The High Alcohol Synthesis Over Promoted Copper/Zinc Oxide Catalysts. Can. J. Chem. Eng., **1983**, 61, 40-45.

Smith, K.J., Young, C.-W., Herman, R.G. and Klier, K., Development of a Kinetic Model for Alcohol Synthesis over a Cesium-Promoted Cu/ZnO Catalyst. Ind. Eng. Chem. Res. **1991**, 30, 61-71.

Sofianos, A., Production of Branched-Chain Hydrocarbons via Isosynthesis. Catal. Today, **1992**, 15, 149-175.

Tronconi, E., Forzatti, P. and Pasquon, I., An Investigation of the Thermodynamic Constraints in Higher Alcohol Synthesis over Cs-Promoted ZnCr-Oxide Catalyst. J. Catal., **1990**, 124, 376-390.

Tronconi, E., Lietti, L., Groppi, G., Forzatti, P. and Pasquon, I., Mechanistic Kinetic Treatment of the Chain Growth Process in Higher Alcohol Synthesis over a Cs-Promoted Zn-Cr-O Catalyst. J. Catal., **1992**, 135, 99-114.

Vedage, G.A., Himelfarb, P., Simmons, G.W. and Klier, K., Alkali Promoted Cu/ZnO Catalysts for Low Alcohol Synthesis. Symposium on the Role of Solid State Chemistry in Catalysis, presented before the Division of Petroleum Chemistry, American Chemical Society, Washington, **1983**.

Xiaodong, Hu., Scientific Basis for Design of Heterogeneous Catalysts . A Study of Alcohol Synthesis Catalysts. PhD Thesis, Department of Chemical Engineering, University of Delaware, Delaware, USA, **1989**.

3: ANALYSIS OF THE EFFECT OF ALKALI METAL DOPING ON THE TEXTURAL PROPERTIES OF THE CATALYST USING PHYSISORPTION TECHNIQUES

3.1 INTRODUCTION

In this chapter a study of the effect of alkali doping on the surface area, pore volume and size distribution of the blank and alkali metal doped catalyst batches are reported. The physical properties of the catalyst were probed using physisorption processes. A critical review of the methods employed is presented with emphasis on their capabilities and short-comings. This sets criteria by which the results are evaluated.

3.2. THEORY

3.2.1 ADSORPTION ISOTHERMS

Physisorption occurs whenever a gas (adsorbate) comes into contact with a solid (adsorbent). This is an adsorption process which is controlled by Van der Waal's forces between the surface and the adsorbate. A number of mechanisms which the process follows have been identified.

The nature of the surface of the solid determines the mechanisms the physisorption processes take. A non-porous solid is considered to possess what is termed external surface area on which multilayer physisorption can occur. In this work the external surface area is described as the area around particles / aggregates and the areas in cavities, pores and cracks whose depths are less than their widths [Haber 1991]. Some solids display limited external surface area and extensive pore area.

Generally pores can be classified into three broad categories [Bond 1987; Sing 1980]. Pores whose internal diameter is less than 20Å are called micropores and those with diameters ranging from 20Å to 500Å are termed mesopores. Pores

whose internal diameters exceed 500Å are called macropores. Depending on the porosity of an adsorbent, physisorption may proceed by any of three mechanisms. In micropores, the process occurs by micropore filling, which is normally called primary physisorption. In mesopores, physisorption is by secondary adsorption. This is a capillary condensation which is preceded by formation of adsorbed multi-layer physisorption on the pore walls. In macropores, capillary condensation occurs when adsorbate vapour pressure approaches its saturated vapour pressure at the working temperature. The vapour pressure of the adsorbate will be shown to control the extent to which physisorption takes place.

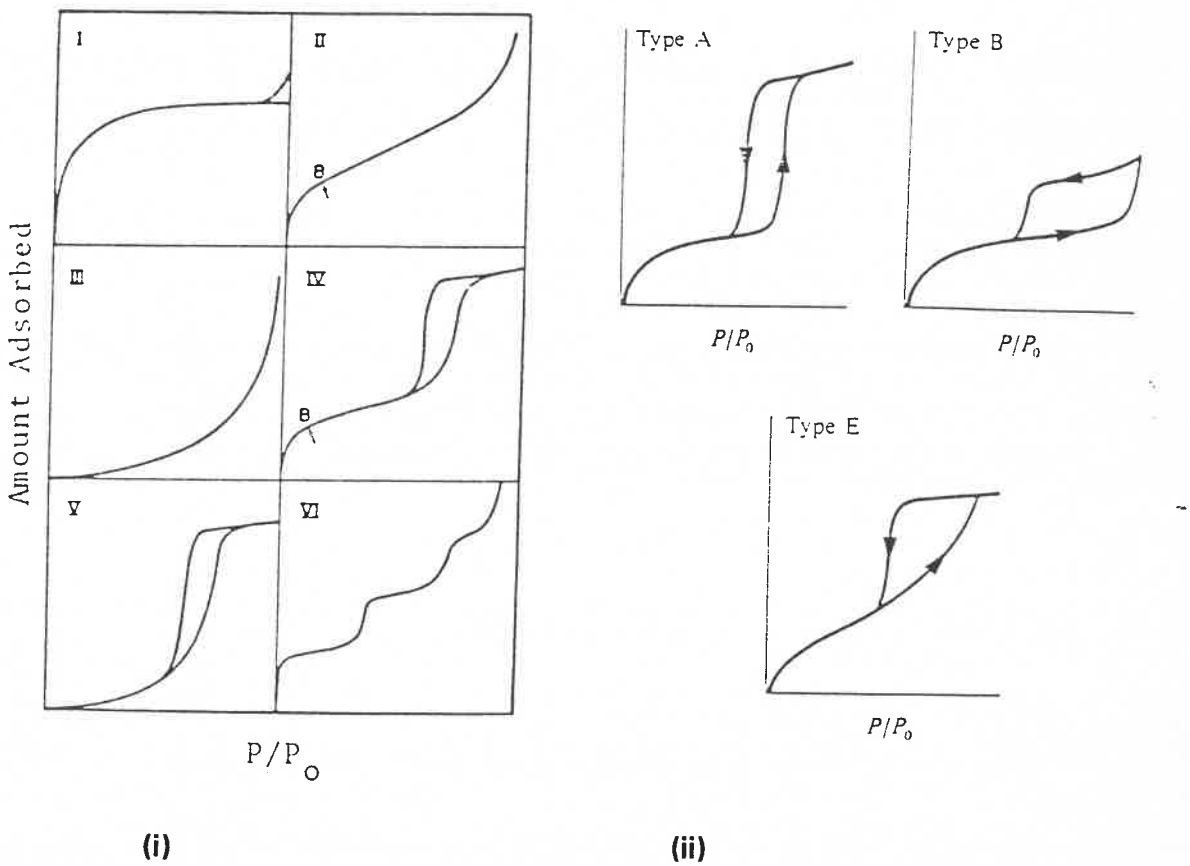

(i) (ii)

Figure 3.1: The physisorption isotherm types (i) and the different Type IV hysteresis loops (adopted from Sing 1980).

A plot of the quantity of gas adsorbed on a solid, at constant temperature, against the pressure with which it is in equilibrium is called an isotherm.

Isotherms are classified according to their shapes. There are six different classes of isotherms which are labelled Type I, Type II.... Type VI (see Figure 3.1). The shape of the isotherm is dependent on the nature of the adsorbent and the adsorbate. As a consequence, one can readily deduce whether the adsorbing surface is completely non-porous or not by simply examining the shape of the isotherm. Furthermore, the shapes of the Type IV isotherms have been shown to be dependent on nature of pores the adsorbent has [Ponec et al. 1974; Bond 1987; Allen 1981]. The importance of this fact will be discussed in detail later.

In Figure 3.1 it can be seen that Type IV isotherms are not reversible and show hysteresis loops. It has been suggested that the presence of the hysteresis loops is due to adsorption by capillary condensation which takes place **simultaneously** with multilayer adsorption. This results in different radii of curvature for adsorption and desorption processes at any particular relative pressure which falls within the hysteresis [Allen 1981]. The Kelvin equation [Eq. 3.1] shows that the relative pressure of a gas in equilibrium in such a pore is different for adsorption and desorption processes due to different **core** radii. The Kelvin equation has this form:

$$\ln (p/p_0) = \frac{-2Vv\cos\theta}{rRT} \qquad (3.1)$$

where p/p_0 is the relative pressure, V is the molar gas volume, v is the surface tension of the liquid whose meniscus in a pore of radius (r) forms a contact angle of θ. This contact angle is normally equated to zero. The practice is acceptable for the desorption branch of the hysteresis loop but questionable for the adsorption side [Baiker 1985]. This is the reason why desorption isotherms are regarded as depicting the true picture about the surface textural properties [Richardson 1989].

In Figure 3.1 three different classes of Type IV isotherm are shown. Mesopores

which are open ended and cylindrical show a Type IV (A) hysteresis while the "ink bottle"mesopores show Type IV (E) hysteresis loops. A Type IV (B) isotherm is characterised by mesopores which are constricted in a certain way. This analysis is currently the accepted position [Bond 1987; Richardson 1989; Ponec et al. 1974]. The hysteresis loops are valuable in determining a suitable model for the volume and area analysis of the pores.

Various methods for pore volume analysis, depending on the pore shape, are now in use. For pores whose shapes are unknown the modelless method is used to investigate the pore volume and hence pore area. Depending on suitability, pore volume analysis can be attained by the parallel plate model, the cylindrical core model or the cylindrical pore model. In this work the catalyst was shown to possess cylindrical pores and therefore, the cylindrical pore model was adopted and the pore volumes and areas evaluated.

A number of empirical methods to evaluate isotherms have been advocated. One procedure reviewed here is the BET method which is used to evaluate the total surface area (the sum of the external surface area and the micropore area). The t-method is used to further understand the BET surface area in terms of its constituents. Additionally, the analysis of mesopores and macropores using the BJH method is critically analyzed.

3.2.2 THE BJH METHOD

For analysis of the catalyst pore volume and area we used the BJH method which was developed by Barrett, Joyner and Halenda [1951]. It is a desorption procedure method. It applies to materials of variable pore radii and is based on the following assumption. At liquid nitrogen temperatures and at a given relative pressure the equilibrium between the adsorbed liquid-like N_2 on the adsorbent surface and the gas phase depends on two factors. It is a function of multilayer adsorption on the walls of a pore and capillary condensation in the core of the

pore (see Figure 3.2).

In probing the pore surface area and volume, the desorption isotherm is used from a relative pressure value close to unity to a relative pressure which corresponds to the closing of the hysteresis. When the relative pressure is decreased, certain pores lose the condensate in their cores leaving behind adsorbed layers on their walls. To be able to calculate the pore surface area and volume, the core volume and the average thickness ($\bar{t}$) of the layer still adsorbed on the pore wall have to be determined (see Figure 3.1). The average radius of cores emptied, at the end of that relative pressure interval, is calculated from the Kelvin equation. The value of $\bar{t}$ at a particular relative pressure, is determined from an appropriate t-curve (see section on the t-method).

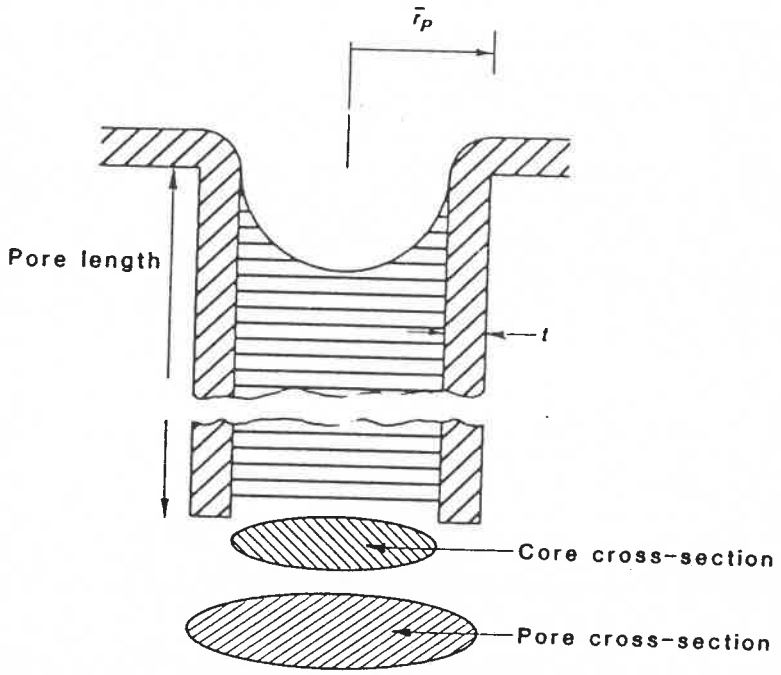

Figure 3.2: The model of adsorption in a cylindrical pore (from Allen 1981] where both the core and the adsorbed layer thickness (t).

Subsequent lowering of the relative pressure results in either the thinning of $\bar{t}$ or

an evaporation of cores of another set of pores accompanied by thinning of their adsorbed layers at the end of the relative pressure interval. This means that after every desorption step (j), the desorbed liquid could be a measure of one of two things. It could be an estimation of the total core volume of new sets of pores emptied plus a volume equivalent to the first thinning of layers remaining adsorbed on the pores walls at the end of the relative pressure interval. Alternatively, it could be an indication of the thinning out of the adsorbed layers of the previously opened pores. Barrett et al. showed that the volume of adsorbate evaporated could be related to pore volume using the following equation:

$$V_{pn} = R_n \Delta V_n - R_n c\, dt \sum_{j=1}^{n-1} A_{pj} \qquad (3.2)$$

where V_{pn} is the mesopore incremental volume, R_n is the ratio of the square of the pore radius (r_p) to the square of the sum of the Kelvin radius (r_k) and dt(i.e. the change in wall thickness), ΔV_n is the volume desorbed in the n-th desorption step, c is the ratio of the average core radius to the average pore radius, and A_{pj} is the pore area of pores which undergo a thinning step (step j) of their adsorbed layers on their walls due to a desorption step (i.e. step n). The summation of the area of these pores is over the steps j = 1 to j = n-1.

The incremental surface area of pores is calculated using the following formula:

$$S = 2V_{pn} / \check{r}_p \qquad (3.3)$$

where $\check{r}_p$ is the average pore radius. The value of $\check{r}_p$ is evaluated from Equation (3.4) below:

$$\check{r}_p = r_k + \bar{t} \qquad (3.4)$$

where r_k is the Kelvin radius and $\bar{t}$ is the average thickness of the adsorbed layer,

values of which can be calculated as shown in the section on t-method. The summations of the above incremental pore volumes and areas yield the total pore volume and total mesopore surface area, respectively. A detailed set of calculations is presented in Micromeritics ASAP 200 operator manual [1989].

From these calculations the following can be obtained:

- incremental pore volumes and surface area,
- cumulative pore volumes and surface area and
- data for distribution curves.

The BJH method has not been widely used because of its complexity.

3.2.3 THE BET METHOD

The key parameter in surface area determination in the BET method is the volume of monolayer coverage (V_m). This is the volume required to form a monolayer on the adsorbent surface thereby completely covering it. The first quantitative determination of V_m was suggested by Langmuir [1918] in his equation which described an isotherm similar to what is now known as the Type I isotherm. In its derivation it was assumed (i) that a single molecule adsorbed as a whole entity at a single point which was big enough for a single molecule only, and (ii) that all adsorbing sites had equal energy. The equation took the form of Equation 3.5 below:

$$V/V_m = [Kp / p_0] / (1 + Kp / p_0) \qquad (3.5)$$

where V_m was the monolayer volume, V was the total volume adsorbed at pressure p, p^0 was the saturated vapour pressure of the adsorbate at the working temperature and K was a constant. The equation fits the first few segments of S-shaped isotherms.

In Types II and IV isotherms the monolayer volume can be determined from point B(see Figure 3.1) although this point cannot be accurately located, especially in certain Type II isotherms. In order to mathematically describe the isotherm at higher relative pressures Brunauer et al. [1938] extended the Langmuir analysis by including a few more assumptions. They advocated a multilayer model of adsorption on the solid surface and assumed that:

- the binding energy of multimolecular adsorption was due solely to condensation forces,
- adsorption sites for molecules in the second layer were the tops of the molecules on the first layer and the same was the case for subsequent layers,
- molecular vibrations were different for different layers and
- that, from the second layer upwards, the condensation and evaporation behaviour were similar to those of the liquid state and were equated to them.

The equation they derived for the isotherm took the form:

$$V = \frac{V_m C p}{(p_0 - p)\{1 + (C-1)(p/p_0)\}} \qquad (3.6)$$

where all the other symbols retained their meaning as in the Langmuir equation. The free energy term (C) was equal to:

$$C = \exp[(H_a - H_1)/RT] \qquad (3.7)$$

where H_a was the enthalpy of adsorption of the first layer and H_1 was the enthalpy of formation of the second and subsequent layers and was taken to be equal to enthalpy of liquefaction of the adsorbate.

Equation (3.6), now known as the BET equation, was rearranged to the linear form in Equation (3.8).

$$\frac{p}{V(p_0-p)} = \frac{1}{V_mC} + \frac{(c-1)\ p}{V_mC\ p_0} \qquad (3.8)$$

A plot of $1 / V((p_0/p)-1)$ against p/p_0 gave a straight line from whose slope and intercept the values of V_m and C were determined. The magnitude of C is a measure of attraction between the surface and the adsorbate. High cohesion forces among the adsorbate molecules result in a low C value while high attraction forces between the adsorbent and the adsorbate result in a high value of C. Normally C falls within the range 80 to 120. In surfaces which have micropores and extensive external surface area C is found to be higher than 120 and this is taken to mean that surface adsorption due to micropore filling and monolayer adsorption are taking place at the same time [Sing 1980].

The parameter V_m is used to determine surface area (S) by using Equation 3.9 below [Baiker 1985]:

$$S = V_mNa_m/M_v \qquad 3.9)$$

where N is the Avogadro's number, a_m is the surface area per molecule of the adsorbing gas and M_v is the molar gas volume. In a case where the value of C is known, the intercept can be ignored and C could be equated to C-1 to modify the rearranged BET equation to the form as in Equation (3.10):

$$V_m = V(1-p/p_0) \qquad (3.10)$$

By using a single point of V, a reasonably accurate estimate of the value of V_m and hence the surface area can be quickly determined. This is the basis for the so-called Single Point method. It is a fast and reasonable method for estimating

the surface area.

Brunauer et al. [1938] found the method to be consistent over a wide range of adsorbate-adsorbent systems. Much work was devoted to investigating the surface areas of catalysts whose isotherms were S-shaped. Many authors have applied the BET method to many systems with satisfactory results which could be independently verified [Allen 1981]. The BET equation holds within the relative pressure range 0.05 to about 0.35 when measurements are taken at temperatures close to the boiling point of the adsorbing gas. The range over which the method is valid shifts to lower relative pressure values when measurements are made at temperatures close to the melting point of the adsorbate [Ponec et al. 1974]. The BET procedure is therefore a method of choice for many surface area determinations because of its simplicity, reproducibility and soundness of its theoretical basis, but it also has its shortcomings.

At very low relative pressures the BET theory predicts less coverage than is actually determined experimentally. The major problem here is that the adsorbed gas is so minimal that its accurate determination cannot always be accomplished. At high relative pressures the BET method predicts too high a surface area and has to be modified accordingly [Ponec et al. 1974]. This raises questions about some of the assumptions in the derivation of the theory.

The deficiencies of the BET method could be traced to some of the reservations expounded below. Experimental data have shown that C is not always a constant as was initially assumed. The absence of horizontal interactions among adsorbate molecules on the adsorbent surface, as required by the theory, is highly unlikely. Furthermore, the need to treat molecules in the second and subsequent layers as equal is questionable in the light of the work by Halsey [1948]. He showed that, in practice, a situation where a molecule in the second layer could adsorb onto one in the first layer and have another adsorbed onto it

giving rise to a third layer with concomitant release of all the energy of liquefaction, could not be attained. It has been found experimentally that B is located in the pressure range $0.05 < x < 0.15$ but, the BET theory predicts B at variable coverages which are influenced by the value of C.

Gregg and Jacobs [1948] showed that the BET calculations were still valid even when any constant other than p_0 was used and the adsorbed gas was assumed not to have liquid properties [Allen 1981 and references therein]. Despite these setbacks the BET method is still widely used. In conjunction with the t-method, the BET method can additionally probe the micropore area and volume and the external surface area.

3.2.4 THE t-METHOD

By assuming that the molar volumes of adsorbed N_2 gas and liquid N_2 are equal, a nitrogen isotherm can be converted to a t-curve. This is a plot of relative pressures (x) as a function of the thickness (t) of the layers of adsorbed gas. The analysis is based on research by Lippens and de Boer [1965] and Mikhail et al. [1968]. The first step is to convert adsorbed gas volumes into t values corresponding to the same quantity of gas when it is adsorbed on a non-porous adsorbent. This can be accomplished by using Equation 3.11.

$$t = \frac{MV_{sp}}{M_v}\,\frac{V}{S_w} \qquad (3.11)$$

where: M = the molecular weight of the gas

V_{sp} = the specific volume of the adsorbate ($cm^3\ g^{-1}$)

S_w = the BET specific surface area in $m^2\ g^{-1}$

M_v = 22 140 cm^3

V = adsorbed volume

The t-curve can be described by the Harkins and Jura equation (Eq. 3.12).

$$t = [13.99 / (0{,}034 - \log x)]^{.500} \qquad (3.12)$$

The t-curves are used to evaluate the adsorbed layer thicknesses in the mesopores and macropores as required for the BJH calculations. In such a case the material whose t-curve is used must have properties as close as possible to those of the adsorbent being studied and its structure must be known too [Sing 1980].

A plot of V against t, at low relative pressures, is a straight line the slope of which is used to calculate external surface area. The area is calculated from

Equation 3.13 which is derived from Equation 3.11 by simply inserting all constants and rearranging terms.

$$S = 15.47\ V/t \times 10^4 Å \qquad (3.13)$$

where:

0.001 547 = conversion factor of N_2 gas volume to its liquid equivalent.

The micropore surface area is the difference between the BET surface area and the external surface area [Micromeritics 1989]. The intercept (Y_{INT}) of the line is used to evaluate the micropore volume (V_{mp}) (See Equation 3.14 below).

$$V_{mp} = Y_{INT}\ (cm^3/g\ STP) \times 0.001\ 547\ (cm^3\ liquid/cm^3\ STP) \qquad (3.14)$$

At higher t values the V-t curve might deviate from linearity. A positive deviation is associated with the onset of capillary condensation in mesopores while a negative deviation implies the decrease of accessible surface area because of macropore blocking [Allen 1981]. The main drawback of the t-method is the need to find a suitable material for the determination of t-values. Summaries of results from the above methods are presented below. The detailed results are in

Appendices 1, 2, 3 and 4.

The ASAP 2000 Accelerated Surface Area and Porosimetry System from Micromeritrics was used in the surface area and pore size distribution analysis. The apparatus could be used for analyses in the BET, BJH and the t-methods. It has already been mentioned that N_2 gas was used to determine the shapes of isotherms our alkali-doped catalyst batches gave rise. Analysis of quantities of gas desorbed were volumetrically determined. In all the investigations where desorption was varied with relative pressure, equilibration time allowed for was 5 seconds. In this chapter the results of the textural properties evaluated before and after alkali metal impregnation are presented and discussed.

3.3. RESULTS AND DISCUSSION

The total BET surface area which includes the external surface and micropore area, the BJH mesopore and macropore surface areas (from the t-method) together with their respective volumes and diameters (where applicable) were the criteria employed to characterize the textural properties of the undoped ISO 63 catalyst. The same parameters were used to investigate the effect of alkali impregnation on the surface properties of the said catalyst.

The BET surface area of 57.36 m^2/g for ISO 63 (blank) is moderate by normal standards (See Table 3.1 and Appendix 2). The catalyst has a micropore area of about 4 m^2/g which is very small compared to the BET area. The rest of the BET surface area was due to external surface area. This is an ideal situation, for the catalyzed reaction does not suffer transport limitations as normally found in microporous catalytic systems.

As indicated in Table 3.2 and Appendix 4 the BJH desorption surface areas are larger than the BET areas. The most important reason for this discrepancy is that the BJH method evaluates the areas of all pores including the interconnecting

TABLE 3.1

The total BET surface area for different catalyst batches is shown in terms of its components i.e. external surface area (ESA) and micropore area (MA).

Catalyst batch	BET SURFACE AREA ($m^2/g_{cat.}$)		
	Total SA	ESA	MA
ISO 63 (Blank)	57.36	53.39	3.97
ISO 63 + Li	58.05	58.05	-
ISO 63 + Rb	64.77	64.77	-
ISO 63 + K	44.90	44.90	-
ISO 63 + Cs	39.13	39.13	-
ISO 63 + Na	40.51	38.83	4.68

ones which cannot be accessed by the BET method [Allen 1981]. This implies that the BJH method is sensitive to both the BET area and the area of interconnecting pores. A good example is the BJH desorption method area result of the Rb-doped catalyst in pores within the range 17.00Å to 3000.00Å. The increase in the surface area of the Rb-doped catalyst batch was detected by both the BET and the BJH methods.

The volumes and areas obtained by the BJH desorption method for pores whose diameters fall within the range 17.00Å to 3000.00Å show that the different catalyst batches have both mesopores and macropores. From both Tables 3.1 and 3.2 the presence of the micropores, mesopores and macropores in the catalyst is confirmed (as already noted the micropore volume was found to be very small). The average pore diameters which are functions of both the total pore areas and total pore volumes show the dominance of mesopores in the

TABLE 3.2

The BJH total pore volume (TPV), total pore area(TPA) and average pore diameters(APD) of the blank and alkali impregnated catalyst batches for pores of sizes 17.00Å to 3000.00Å

Catalyst Batch	BJH Results		
	TPV (cm^3/g)	TPA (m^2/g)	Average PD (Å)
ISO 63 (Blank)	0.2989	84.32	141.79
ISO 63 + Li	0.2143	79.47	107.87
ISO 63 + Rb	0.2674	98.95	108.11
ISO 63 + K	0.1878	73.05	102.86
ISO 63 + Cs	0.1649	62.81	105.04
ISO 63 + Na	0.1824	64.91	112.44

catalyst. The BJH desorption average diameter is 176Å. This falls within the mesopore range of diameters, thereby emphasizing the importance of the contribution of mesopores towards the total surface area and pore volume.

An inspection of the detailed analysis data from all methods (Appendices 1 to 4) highlighted many important points. The catalyst gives rise to a Type IV (A) isotherm which implies that it consists mainly of open ended cylindrical pores. This is the reason why the cylindrical pore model was used to analyze pore volumes and areas in the BJH method. Since the BET method is known to describe the Type II and IV isotherms accurately [Baiker 1985], its suitability in characterizing the catalyst is implied.

The BET surface area data in Appendix 1 show that errors in the determinations

of the slope and Y-intercept hence, the surface area, are very low. The same accuracy can be detected in the micropore analysis data where the slope and the Y-intercept were used to determine/ the external surface area and micropore volume respectively. The above situation was true even in alkali-doped catalyst batches. The value of C, which was found to be 116.75, is of acceptable magnitude such that the estimation of V_m is of reasonable accuracy [Brunauer et al. 1938]. The BET plot in the zero to 0.22 relative pressure range was a straight line facilitating the accuracy with which the slope and Y-intercept could be determined. The plot of V against t-Harskins and Jura (the thickness was calculated by the Harskins and Jura formula) is convex to the t-axis, indicating that capillary condensation occurs in mesopores at higher relative pressure values. Further evaluation of mesopore volume and hence area was done by the BJH method.

The BJH desorption pore volume distribution graph in Appendix 4 is a sum of two bell shaped curves with the major curve having a mode at about 150Å and the minor one at approximately 300Å. The curve in conjunction with the BJH desorption pore volume distribution data shows that a significant pore volume fraction is due to pores in the diameter range 350Å to 60Å. Pores of diameter above 350Å have the second largest total pore volume while pores of diameter less than 60Å have the least total pore volume. This behaviour is a reflection of the variation of pore surface area with pore diameters. The textural properties of the catalyst batches doped with equal moles of Li, Na, K, Rb and Cs were studied as above.

The V-t(Harskins and Jura) plots in Appendix 3 for all alkali metals, except Li, are convex with respect to the t-axis, indicating that capillary condensation occurred in mesopores at higher relative pressures. For the Li-doped catalyst the plot shows a downward curvature which implies that accessible surface area decreased as macropores were blocked. Both these results indicate the presence of both mesopores and macropores in alkali doped catalysts.

The isotherm plots of all the alkali doped catalyst batches are similar to that of the blank catalyst batch and are all of Type IV A. It can be concluded that impregnation with alkali metal salts does not have a serious effect on the shape of the catalyst pores. Except for Na, impregnation of the catalyst with alkali metal salts resulted in reduction of the value of C. This implies that the catalyst surface was made less adhesive to the adsorbate than the undoped one. The high value of C in the Na-impregnated catalyst means that the adhesive capacity of the surface towards N_2 gas was enhanced by the sodium salt impregnation.

The BJH total desorption pore volumes of the alkali-impregnated catalysts are lower than those of the blank. It is thus apparent that alkali-impregnation decreases the pore volumes for pores in the range 17.00Å to 3000.00Å. The dv / d log (D) desorption pore volume plots in Appendix 4 are approximately Gaussian and have narrower bases than those of the undoped catalyst. For all the alkali-doped catalyst batches many pores fall within a narrower pore diameter range (i.e. smaller than the 350Å-to-60Å range of the undoped catalyst batch). The upper and lower limits of this range are shifted towards smaller pore diameter values. The distribution curves, in conjunction with cumulative desorption pore distribution data, show that for this catalysts large fractions of pore volumes stem from pores of smaller diameters than in the case of the undoped catalyst batch. It appears that alkali-impregnation of ISO 63 not only decreases its total pore volume but also increases the populations of small diameter pores. This means there is pore blocking. It will be shown later that alkali salts and catalytic material (which is soluble in the doping solution) are responsible for pore blocking. The decrease of the average pore diameters of the alkali-doped catalyst batches, as compared with the undoped catalyst, confirms this assertion (see Table 3.2). The effect of alkali doping on the BET surface area is not as clear-cut as in the case above.

Two general patterns emerge from the BET surface area results of the alkali-doped ISO 63 catalyst. Firstly, there are alkali metal impregnations which led, to

a marginal increase of the BET surface area. This behaviour was observed for Li and Rb doping. The effect of alkali impregnation with a second group of metals led to the decrease in BET surface area. This was found in cases involving Cs, Na and K doping. The first case to be considered is the one where BET surface area increased with alkali doping.

The catalyst batches impregnated with Li and Rb showed increases in their BET surface areas and by as much as 13% in the case of Rb. For Li-doped catalyst the area increase was marginal. From Table 3.1 it is apparent that alkali impregnation not only did it eliminate micropore volume but also increased the external surface area by more than 9% in the case of Li and 40% in the case of Rb. The external surface area increase is a major contributing factor towards the overall surface area increase in the Li- and Rb-impregnated catalyst batches.

The external surface area increase balances the negative effects of possible pore blocking (explained above) on the BET surface area. This increase in external surface area will be related to increase in surface concentrations of the copper and zinc components of the catalyst batches in Chapters 4 and 5. As mentioned there were cases where BET surface area decreased due to alkali-impregnation.

The impregnation of the catalyst batches with solutions of formates of K, Cs and Na resulted in the decrease of the BET external surface areas. The decrease was minimal (7%) for the K-doped catalyst while it was large for catalyst batches doped with Cs (25%) and Na(34%) dopants. This is a major contributing factor towards the decrease of the total BET surface area. It seems that another process effected changes on this catalyst surfaces. We believe that this decrease in surface area could be due to surface restructuring. A possible explanation for this restructuring will be advanced in Chapter 5.

Save for the Na-doped catalyst batch, alkali impregnation by other alkali metal salt solutions resulted in the loss of micropore area and volume. These results

point to possible pore blocking as explained above. In the Na-doped catalyst the micropore volume and area were increased by alkali impregnation. This could imply that the material that was re-deposited on the surface developed some micropores.

3.4 CONCLUDING REMARKS

Characterization of ISO 63 showed that the catalyst had moderate surface area. It has been shown that the alkali-impregnated catalyst had macropores (micropores were present in the case of Na-doped catalyst batch) but was predominantly mesoporous. The catalyst had pores which were open-ended and cylindrical in shape. Alkali-doping of the catalyst causes the blocking of pores by deposition of material on the pore walls. Although the effect decreases the catalyst pore area, it does not change the shape of pores. The pore diameters do not decrease drastically, i.e. they still remained mesopores. This has a significant advantage in that the alkali-doped catalyst does not suffer mass transfer effects in the course of the HAS reaction. It was shown that another effect of alkali doping is to decrease the external surface area for the catalyst batches doped with Cs, K and Na salts due to possible surface restructuring. In the case of Li- and Rb-doped batches external surface area is increased by the alkali doping process. It will be shown later that this increase in the external surface area in those catalyst batches is due to increase in surface concentrations of copper and zinc components of the catalyst. The above effects on the catalyst surfaces cannot be correlated with the catalytic performance of the above metal salts i.e. the changing of the reaction selectivity of the ISO 63 catalyst towards the production of HA.

3.5 REFERENCES

Allen, T., (ed), Particle Size Measurement, Chapman and Hall, London, 1981.

Baiker, A., Experimental Methods for the Characterization of Catalysts. I. Gas Adsorption Methods, Pycnometry and Porosimetry. Intern. Chem. Eng., **1985**, 25, 1, 16-28.

Barrett, E.P., Joyner, L.G. and Halenda, P.P., The determination of Pore Volume and Area Distribution in Porous Substances. I. Computations from Nitrogen Isotherms. J. Am. Chem. Soc., **1951**, 73, 373-380.

Bond, G.C. (ed), Heterogeneous Catalysis. Principles and Applications, 12-22, Clarendon Press, Oxford, **1987**.

Brunauer, S., Emmett, P.H. and Teller, E., Adsorption of Gases in Multimolecular Layers. J. Am. Chem. Soc., **1938**, 60, 308-319.

Greggs, J. and Jacobs, J., Trans. Faraday Soc., **1948**, 44, 574.

Haber, J., Manual on Catalyst Characterization. Pure & Appl. Chem., **1991**, 63, 9, 1227-1246.

Halsey, G.D., J. Chem. Phys., **1948**, 78, 117.

Langmuir, I.J., J. Am. Chem. Soc., **1918**, 40, 1361.

Lippens, B.C. and de Boer, J.H., J. Catal., **1965**, 4, 319.

Michail, R.Sh., Brunauer, S. and Bodor, E.E, J. Colloid Interface Sci., **1968**, 26, 45.

Micromeritrics, ASAP 2000 Accelerated Surface Area and Porosimetry System Operator's Manual. **1989**.

Richardson, J.T., Catalyst Preparation: How they are Made. In: Principles of Catalyst Development, Chapter 6, pp 95-134, Plenum Press, New York, **1989**.

Ponec,V., Knor, Z. and 'Cerny', S. (ed), Mechanisms of Physical Adsorption. in Adsorption on Solids, 419-447, Butterworth, Durban (SA), **1974**.

Sing, K.S.W., The Use of Physisorption for the Determination of Surface Area and Pore Size Distribution. in Characterization of Catalysts, Thomas, J.M. and Lambert, R.M., Ed:, 11-29, Wiley, Chichester, **1980**.

4: A STUDY OF THE EFFECT OF ALKALI METAL DOPING ON THE Cu COMPONENT OF THE CATALYST BY TPD AND XRD METHODS

4.1 INTRODUCTION

With the objective of further understanding the effect of alkali doping on the properties of our catalyst, a study of the Cu surface area and of the CuO crystallite size distribution was undertaken, using hydrogen temperature-programmed desorption (H_2 TPD) and X-ray diffraction (XRD) methods, respectively. Characterization of the Cu component is crucial as this component is related to catalyst activity [Duprez et al. 1984; Pan et al. 1988]. A review of the processes used in the study is presented with the aim of assembling a framework through which the results can be analyzed. Firstly, the chemisorption of H_2 on Cu is looked into.

H_2TPD: The understanding of the adsorption / desorption of hydrogen on copper is developing rapidly. This is matched by the speed with which this information is put to practical use. The kinetics of the process was elucidated by Anger et al. [1989]. The work of Chorkendorff and Rasmussen [1991] highlights an important property of Cu, i.e. the restructuring of Cu(100) plane due to adsorption of atomic hydrogen. Significantly it was Muhler et al. [1992] who first proposed a quantitative evaluation of the H_2 TPD spectrum on copper containing catalysts for purposes of specific copper surface area determination.

H_2 TPD is one of the many desorption methods used to probe catalyst surfaces. The method is based on the principle of chemisorption. The analysis is *in situ* and conditions under which the analyses are conducted can be very close to the industrial testing conditions. It was noted that H_2 desorption from Cu was an activated adsorption phenomenon [Anger et al. 1989]. This presented an advantage in that the desorbed gas could not readsorb thereby minimising difficulties in its detection and evaluation. This is but one advantage of the

process and hence the method.

The method is considered to be superior to the commonly used N_2O frontal chromatography in that it does not alter the structure of the catalyst. Another advantage of the method is that the nature of exposed copper crystallographic planes can be probed [Roberts and Griffin 1988; Muhler et al. 1992]. This becomes clearer in the actual calculation of the specific copper surface area is discussed in the paragraphs that follow.

The copper surface area (A) is a function of monolayer coverage (n^s_m) of Cu by H_2, the stoichiometry of H_2/ Cu (X_m) and the density of exposed Cu surface atoms per unit area (n_s). The value of n_s is related to the copper planes exposed to H_2 adsorption can be obtained from the literature [Anderson and Pratt 1985].

$$A = n^s_m X_m / n_S$$

The crucial task of H_2 TPD is to establish n^s_m. This is achieved in a number of steps. Firstly, the H_2 peak from the metallic copper is identified from the TPD trace and integrated. Then peak areas are converted to H_2 moles using a calibration factor. These are converted to n^s_m values by taking into consideration the saturation coverage of the surface at T and P conditions of the experiment [Muhler et al. 1992; Anderson and Pratt 1985]. This is the coverage when the H/Cu ratio is 1/2. For experimental conditions used, the coverage can be determined as in Anger et al. [1989]. Experimental conditions have to be chosen such that the desorption peaks are well resolved and can be integrated with acceptable accuracy. The importance of experimental conditions is apparent from the work of Bailey and Waugh [1993]. Attainment of an acceptable hydrogen desorption peak is one of the variables which can seriously affect the accuracy of the method. Apart from this drawback other problems exist too.

The main problem of the method is the value of n_s. An average of the densities of copper low index planes is used as there is evidence of H_2 adsorption on such planes in the $Cu/ZnO/Al_2O_3$ catalyst of Muhler et al. [1992]. This poses a problem in that research by Roberts and Griffin [1988] indicated that there was evidence of H_2 adsorption on the high order planes of their Cu/ZnO catalyst. This implies that, for better results, the nature of planes present should, whenever possible, be probed. This adds another complicated step to the method. The H_2 TPD method is relatively new and its accuracy and shortcomings still have to be encountered. In this work, the specific copper surface areas for blank ISO 63 catalyst batch and alkali-impregnated batches were analyzed with the aim of investigating the effect of alkali impregnation on the said area.

XRD EVALUATIONS AND CRYSTALLITE SIZES: Many definitions of crystallite size have been proposed [Allen 1981]. In this work, suitable definitions of crystallite size as used in catalysis are explored and relevant methods for measuring them are highlighted. In a supported metal catalyst, crystallite size can be equated to "diameter" (d). In this case the d is defined as a straight line whose length is confined within the boundaries of the particle and which goes through the centre of the particle. A two dimensional projection of the particle shows that such diameters vary depending on the axis of the particle considered. This means that a diameter parallel to the long axis is different from one along the shorter axis. Many different definitions of the d in relation to an axis have been adopted e.g.Martin's diameter, Feret's diameter, maximum calliper diameter etc. [Matyi et al. 1987]. An appropriate definition for any particular situation will depend on the solid measured and the reasons for measuring it. The above argument implies that different size definitions will show different numerical values for a single sample. Therefore, interpretation of the particle size data has to be treated cautiously, with due consideration given to the size definition and the method of its measurement.

Particle size measurements are only useful when distributions are considered The size distribution is a consideration of particle size as a function of its frequency of occurrence. In a particle size distribution analysis, one normally refers to average particle sizes. In this case the average means the geometrical mean [Matyi et al. 1987]. An inherent assumption is that particle shape variation is minimal.

High particle shape variation has an impact on observed particle size distribution. Quantitative particle shape analysis is still at infancy and its application on supported metal catalysts is almost non-existent. The extent of its effect on the results cannot be quantified. Generally, it has been noted that narrow shape, as compared to size distribution, has little effect on size distribution. For particles of comparable size, shape distribution broadens measured size distribution. This means that broad shape distribution will be relatively insensitive to small changes in size [Allen 1981 and references therein]. From Table 4.1, it is noted that different characterization methods determine different particle averages. In this work a "volume weighted" average is the particle size of interest. This is measured by the XRD procedure using the Debye-Sherrer method.

The Debye-Sherrer method has been used extensively in catalyst characterization. The method is based on X-ray peak broadening, which is a function of the average particle size (d) of the sample. The exact relationship is shown in Equation 4.1 below:

$$d = k\lambda/\beta.\mathrm{Cos}\theta \qquad (4.1)$$

where λ is the wavelength of monochromatic X-ray radiation, β is the particle size dependent line broadening, k is a constant which is controlled by shape of the particle and the method of evaluating the X-ray peaks i.e. be it the width at half peak height or peak area. For Gaussian peaks the value of β is evaluated from Equation 4.2.

$$\beta = B^2 - b^2 \qquad (4.2)$$

TABLE 4.1

Different definitions of the particle size distribution and methods of their determination where d is the diameter of interest and n is the frequency of occurance of d in a particle population of interest.

Name	Definition	Method of Measurement
"Volume weighted"	$\sum n_i di^4 / \sum n_i d_i^3$	Debye-Sherrer method (XRD)
Volume-Area	$\sum n_i d_i^3 / \sum n_i d_i^2$	Fourier Analysis
Radius of gyration	$\sum n_i d_i^8 / \sum n_i d_i^6$	SAXS
Surface Area	$\dfrac{\sigma/v}{\sum n_i d_i^3 / \sum n_i d_i^2}$	Chemisorption

where B is obtained from the diffractogram as the sum of β and line broadening due to the instrument (b) [Baiker 1985]. The major drawback of the method is that line broadening due to structural defects and lattice stresses are very difficult to estimate. In most cases they cannot be corrected for. In this work, no corrections were made for line broadening from lattice stresses and structural defects. It was assumed they were similar for the alkali-doped catalyst and blank catalyst batches. In this work XRD was used to determine the effect of alkali doping on the CuO crystallite size distribution. From the XRD diffraction patterns

a limited information on the nature of phases present in the catalyst bulk was extracted.

4.2 EXPERIMENTAL

XRD Analysis: X-ray diffraction powder patterns were obtained utilising a Rigaku (Model DMax-3) diffractometer equipped with a graphite monochromator. The CuKα radiation was used in all cases. The Debye-Sherrer equation was used to evaluate the CuO crystallite sizes for the blank and alkali doped catalyst batches. The peak widths of the main reflex were used in probing line broadening. Some 2θ angles of the XRD diffraction patterns were used to identify some of the phases present in the bulk of the different catalyst batches.

TPD Analysis: The H_2 TPD analysis involves three broad steps. These are catalyst reduction, H_2 chemisorption on the surface and the TPD step. Catalyst reduction was accomplished in the TPD rig shown in Figure 4.1. The tubing material of the gas flow system was stainless steel. Gas flows were controlled by Brooks mass flow controllers and Nupro valves were used to redirect gases to appropriate directions. The reduction process and TPD tests were performed on a catalyst in a reactor (R1) which could be heated or cooled, depending on the requirement. The gas which probes the surface, in this case H_2, was desorbed into a He stream and its quantity was evaluated by a TC detector.

The reduction process was similar to the method used in HAS tests with slight modifications. The gas mixture for reduction was 2% H_2 in argon, and no pressure was applied to the reactor. The experimental routine was as follows:

- Desorption of adsorbed impurities by flushing the catalyst with N_2 gas.
- Reduction with 2% H_2 in Argon over at least 24h.
- Adsorption of pure H_2 at 493K, cooling in H_2 to 250K and holding for 60min

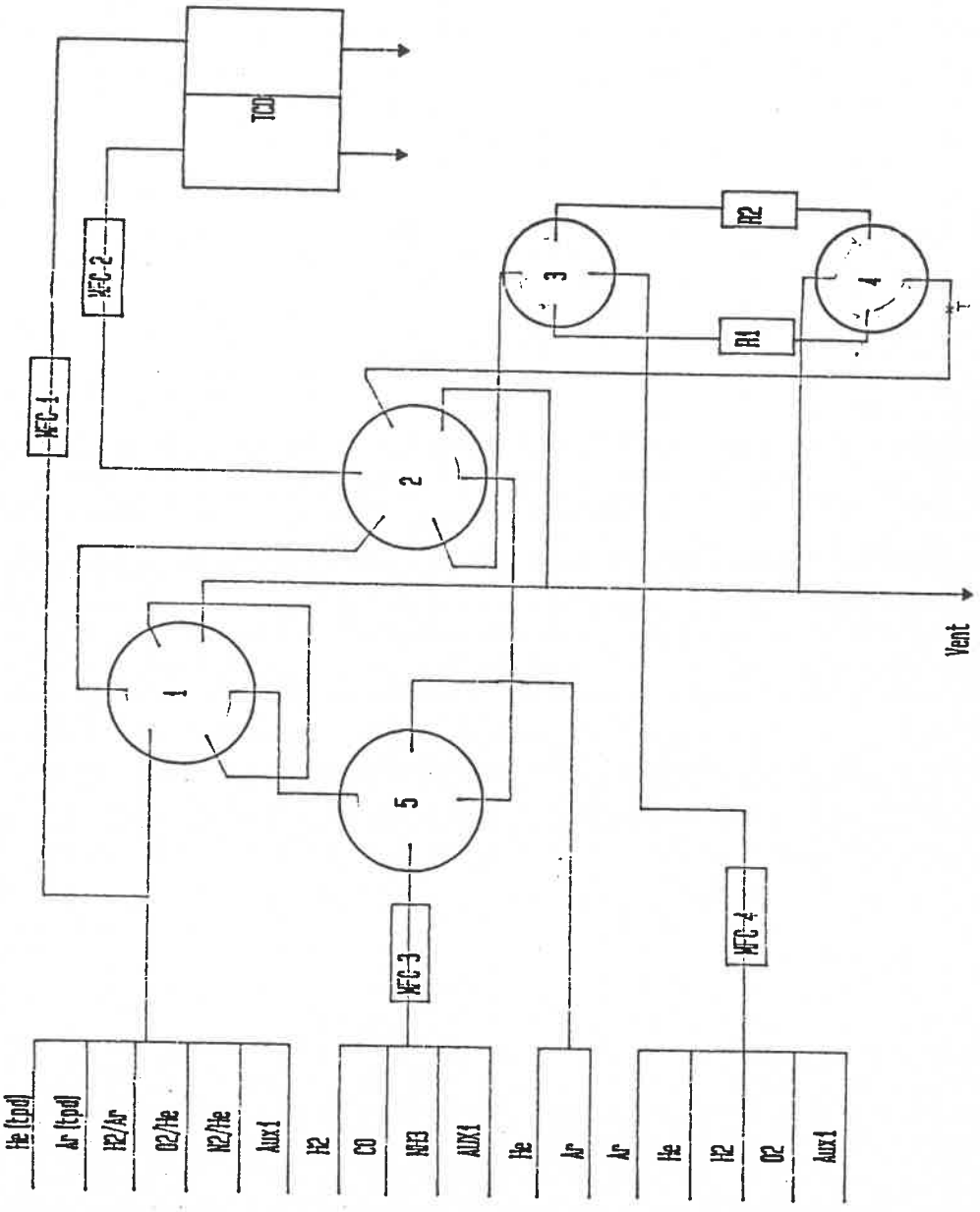

Figure 4.1: The TPD rig where the positions of the mass flow controllers (MFC1 to MFC4), valves(1 to 5), reactors (R1 and R2) and the detector (TCD) are shown.

with subsequent cooling to 78K.

- Flushing with helium so that physisorbed hydrogen was removed and finally,
- TPD was carried out with hydrogen being desorbed into a stream of helium.

This was accomplished by allowing the reactor to warm to room temperature. It was then heated gently (10° C/ min) to 350°C using a temperature programme. The quantities of hydrogen desorbed were traced by a TC detector. A print-out similar to the one in Figure 4.2 was obtained. The hydrogen desorption peak from the copper component of the catalyst was identified and integrated. The area of the peak was then related to specific copper surface area [Anderson and Pratt 1985].

4.3 RESULTS AND DISCUSSION

TPD Analysis: A TPD trace for the K doped catalyst is shown in Figure 4.2 below. The peak at about 300K was assigned to hydrogen desorbing from the copper component of the catalyst. This assignment was based on the work of Pan et al. [1988]; Roberts and Griffin [1988]; Anger et al. [1989] and Muhler et al. [1992]. The slight taper to the front of the peak is related to hydrogen desorption from the Cu(110) crystal plane [Pan et al. 1988]. The second and largest peak is due to hydrogen desorption from the Zn Type II site [Pan et al. 1988]. Since the peak is of no primary interest in this work it will not be discussed any further.

The copper surface areas of the different catalyst batches are shown in Table 4.2. Since the TPD test is **in situ** the results were expected to represent the copper surface area conditions immediately before the HAS catalytic test. The areas are very small. In all the cases investigated the Cu surface areas did not exceed 10% of the total surface area. The problem associated with the integration of the copper peaks is believed to be the main reason for this discrepancy. Nevertheless, trends which emerge from a comparison between the blank and alkali metal impregnated catalyst batches are regarded to be valid. This

can only be said if an assumption is made that there was a systematic error common to all the above results.

Comparison of the specific Cu surface area of the blank and the alkali-doped catalyst batches indicates an increase in that area as a result of the impregnation process. This is in contrast with the known fact that the specific surface area is normally decreased after impregnation because part of the alkali salts sits on the copper component of the catalyst. The above observation can only be caused by a phenomenon other than deposition of material on copper surface. In Chapter 5, the pH of the impregnating solutions and the effect of the high calcination temperature will be shown to be responsible for the above behaviour of specific Cu surface area when doped with alkali metal salt solutions.

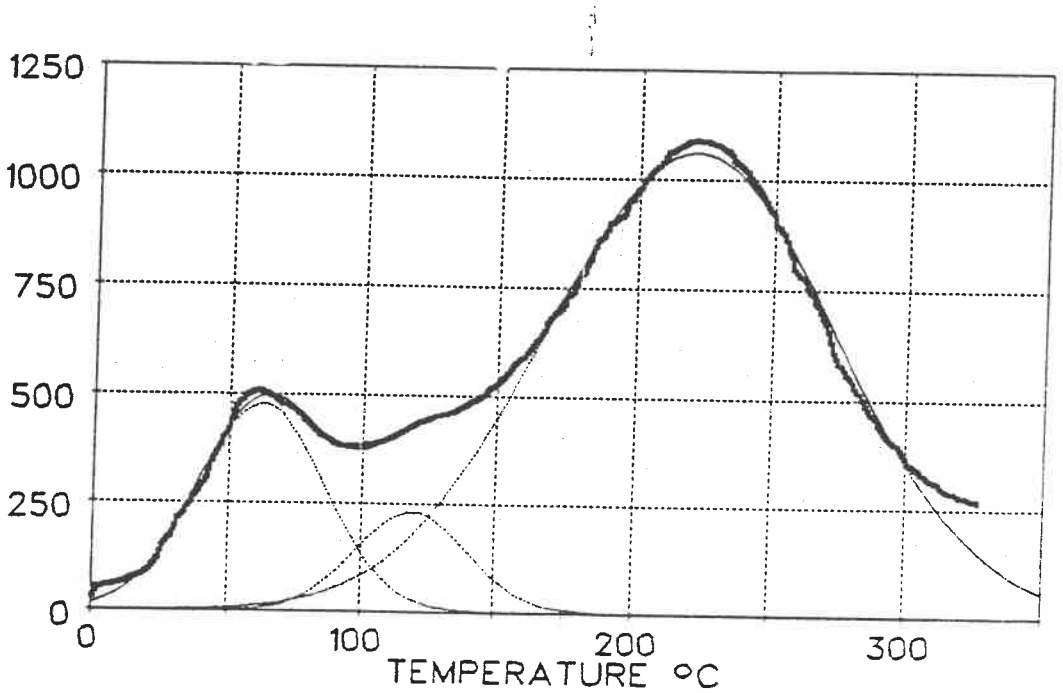

Figure 4.2: A trace of hydrogen desorption from the copper and zinc components of the Cu/Zn/Cr catalyst impregnated with potassium formate.

The extent of the specific Cu surface area change as a result of alkali-doping

proceeds in the following order:

$$Rb > Li > K > Cs > Na$$

With the exception of K, the above pattern is the same as that observed for the external surface area determined by the BET method:

$$Rb > Li > Cs > K > Na$$

TABLE 4.2

Copper surface areas of ISO 63 impregnated with $2.26*10^{-4}$moles alkali metal/ $g_{cat.}$ for different alkali metal formates.

CATALYST BATCH	Cu Surface Area m^2/g_{cat}
ISO 63 (BLANK)	3.09
ISO 63 + Rb	4.47
ISO 63 + Li	4.22
ISO 63 + Cs	4.04
ISO 63 + K	3.83
ISO 63 + Na	3.65

The above trends show that processes that affect the external surface area, as detected by the BET method, affected the specific copper surface area in the same way. It appears that the overall increase in the Li and Rb impregnated

catalyst batches could in part be related to copper surface area enrichment in those batches. This will be shown later to be related to catalyst treatments that accompany impregnation processes not the actual deposition of alkali metal dopants on the surface.

XRD Analysis: An XRD diffraction pattern of a Cu/Zn/Cr catalyst impregnated with Cs is shown in Figure 4.3. The pattern reveals the presence of ZnO and CuO peaks. This clearly shows that the bulk of the calcined catalyst is dominated by the oxides of the metals constituents. The zincite peaks at 2θ angles of about 30 and 36 are preceded by shoulders. The shoulders are found at the 2θ angles 30.3 and 35.5. The above angles indicate the presence of the

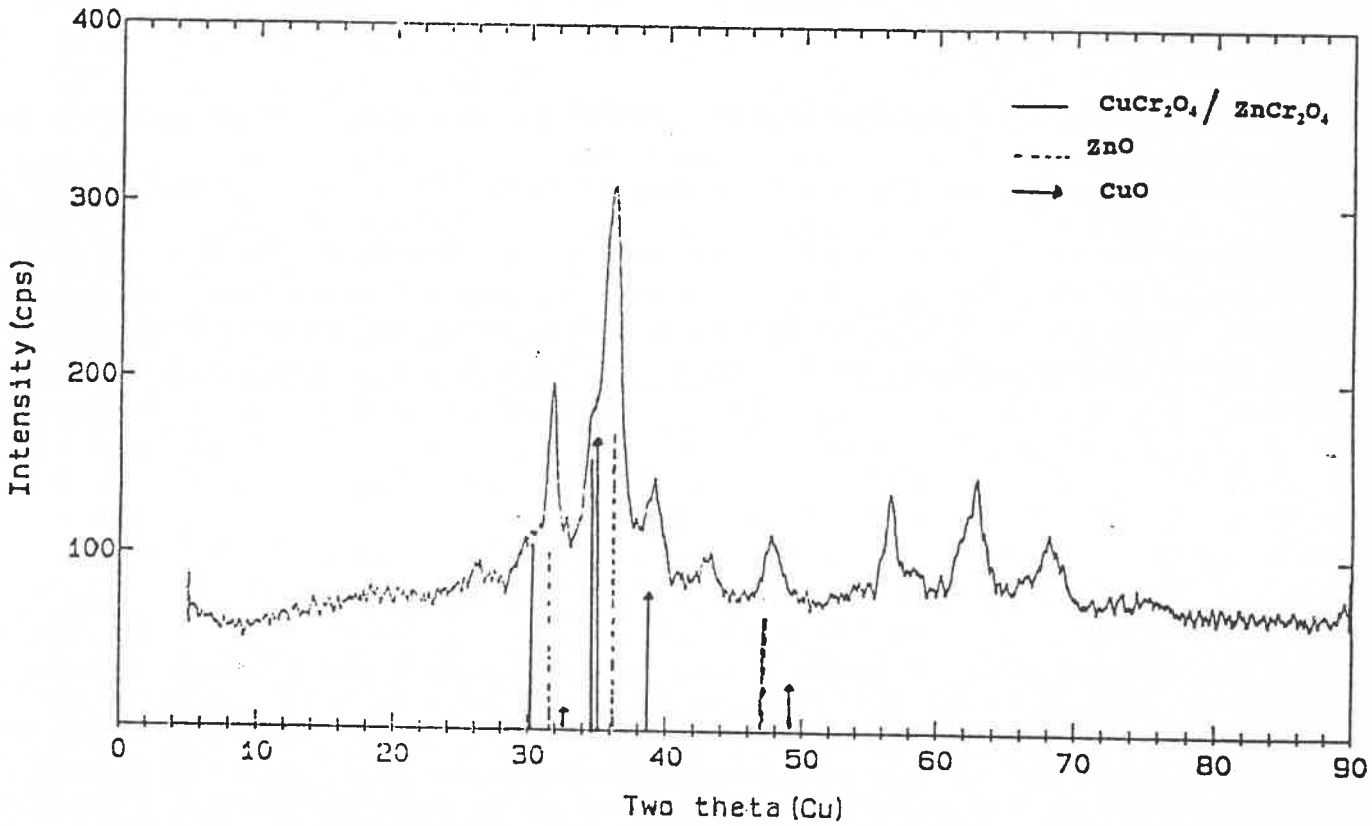

Figure 4.3: XRD pattern for ISO 63 + 3% Cs, showing the reflections of the CuO, ZnO and $CuCr_2O_4/ZnCr_2O_4$ spinel(s).

$CuCr_2O_4$ / $ZnCr_2O_4$ spinels.

All the alkali metal impregnated catalyst batches showed XRD diffraction patterns similar to that in Figure 4.2. One can deduce that the above phases can be found in all the catalyst batches.

TABLE 4.3

Average crystallite sizes of CuO in the Cu/Zn/Cr catalyst samples impregnated with different alkali metal formates.

IMPREGNATING FORMATE	CuO CRYSTALLITE SIZE (Å)
ISO 63 (BLANK)	50
ISO 63 + Cs	79
ISO 63 + Rb	72
ISO 63 + K	77
ISO 63 + Na	80
ISO 63 + Li	84

The average CuO crystallite sizes for catalyst batches impregnated with different alkali metals are summarized in Table 4.3. It appears that alkali impregnation increased the CuO crystallite size. From the table it can be seen that copper exists as small crystallites in all catalyst batches. The differences in the CuO crystallite size increase for the different alkali-impregnated batches is not clear at the moment. The effect could be the result of dissolution of alkali metals in CuO [Slaa and references in 1991]. It is evident from the above results that the near optimal HAS catalyst has CuO crystallite size of 78 ± 6 Å in diameter, which is comparable to that of the active industrial methanol synthesis systems.

4.4 CONCLUDING REMARKS

It is concluded that alkali doping processes (not the actual deposition of alkali metal dopant on the copper component of the catalyst surface) increased the specific copper surface area. The correlation between the BET external surface area change due to alkali doping with specific copper surface areas of the alkali doped catalysts, supports the above assertion. It will later be shown that the pH of the impregnating solution and the calcination and drying procedure affect the two surface areas in the same way. It is again concluded that alkali impregnation increased the CuO crystallite size. The near optimal HAS catalyst has an average CuO crystallite size of 78 ± 6 Å in diameter. It was shown that at least three phases i.e. CuO, ZnO and $CuCr_2O_4$ / $ZnCr_2O_4$ constitute part of the bulk of the catalyst.

4.5 REFERENCES

Allen, T.,(ed), Particle Size Measurement, Chapman and Hall, London, **1981**.

Anderson, J.R. and Pratt, K.C., Surface Area Measurement, In: Introduction to Characterization and Testing of Catalysts., 1-49, Harcourt Brace Jovanovich, Sydney, **1985**.

Anger, G., Winkler, A. and Rendulic, K.D., Adsorption and Desorption Kinetics in the Systems H_2/Cu(111), H_2/Cu(110), H_2/Cu(100). Surface Science, **1989**, 220, 1-17.

Baiker, A., Experimental Methods for the Characterization of Catalysts.II. X-ray Diffraction, Temperature-Programmed Desorption and Reduction, Thermogravimetry and Differential Thermoanalysis. Intern. Chem. Eng., **1985**, 25, 1, 30-37.

Bailey, S. and Waugh, K.C., Comment on the Use of Temperature-Programmed Desorption of H_2 as a Tool to Determine Metal Surface Area of Cu Catalysts. Catal. Lett., **1993**, 371-374.

Chorkendorff, I. and Rasmussen, P.B.,Reconstruction of Cu(100) by Adsorption of Atomic Hydrogen. Surface Science, **1991**, 248, 35-44.

Duprez, D., Barbier, J., Ferhart.Hamida and Bettahar, M., Characterization of Copper-Zinc Catalysts by Hydrogen Thermodesorption. Appl. Catal., **1984**, 12, 219-225.

Matyi,R.J., Schwartz, H.L. and Butt. J. B., Particle Size, Particle Size Distribution, and Related Measurements of Supported Metal Catalysts. Catal. Rev.-Sci. Eng., **1987**, 29, 1, 41-99.

Muhler, M., Nielsen, L., Tornqvist, E., Clausen, S.B. and Topsoe, H. Temperature-programmed Desorption of H_2 as a Tool to Determine Metal Surface Areas of Cu Catalysts. Catal. Lett., **1992**, 14, 241-249.

Pan, W. X., Cao, R., Roberts, D.L. and Griffin, G.L., Methanol Synthesis Activity of Cu/ZnO Catalysts. J. Catal., **1988**, 114, 440-446.

Roberts, D.I. and Griffin, G.L. Temperature-Programmed Desorption and Infrared Study of CO and H_2 Adsorption on Cu/ZnO Catalyst.J. Catal., **1988**, 110, 117-126.

Slaa, J.C., $Cu/ZnO/Al_2O_3$-based Catalysts for the Synthesis of Methanol and Higher Alcohols from H_2 and CO. PhD Thesis, Catalytic Processes and Materials Group, Faculty of Chemical Technology, University of Twente, AE Enschede, The Netherlands, **1991**.

5: AN INVESTIGATION OF THE EFFECT OF ALKALI DOPING ON THE CHEMICAL PROPERTIES OF THE Cu/Zn/Cr CATALYST USING XPS

5.1 INTRODUCTION

In this discussion the concepts of X-ray photoelectron spectroscopy (XPS), including binding energies (BE's) and chemical shifts, are critically reviewed. Special attention is paid to their use in characterizing catalysts. Aspects of the discussion which directly relate to our investigations will be highlighted.

The principle behind XPS is photoemission. Irradiation of a sample with X-rays of sufficient energy results in the emission of electrons from its atoms and molecules. These electrons are referred to as photoelectrons. Their kinetic energy (E_{KE}) is a function of the photon energy of the irradiating X-rays ($h\nu$), the Fermi-referenced binding energy and the work function of the spectrometer (Φ_{SP}). Therefore, the BE can, in fact, be expressed as follows [Baiker 1985; Delgass et al. 1979; Ebsworth 1984; Mouler et al. 1992]:

$$BE = h\nu - E_{KE} - \Phi_{SP} \qquad (5.1)$$

The magnitude of an electron's BE is dependent on its atom of origin and its electronic energy level. These are different and unique for different atoms. Tabulated BE values for different elements with their different electron energy levels are now available [Mouler et al. 1992]. Comparisons of experimental and tabulated values of BE's can be used to determine the atomic constituents of samples. In this way, much qualitative information can be obtained from an XPS run.

The above information can be used in catalysis to investigate the identity of surface compounds, be they catalyst components or impurities related to catalytic activity, as work by Herman et al. [1979] shows. Again, XPS has been used to investigate the presence of different chemical phases on the surfaces of

catalysts. In the work of Okamoto et al. [1983a] the presence of two unique surface phases of Cu(II) ions dissolved in ZnO phase and Zn in CuO in catalysts of certain Cu/Zn ratios were confirmed by XPS. The MoS_x-K^+/SiO_2 catalysts for higher alcohol synthesis were characterized by Hong-Bin Zhang et al. [1992]. The formation of a new phase in the working catalyst, due to potassium impregnation, was determined by XPS and confirmed by other methods. Such information is very important as it can be related to catalyst deactivation or activity. A broader picture is obtained from the quantitative analysis of materials by XPS.

The analysis of all factors contributing to the intensity of photoelectron currents (I) has been carried out by various researchers [Davies 1980; Delgass et al. 1979; Mouler et al. 1992]. Excitation cross-section (δ) of the photoelectrons, electron escape depth (λ) and its dependence on exciting energy, efficiency of the analyzer of the spectrometer, chemical and physical inhomogeneity have to be considered in the evaluation of I. For homogeneous samples the value of I, for a particular atom, can be related to the above variables, as shown in Equation (5.2) below:

$$I = k\, n\, \delta\, \lambda\, L \qquad (5.2)$$

where k is a constant, n is the number of atoms of interest per unit volume and L is the analyzer luminosity. The values of δ and λ are tabulated [Davis 1980]. The sensitivity factor (S_x) is a parameter used to evaluate atomic fraction (c_x) of atom x from measured values of I. S_x can be calculated from Equation 5.3.

$$S_x = k\, \delta_x\, E_x \qquad (5.3)$$

where E_x is the energy of the irradiating flux. The value of c_x can be obtained as shown in Equation 5.4 below.

$$c_x = (I_x/S_x)/(\sum i_i/S_i) \qquad (5.4)$$

where i is summation over all elements. For a multi-component heterogeneous catalyst the quantitative surface analysis discussed above will not show its true surface character because of its non-uniformity. Results from such surfaces will only reflect the catalyst properties analyzed on the spot and this cannot be said to be representative of the whole catalyst surface. The value of such an analysis has been extended to investigate the concentration of Cs on a Cu/ZnO catalyst by Klier et al. [1988] using a mathematical model. This is an isolated case whose success was based on the knowledge of the composition of the surface, which was very simple in that case. We wish to emphasize that characterization of heterogeneous surfaces by XPS is still at best semi-quantitative. Nevertheless, important information can be extracted from these results. Delgass et al. [1979] noted that the quantitative analysis of a heterogeneous surface could be used to study the effect of any treatment of a particular catalyst surface. A comparison of the intensity ratios of elements of interest before and after treatment can reveal the effects (chemically or physically) the treatment has had on the catalyst surface. This approach was used extensively in our study to establish whether alkali-doping of the catalyst influenced in any way the chemical and physical properties of the parent catalyst surface.

It has already been noted that the BE's of electrons in atoms at their standard environments are known. The BE of an atom's core level electron in a particular compound is influenced by the environment in which it exists. This means that the BE of an electron at a certain level e.g. Cu $2p_{3/2}$ is not only different for different copper compounds but is also not the same for a particular Cu compound in different matrices. The difference between the BE's is referred to as a chemical shift. This should not be mistaken with shifts of the BE's which are attributed to the following [Delgass et al. 1979, Ebsworth et al. 1987]:

- spectrometer
- sample effects e.g. charging, and
- energy loss processes which sometimes result in satellite peaks.

When BE is defined as the difference between the energies of a final state of a system after photoemission and its initial state, parameters which constitute a chemical shift can clearly be identified. The theoretical accounting for chemical shifts has necessarily to involve changes in both the initial and final states of the system. There is overwhelming evidence to suggest that BE's are associated mainly with the distribution of charge around atoms and molecules [Delgass et al. 1979]. Atomic charge and extra-atomic potential determine the BE of the initial state of a system. A change in the above states constitutes a chemical shift which can be detected. From this argument it is expected that the oxidation state of an atom can easily be determined from the XPS data. This indeed is the case. Atoms in higher oxidation state experience greater electron shielding of the positive charge than in lower states. As a consequence, higher oxidation state atoms exhibit chemical shifts towards higher BE's. This implies that reduction of an atom of interest will shift its BE in the opposite direction.

It follows from the above argument that the electronegativity of a counter-ion in a molecule, plays a role in explaining the chemical shifts of certain ions / ion groups, associated with the counter ions. The chemical shifts of the carbonate group in the alkali metal carbonates in the work by Sheffer and King [1989] were clearly explained by electronegativity difference among alkali metal ions. By studying their chemical shifts, certain electron transfers between atoms in certain metal interactions of catalytic materials have been determined. XPS analysis of methanol producing Cu metal promoted by lithium carbonate showed a shift of 1.2 eV in the Cu $2p_{3/2}$ line [Sheffer and King 1989]. The shift could only be explained by electron donation by Li to Cu. Results from the XPS work of Okamoto et al. 1983b, on the Cu/Zn catalyst, provide evidence of electron transfer from Zn to Cu in catalyst batches of lower Cu content.

Campbell et al. [1992] studied the properties of ultrathin Cu and Pd films on different metal substrates. XPS and other methods were used to determine the nature of the substrate-overlayer bonds. The chemical shifts of the peaks of the overlayer compound e.g. Cu $2p_{3/2}$ showed that if the overlayer was electron deficient as compared to the substrate, there would be electron donation from the substrate to the overlayer and vice versa. In this context, electron deficient substances were those whose valence d-bands were "less than half occupied". In this way the direction of charge transfer between the overlayer and the substrate and the nature of the bond between the two could be studied. The above facts are widely used in catalysis where the composition of surface compounds has to be determined. In this work the concept of chemical shifts is extensively used in determining the chemical states i.e. oxidation states and possible counter ions of the different atoms of interest.

A product of an XPS analysis is a spectrum which reflects the BE's of atoms of compounds present in a sample as functions of intensities of their photoelectron currents (I). Additionally, XPS spectra are characterized by the presence of satellite and split peaks. The latter are associated with 3d metals. Configuration interactions, discrete energy losses in the irradiated samples e.g. plasmon formations, unchromated radiation sources and "shake-ups" (where an atom gets excited without releasing a photoelectron) [Delgass et al. 1979] are some of the causes of satellite peaks. Peak splitting is attributed to spin-orbital coupling and exchange interactions between unfilled valence electrons and electrons in the core level which suffered photoemission [Mouler et al. 1992]. These features are documented for various atoms and should always be recognised in XPS spectra because failure to do so leads to incorrect chemical identifications. This factor was taken into consideration in interpretations of our XPS spectra.

Satellite peaks have been used in studies of some catalyst surfaces. For instance, the ratio of a satellite peak to the parent peak (I_s/I_p) was used by Okamoto et al. [1983b] to demonstrate variation of bonding between Cu^{2+} and

its matrix. The authors demonstrated that the nature of interactions was dependant on the CuO composition in ZnO. This was achieved by using the $Cu(2p_{3/2})$ band as the parent peak. The above example clearly shows that a lot of effort is devoted to exploiting all aspects of XPS to the benefit of the analyst. It is recognised that the method has not been utilized to its full potential. Some problems which still have to be overcomed are discussed below.

An appreciation of the limitations and strengths of the XPS technique is central if a catalytic chemist is to derive maximum benefit from the method. We already have mentioned that for heterogeneous catalysis XPS method is essentially only semi-quantitative in nature. The limitations associated with this have already been elucidated. Since XPS analysis requires semi-vacuum conditions, it cannot be used to analyze surfaces under dynamic reaction conditions.

The depth to which a surface can be probed is between 0.5 to 3nm [Davies 1980]. This implies that the method is essentially a surface analysis technique. Although this is an important aspect of the method, it has its drawbacks too. For highly porous catalysts, a large part of their surface areas lie deep in the pores. Therefore, analysis by XPS may fail to elucidate completely the nature of such surfaces. This calls for extreme caution when interpreting such results. Again, XPS has to be used in conjunction with ion sputtering techniques for a depth profile analysis of a sample, as the method alone cannot achieve this.

It has been found that certain elements in different oxidation states cannot be distinguished by BE alone as they show similar BE values. The compounds Fe_2O_3 and Fe_3O_4 have similar BE values [Davies 1980]. The same applies to Cu^0 and Cu^I and Mo^{IV} and Mo^V in certain complexes [Ebsworth et al. 1987]. Currently, an acceptable method for distinguishing between the Cu^0 and Cu^I is the use of Auger parameters [Sheffer and King 1989]. We see an increasing tendency to use XPS in conjunction with other methods to extend its value. This trend is likely to increase in the future and XPS will undoubtedly emerge as a very

important tool in catalyst design and characterization. In this study XPS is used to evaluate the effect of alkali doping on the surface properties of our catalyst.

5.2 EXPERIMENTAL

The XPS analysis was conducted using a VG ESCALAB MkII spectrometer. Magnesium Kα radiation (1253.6 eV) at an angle of 45°, at 15kV/20mA was used in analyzing all the catalyst batches. In exceptional cases aluminium Kα radiation (1486.6 eV) was employed to verify BE's of some compounds. A pass energy of 50 eV was used for wide scans and 20 eV for narrow scans. The slit is three-by-six in width. Linear background subtraction and a least-square fitting procedure were used to determine the peak positions, line widths and peak areas.

The effects of charging were studied and corrected for by plating samples with 15Å Au. The 4f Au line was assumed to have a BE of 84.0 eV [Mouler et al. 1992]. All the peak binding energies were referenced to C 1s peak of CH_x whose BE was taken as 284.7 eV [Hong-Bin Zhang et al. 1992; Mouler et al. 1992]. The CH_x was assumed to be associated with or related to sodium acetate which was used in catalyst preparation. This carbon species found in all catalyst batches was used as an internal standard.

Sample treatment was simple and involved two basic steps. Samples were mounted using adhesive tape where volatile and adsorbed gases were desorbed from the surface by evacuation techniques. Surface sputtering by argon gas was performed only on the blank sample to confirm the presence of carbon in the body of the catalyst. The quantitative analysis without standards has an uncertainty of 10% which improves to less than 5% in the presence of standards.

5.3 RESULTS

TABLE 5.1

XPS results of ISO 63 catalyst (blank) showing different compounds, values of BE's of their peaks and their atomic percentages (At %).(The same information is shown for ISO 63 + Li (Table 5.2), ISO 63 + Na (Table 5.3), ISO 63 + K (Table 5.4), ISO 63 + Rb (Table 5.5) and ISO 63 + Cs (Table 5.6))

ELEMENT	PEAK eV	At %	COMPOUND
Cu $2p_{3/2}$	933.5	1.2	CuO
Zn $2p_{3/2}$	1021.8	8.1	ZnO
Cr $2p_{3/2}$	574.6	0.3	Cr^0
Cr	576.5	2.5	Cr_2O_3
Cr	579.9	2.4	Na_2CrO_4
Na 2s	63.0	2.5	Na_2CrO_4
C 1s (1)*	280.3	10.0	?
C (2)	282.9	8.8	Cr_3C_2 / ?
C (3)	284.7	12.5	CH_x
C (5)	287.8	3.3	CO_3^{2-}
O_{1s}	531.1	48.5	CuO, ZnO, Cr_2O_3

* carbons were numbered from one to five for convenience.

TABLE 5.2: ISO 63 + Li

ELEMENT	PEAK eV	At %	COMPOUND
Cu	933.7	1.4	CuO
Zn	1021.9	6.7	ZnO
Cr	574.5	0.5	Cr^0
Cr	576.4	1.5	Cr_2O_3
Cr	578.0	3.1	Na_4CrO_4
Cr	579.9	2.2	Na_2CrO_4
C(1)	281.1	6.4	?
C(2)	282.5	3.9	Cr_3C_2/?
C(3)	284.7	5.7	CH_x
C(4)	286.1	3.2	?
O	531.1	65.2	CuO, ZnO, Cr_2O_3
Li	56.0	0.2	Li_2O

TABLE 5.3 ISO 63 + Na

ELEMENT	PEAK eV	At %	COMPOUND
Cu	933.1	1.4	CuO
Zn	1021.5	9.3	ZnO
Cr	575.9	0.4	Cr_2O_3 / Cr(O)
Cr	577.3	3.4	$ZnCr_2O_4$ $CuCr_2O_4$ $NaCrO_2$
Cr	579.2	2.3	$Na_2Cr_2O_7$
Na 2s	62.9	7.8	$Na_2Cr_2O_7$ Na_2CrO_4 $NaCrO_2$
C (1)	280.9	7.1	?
C (2)	282.3	4.4	Cr_3C_2 / ?
C (3)	284.7	6.5	CH_x
C(5)	288.7	1.6	CO_3^{2-}
O	530.2	55.3	CuO, ZnO, Cr_2O_3

TABLE 5.4: ISO 63 + K

ELEMENT	PEAK eV	At %	COMPOUND
Cu	934.2	2.8	$CuO/CuCr_2O_4$
Zn	1022.1	11.6	$ZnO, ZnCr_2O_4$
Cr	575.5	0.8	Cr^0
Cr	577.3	3.9	$ZnCr_2O_4, Cr_2O_3$
Cr	580.0	3.9	Na_2CrO_4 $Na_2Cr_2O_7$
Na	63.2	2.7	Na_2CrO_4 $Na_2Cr_2O_7$
C(1)	280.6	5.6	?
C(2)	282.6	1.9	Cr_3C_2
C(3)	284.7	1.9	CH_x
C(4)	287.3	1.6	?
K $2p_{3/2}$	293.2	0.5	
O	531.3	61.2	CuO, ZnO, Cr_2O_3

TABLE 5.5: ISO 63 + Rb

ELEMENT	PEAK eV	At %	COMPOUND
Cu	934.5	3.0	CuO, $CuCr_2O_4$
Zn	1022.0	13.4	ZnO, $ZnCr_2O_4$
Cr	577.0	0.8	$CuCr_2O_4$ $ZnCr_2O_4$ $NaCrO_2$, Cr(O)
Cr	580.5	3.4	Na_2CrO_4
Na	64.5	3.1	$NaCrO_2$
C(1)	281.1	6.2	?
C(2)	283.1	2.4	Cr_3C_2 / ?
C(3)	284.7	1.4	CH_x
C(4)	286.6	2.4	?
Rb	110.6	3.2	
O	531.3	56.1	CuO, ZnO, Cr_2O_3

TABLE 5.6 ISO 63 + Cs

ELEMENT	PEAK eV	At %	COMPOUND
Cu	932.6	1.8	Cu_2O
Zn	1021.3	11.0	ZnO
Cr	574.4	1.0	Cr
Cr	576.7	3.5	Cr_2O_3
Cr	579.0	1.3	$Na_2Cr_2O_7$
Na	63.5	3.3	Na_2CrO_4
C(1)	281.2	5.2	?
C(2)	282.7	3.3	Cr_3C_2 / ?
C(3)	284.7	3.7	CH_x
C(5)	289.2	2.2	CO_3^{2-}
Cs	724.9	7.7	Cs_2O
O	529.9	56.0	CuO, ZnO, Cr_2O_3

5.4 DISCUSSION

In Figure 5.1 below an XPS spectrum and identification of peaks is shown. In the catalyst batches tested, the presence of the following elements is common to all; Cu, Zn, Cr, Na, C and O. This is no surprise because the catalyst was prepared with compounds that were composed of the above elements.

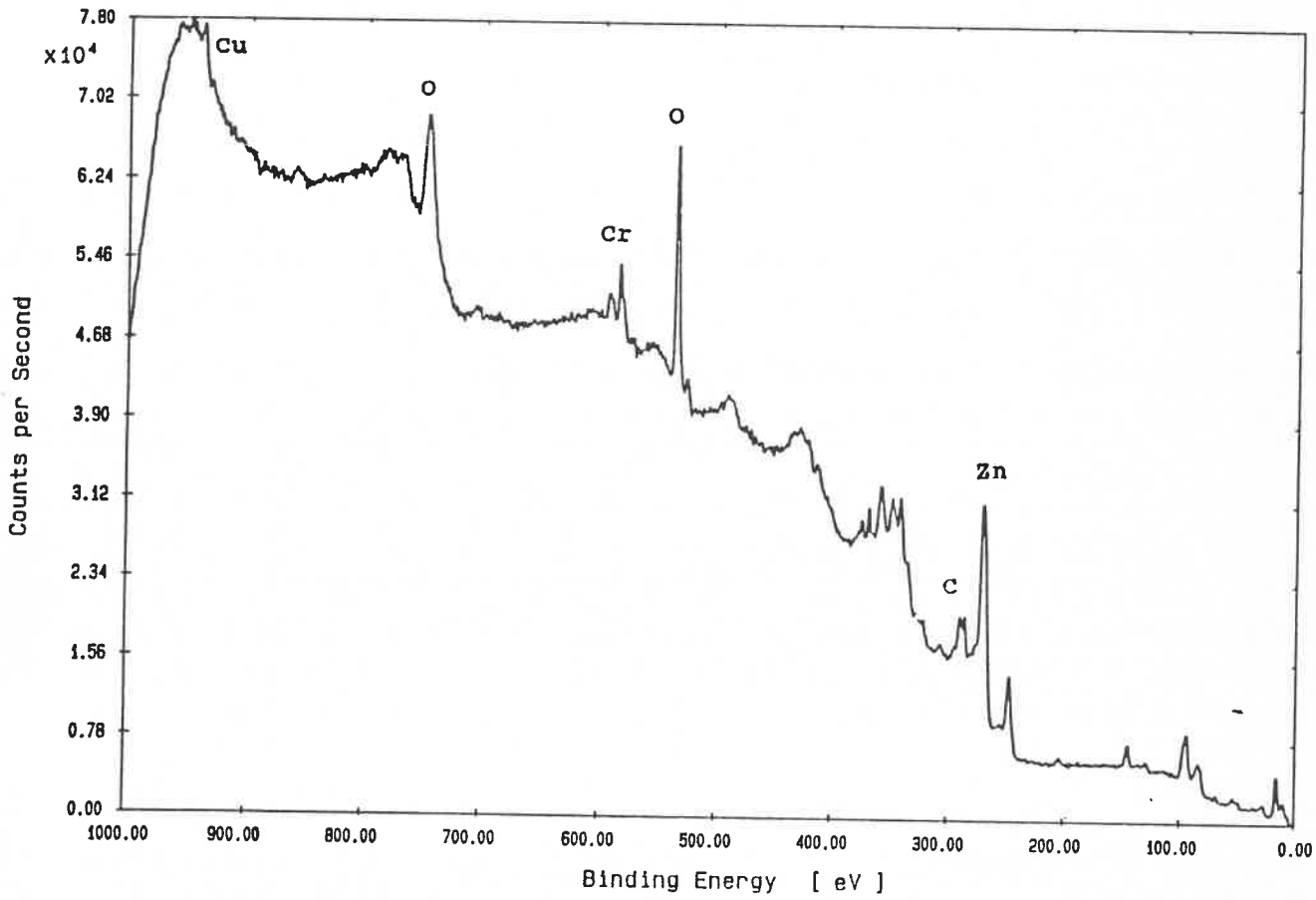

Figure 5.1: The XPS spectrum of the blank ISO 63 catalyst showing peaks of the different elements in the catalyst.

The relative atomic percentages of Cu, Zn and Cr on the catalyst surface are shown in Table 5.7 for all catalyst batches tested. The results in the table are ratios of atomic percentages of individual elements relative to the copper atomic percentages in individual tests. The catalyst was designed to be 38% in Cu,

38% in Zn and 24% in Cr. The difference in the surface composition of the blank batch and the composition of the catalytic material mirror the difference between

TABLE 5.7

Relative atomic percentages of Cu, Zn and Cr (taken as the ratios of atomic percentages of each element to that of Cu) in the surface layers of the different catalyst batches.

Element	Doping Metal					
	blank	Rb	K	Li	Na	Cs
Cu	1	1	1	1	1	1
Zn	7	5	4	5	7	6
Cr	4	1	3	5	4	3

the bulk and the surface of the catalyst. From Table 5.7 it can be seen that the relative ratios of Cu, Zn and Cr are similar for the Na-doped and blank catalyst batches although the former has higher atomic percentages than the latter (see Tables 5.1 and 5.3). The Cs, Rb, K and Li catalyst batches show either a Cu or a Cr concentration increase on the surface. It is noted that of all six cases, the Rb-doped catalyst batch has the highest surface atomic percentages of the three basic elements (see Table 5.5). This shows that the alkali doping of the catalyst was accompanied by a change in the composition of the surface.

The pH of different impregnating formate solutions and calcination temperatures are shown in Table 5.8. Save for the Rb solution, all the other impregnating solutions showed an acidic pH. This is mainly due to formic acid being a little in

excess of the carbonate / bicarbonate salts. The acidic pH of the solutions is conducive for dissolution of catalyst CuO, and this, in conjunction

TABLE 5.8

The pH of formate solutions used in alkali-doping of different catalyst batches and conditions under which they were calcined.

Formate Solution	pH	Calcination conditions Time (h)	Temper. (°C)
Li	4.03	1.66	350
Na	4.11	1.16	350
K	4.02	1.16	350
Rb	8.61	1.25	390
Cs	4.26	1.15	350

with its subsequent deposition on the catalyst surface might explain its relative percentage increase on the surface in all catalyst batches. The basic pH of the impregnating solution of the Rb salt is favourable for Zn solvation and its ultimate deposition on the surface after the drying process [Vedage et al. 1983]. We believe that the above phenomenon happened. The pH of the impregnating solution was one of two factors that influenced the composition of the surface of the catalysts. The other factors related to the change of catalysts' surface composition is the calcination heat.

Comparison of the blank and alkali metal doped catalyst in Table 5.9 shows that the total atomic percentage of carbon decreased with alkali doping. An in-depth

analysis of carbon highlights the reasons for this behaviour. The sources of carbon in the catalyst are the sodium carbonate precipitant, sodium acetate buffer and the formates of the alkali metal dopants. Under calcination conditions the acetate is likely to decompose as follows [Pearson and Stephenson 1981]:

$$2Na\text{-}O\text{-}CO\text{-}CH_3 = (CH_3)_2CO + Na_2CO_3 \qquad (5.5)$$

TABLE 5.9

Relative atomic percentages of different carbon species in the surface layers of the blank and alkali doped batches, where the atomic percentages are relative to the C(3) carbon in the Rb-doped catalyst.

Carbon	Doping Metal					
	blank	Li	Na	K	Rb	Cs
C(1)	7	5	5	4	4	4
C(2)	6	3	3	1	2	2
C(3)	9	4	5	1	1	3
C(4)	-	2	-	1	2	-
C(5)	3	-	1	-	-	2
At % C	34.8	19.1	19.7	12.5	12.2	14.4

The formate salts are likely to decompose as summarized below [Mark et al. 1972]:

$$2HCOONa = (COONa)_2 + H_2 \quad (5.6)$$

$$(COONa)_2 = CO + Na_2CO_3 \quad (5.7)$$

$$Na_2CO_3 = Na2O + CO_2 \quad (5.8)$$

Five carbon atoms in unique chemical and electronic environments were identified (Tables 5.9). The C(1) carbon has a BE which indicates that it is in the same chemical and electronic environment as a carbon in $Cr(CO)_6$. The positive identity of the C(1) compound could not be confirmed. The C(2) carbon was found to be carbon in Cr_3C_2. The formation of the carbide is facilitated by the presence of heat and CO as shown in the reactions 5.6 and 5.7. The C(3) carbon is proposed to be that of a methyl group or its derivative. The C(4) carbon for the Li- and Rb-doped catalyst batches could not be identified. The C(5) carbon was from a carbonate which could be part of a remaining hydroxycarbonate catalyst precursor.

In the XPS analysis of the blank and the Li-, Na- and Cs-doped catalyst batches the C(1) and C(3) carbons show a one-to-one ratio. This means they could be derived from a single compound i.e. the acetate ion. In the case of the Rb- and K-doped catalyst the above relationship is not as clear-cut, probably due to interconversion / decomposition and loss of one of the two carbons. Alkali-doping of the catalyst batches increased the relative atomic percentages of the C(1) carbon in all catalyst batches. This is interpreted as an indication of the fate of the carboxyl group of the formate ion and possibly the acetate ion too. All carbon atoms of the carboxyl group of the acetate or a fraction thereof might have ended up as C(1) atoms or compound(s). In Equations 5.5, 5.6, 5.7 and 5.8 it is apparent that volatile compounds of carbon are products of the reactions. This shows that the heat of calcination results in the loss of carbon of the catalyst. Therefore, the resultant loss of carbon is one of the factors that change the composition of the catalyst surface.

In all cases tested, C(5) has the lowest ratio of all carbons. The presence of C(5) in small quantities is understandable when it is seen in the context of it resulting from the carbonate of the remaining hydroxycarbonate. Much of it would have been lost as CO_2 in the two calcination processes (See Figure 5.2). In the sample batches of the Cs- and Na-doped catalysts, a carbonate peak was identified. The presence of the carbonate of an incompletely decomposed hydrotalcite in this type of catalyst is very important as work by Nunan et al. [1989b] attests. A closer inspection of their result is in order.

The metal ion and carbonate compositions of the $CuO/ZnO/Al_2O_3$ and $CuO/ZnO/Cr_2O_3$ from the work of Nunan et al. [1989] is shown in Table 5.10.

TABLE 5.10

The compositions of the metal ion species and the carbonate species in the Al and Cr based CuO/ZnO catalyst calcined at 350°C for 3h (From Nunan et al. [1989b]).

	Metal composition, atom %			
Catalyst	Cu^{2+}	Zn^{2+}	M^{3+}	CO_3^{2-} / M^{3+}
$CuO/ZnO/Al_2O_3$	30.2	45.6	24.1	0.48
$CuO/ZnO/Cr_2O_3$	29.1	46.6	24.3	0.12

The compositions of the catalysts shown in Table 5.10 were determined before they were impregnated with a solution of Cs. It appears that the Al-containing catalyst had high quantities of remaining carbonate from the hydrotalcite

precursor when one recognizes the fact that a ratio of CO_3^{2-} / M^{3+} = 0.5 means that no carbonate decomposed. The two catalysts in Table 5.10 were impregnated with a Cs solution and tested for HAS. The Cs-doped Al-containing catalyst lost activity as a result of the impregnation process. It was established that the Al-containing catalyst restructured with concomitant loss of activity and surface area [Nunan et al. 1989a]. The reason for that behaviour was the presence of large quantities of the undecomposed hydrotalcite precursor which had its carbonate ions intact but was deficient in water and hydroxyl ions. The

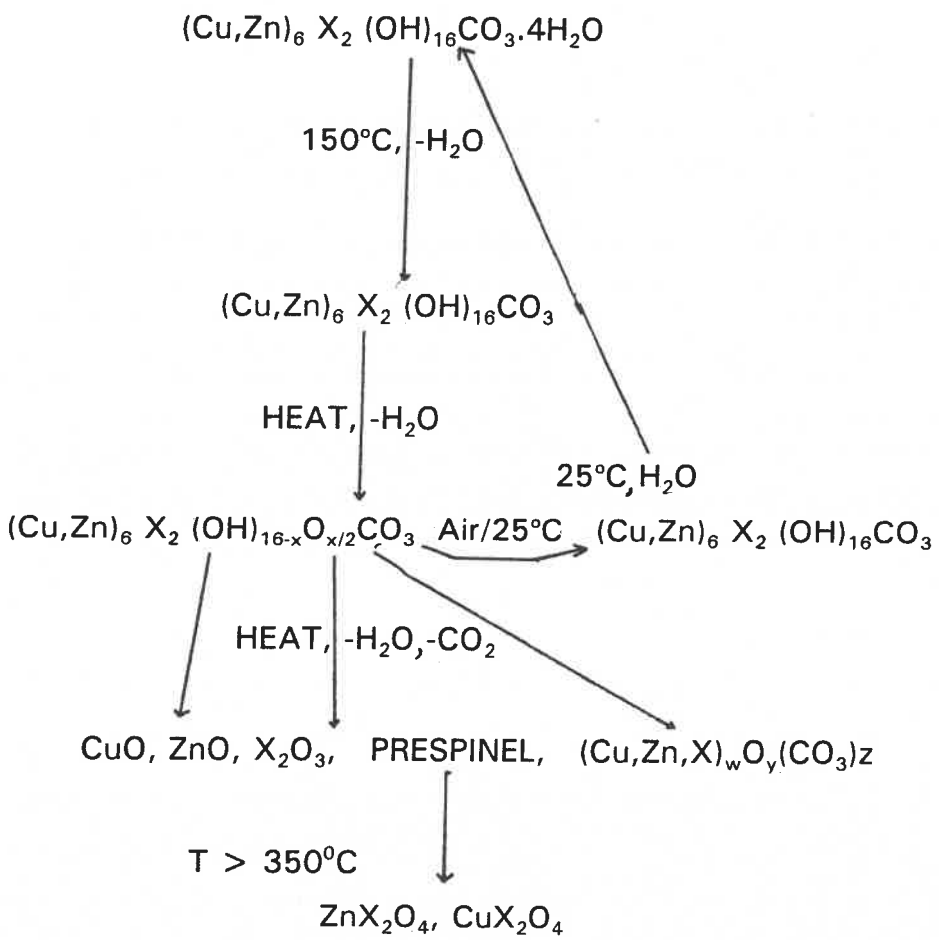

Figure 5.2: Possible decomposition routes of a hydrotalcite-type precursor where X could be Al/Cr with X = Al showing a high tendency to restructure in contact with water [Ross and Kodama 1967, Taylor 1973, Nunan et al. 1989b].

restructuring was triggered by water of the impregnating Cs solution.

It follows from the above argument that the Cr-containing catalyst should suffer minimal restructuring under the above conditions since its CO_3^{2-} / M^{3+} is only 25% of that of the Al-containing catalyst. It is our opinion that the carbonate species detected in our Cs- and Na-doped catalyst could have led to limited restructuring and loss of some external surface area in these catalyst batches. This phenomenon is believed to be the overriding factor in the loss of external surface area in our catalyst batches impregnated with Cs, Na and K formate solutions. Since the loss of external surface area could not be related to the chemical properties of the impregnating salts, it is believed that it is encouraged by the presence of the said phase and water from the impregnating solution.

Figure 5.2, which is a modified version of Nunan's diagram [1989b], highlights other important aspects of the calcination process. This process leads to the formation of the normal oxides; CuO, ZnO and Cr_2O_3. The spinels, $CuCr_2O_4$ and $ZnCr_2O_4$ form during the calcination process. The formation of the spinels is evident in the K, Rb, Na and Li catalyst batches. Although they were not detected in the XPS results of the Cs-doped and blank batches, we think they occurred in all catalyst batches. When the catalyst samples from the blank and Li-doped catalyst batch were dissolved in dilute acid, in a preliminary step for Na analysis by AAS, some portions of the catalyst could not be dissolved. The weak-acid-insoluble portions of the catalytic material could be the spinel phases [Cornthwaite 1972].

The spinels have been shown to be active in methanol synthesis [Cornthwaite 1972; Di Conca et al. 1984], but it cannot be said with certainty that they were active in methanol synthesis in our catalyst, under the reaction conditions we used. Their formation is preceded by the formation a prespinel phase [Nunan et al. 1989b] and this is enhanced by temperatures greater than 350°C. This explains the prominence of spinels in our Rb-doped catalyst batch. By promoting

the formation of this spinels, the high temperature plays a certain role in changing the catalyst surface composition.

According to the XPS results, chromium exists in this catalyst as oxides, chromates and zero valent chromium. The Cr_3C_2 and C(1) formation could have been prompted by the presence of CO as shown in Equations 5.5 and 5.6. The C(1) carbon whose BE indicates that it is in the same chemical and electronic environment as the carbonyl carbon in $Cr(CO)_6$ could account for some fraction of the zero valent chromium. Hydrogen might reduce some metal oxides to their respective metals. The bulk of the chromium is expected to be Cr_2O_3 whose green colour was diagnostic of its presence in all catalyst batches.

All catalyst batches show the presence of Na_2CrO_4, whose yellow colour was distinct in all alkali doped catalyst batches. One possible way for its formation could be through the oxide route shown in Equation 5.9:

$$Cr_2O_3 + 4Na_2CO_3 + O_2 = 4Na_2CrO_4 + 4CO_2 \qquad (5.9)$$

Some exothermic processes during the calcination process might provide the necessary energy for the above reaction.

The presence of a dichromate in some catalyst batches is noted. Its formation can be explained in terms of the presence of an equilibrium between sodium chromate and dichromate in both acidic and basic media as documented by Cotton and Wilkinson [1980]:

$$Cr_2O_7^{2-} + H_2O = 2HCrO_4^- \text{ (pH 4 to 6)} \qquad (5.10)$$

$$Cr_2O_7^{2-} + OH^- = HCrO_4^- + CrO_4 \text{ (basic pH)} \qquad (5.11)$$

The above acidic and basic conditions were noted in different batches of the

catalyst. From the Equation (5.8) above, it seems that alkali metals impregnated on the surface as formates are likely to be oxides at the start of HAS reaction. Only Cs and Li could possibly be said to exist as oxides on the catalyst. The quantities of alkali metal formates on the surface vary from zero for Li to around 8% (atomic) for Cs. The Li result is not a surprise since at least one group (Vedage et al. 1983) found that the metal migrated into the catalyst body after impregnation.

The copper component of the catalyst exists predominantly as CuO though small quantities of Cu_2O and Cr_2O_4 spinel were detected in some catalyst batches. Zinc was found mainly as ZnO with small quantities of $ZnCr_2O_4$ in many catalyst batches. The bulk of oxygen detected resulted from the oxides and chromates in the catalyst. The summation of oxygen atomic percentages of all the compounds identified in each catalyst batch does not account for all oxygen detected. It is postulated that the rest of the oxygen comes from the hydroxides and water of the remaining hydrotalcite.

Analysis of all catalyst batches reveals the presence of sodium as sodium chromate. This means that the sodium is available for HAS reactions in all cases. The high selectivity for HA displayed by the blank catalyst bears testimony to this. In the alkali metal doped catalysts, the activities and selectivities observed are due to a combined effect of sodium chromate and the respective alkali metals. This could explain the high activities and HA selectivities observed in the Na- and Li-doped catalyst batches. Since the sodium salt was located in the parent catalyst batch, its influence must have been exerted in all the alkali-doped catalyst batches tested.

The overall effect of sodium chromate could have been synergistic, additive or even destructive. It therefore follows that the sodium chromate / lithium oxide at 2.26 * 10^{-4}moles $Li/g_{cat.}$ produced a system with the highest selectivity towards isobutanol while sodium chromate / cesium

oxide system at 3% Cs (by mass) showed the highest HA selectivity. In this analysis at least two basic sites which have influence on HAS can be distinguished i.e. sodium chromate sites and sites associated with individual alkali metal dopants.

5.5 CONCLUDING REMARKS

The following conclusions can be drawn from the above work:

a) It has been shown that the catalyst bulk is different from the surface in respect of composition. XPS shows the catalyst surfaces to be dominated by the presence of Zn.

b) The Ph of the impregnating solutions has been shown to be conducive for dissolution of CuO (acid pH) and ZnO (basic pH). The subsequent deposition of the above compounds on the catalyst surface resulted in their increase in surface concentration in different catalyst batches. This, it is believed is responsible for the increase in the external surface area of the Li and Rb-doped catalyst batches. The calcination heat lead to the decomposition of the carbon containing compounds thereby altering the surface composition of the catalyst batches.

c) In our opinion the presence of an incompletely decomposed hydrotalcite precursor in some catalyst batches, especially its carbonate group rendered the catalyst susceptible to surface restructuring. It appears that the decrease of external surface area in the Cs-, K- and Na-doped catalyst batches could be due to limited recrystallization of the remains of the hydrotalcite precursor when it came into contact with water of the impregnating solution.

d) The isobutanol and HA selectivities of the catalysts impregnated with different alkali metals appears to be influenced by the presence of sodium chromate. The influence of sodium chromate was to enhanced the performances of Li and Na

catalyst batches in the HAS reaction.

Water and pH of impregnating solutions, the heat during calcination and not the chemical properties of alkali metal dopants, played a central role in modifying the physico-chemical properties of the ISO 63 catalyst surface during alkali metal salt impregnation. A combination of a mathematical model similar to that of Bhasin and Hendrix [1993] and experimental methods, should be used to study the individual contribution of sodium chromate and alkali metal salt dopants towards the HAS process. The methods could be used to determine combinations of alkali metal dopants and sodium chromate which show the highest selectivity to HA especially isobutanol. Additionally, the optimum doping quantities of each alkali metal for the maximum performance in HAS could be refined.

5.6 REFERENCES

Baiker, A., Experimental Methods for Characterization of Catalyst. III. Electron Microscopy, Electron Probe Analysis, Auger Electron Spectroscopy, Photoelectron Spectroscopy and Secondary-ion Mass Spectroscopy, Intern. Chem. Eng. 25, 1, **1985**, 38-46.

Bhasin, M.M. and Hendrix, C.D., Alkali Promoter Synergism in Selective Oxidation, In: New Frontiers in Catalysis. Proc. 10th Int. Congr. Catal., Guczi et al., 1431-1439, Elsevier Science Publishers, Budapest, **1993**.

Campbell, R.A., Rodriguez, J.A. and Goodman, D.W., Nature of Metal-Metal Bonding in Mixed Metal Catalysis, In: New Frontiers in Catalysis. Proc. 10th Int. Congr. Catal., Guczi et al., Elsevier Science Publishers, Budapest, **1993**.

Cornthwaite, D., Catalyst and Method for Methanol Synthesis, Brit. 1, 296, 212, awarded to Imperial Chemical Industries LTD., **1972**.

Cotton, F.A. and Wilkinson, G., Chemistry of Transition Elements, In: Advanced Inorganic Chemistry. A Comprehensive Text. 4th, 733, John Wiley & Sons, New York, **1980**.

Davies, L.E., Modern Surface Analysis. Metallurgical Applications of Auger Electron Spectroscopy (AES) and X-Ray Photoelectron Spectroscopy (XPS), The Metallurgical Society of AIME, Warrendale, **1980**.

Delgass, W.N., Haller, G.L., Kellermann, R. and Lunsford, J.H., X-ray Photoelectron Spectroscopy, In: Spectroscopy in Heterogeneous Catalysis., 267-322, Academic Press, New York, **1979**.

Di Conca, M., Riva, A., Trifiro, F., and Vaccari, A., The Zinc-Chromium Oxide Potassium Promoted Catalysts for Methanol and High Alcohol Synthesis. Proc. 8th Int. Congr. Catal., **1984**, II-173.

Ebsworth, E.A.V., Rankin, D.W.H. and Cradock, S., Electronic and Photoelectron Spectroscopy, In: Structural Methods in Inorganic Chemistry, 1st, 239-280, Blackwell Scientific Publishers, Oxford, **1987**.

Herman, R.G., Klier, K., Simmons, G.W., Finn, B.P., Bulko J.B. and Kobylinski, T.P., Catalytic Synthesis of Methanol from CO/H_2. I. Phases Composition, Electronic Properties, and Activities of the $Cu/ZnO/M_2O_3$ Catalysts. J. Catal., **1979**, 56, 407-429.

Hong-Bin Zang, Yi-Quan Yang, Hao-Ping Huang, Guo-Dong Lin and Tsai, K.R., Characterization of MoS_x-K+/SiO_2 Catalysts for Synthesis of Mixed Alcohols from Syngas, In: New Frontiers in Catalysis. Proc. 10th Int. Congr. Catal., Guczi et al., Elsevier Science Publishers, Budapest, **1993**.

Klier, K., Herman, R.G., Simmons, G.W., Nunan, J.G., Bogdan, C.E. and

Himelfarb, P.B., Direct Synthesis of 2-methyl-1-propanol / methanol Fuels and Feedstocks. Final Technical Report, DOE # DE-AC22-84PC70021. **1988.**

Mark, H.F., McKetta, J.J.(Jr), Othmer, D.F. and Stander, A., Kirk-Othmer Encyclopedia of Chemical Technology. 2nd, Interscience Publishers, New York, **1972.**

Mouler, J.F., Stickle, W.F. and Sobol, P.E., Handbook of X-Ray Photoelectron Spectroscopy, Chastain, J.,(Ed), Physical Electronics, Eden Prairie,MN, **1992.**

Nunan, J.G., Himelfarb, P.B., Herman, R.G. and Klier, J. Catal., **1989**, 116, 222-a.

Nunan, J.G., Himelfarb, P.B., Herman, R.G., Klier, K., Bogdan, C.E. and Simmons, G.W., Methanol Synthesis Catalysts Based on $Cs/Cu/M_2O_3$ (M = Al, Cr, Ga): Genesis from Co-precipitated Hydrotalcite-like Precursor, Solid-State Chemistry, Morphology and Stability. Inorg. Chem., **1989**, 28, 3868-3874b.

Okamoto, Y., Fukino, K., Imanaka, T. and Teranishi, S., Surface Characterization of CuO-ZnO Methanol-Synthesis Catalysts by X-ray Photoelectron Spectroscopy. 1. Precursor and Calcined Catalysts. J Phys. Chem. **1983**, 87, 3740-3747.a.

Okamoto, Y., Fukino, K., Imanaka, T. and Teranishi, S., Surface Characterization of CuO-ZnO Methanol-Synthesis Catalysts by X-ray Photoelectron Spectroscopy. 2. Reduced Catalysts. J Phys. Chem. **1983**, 87, 3747-3754.b.

Pearson, J.T. and Stephenson, D.K., Kinetic Study of Some Sodium Carboxylate Melts. Proc. Eur. Symp. Ther. Anal., **1981**, 298-301.

Ross, G.J. and Kodoma, H., Properties of a Synthetic Magnesium-Aluminium Carbonate Hydroxide and its Relationship to Magnesium-Aluminium Double

Hydroxide, Manasseite and Hydrotalcite. Am. Mineral., **1967**, 52, 1037-1047.

Sheffer, R.G. and King, G.R., Differences in the Promotional Effect of Group 1A Unsupported Copper Catalysts for Carbon Monoxide Hydrogenation, J. Catal., **1989**, 116, 488-497.

Taylor, H.F.W., Crystal Structure of Some Double Hydroxide Minerals, In: Min. Mag., **1973**, 39, 304.

Vedage, G.A., Himelfarb, P., Simmons, G.W. and Klier, K., Alkali Promoted Cu/ZnO Catalysts for Low Alcohol Synthesis.Symposium on the Role of Solid State Chemistry in Catalysis, presented before the Division of Petroleum Chemistry, American Chemical Society, Washington, **1983**.

6: CONCLUSIONS

6.1 CONCLUDING REMARKS

Catalytic Properties: It is concluded that alkali doping of our Cu/Zn/Cr methanol synthesis catalyst resulted in both an increase in selectivity towards HAS and a decrease in alkane selectivity. Catalytic activity was only enhanced in Li-, Na- and K-doped catalyst batches. Catalytic activity, selectivity towards alkanes, HA selectivity and selectivity towards isobutanol all decrease with an increase in GHSV because of decreased gas residence time in the reactor. This situation does not favour products formed through a chain of steps. In this particular catalyst, alkali doping increased the methanol selectivity and activity, especially at 4 000 $ml/g_{cat}/h$. All of the above conclusions are in good agreement with the results of Klier et al. [1988]. Relative quantities of different reaction products shows that HAS by our catalyst shows a resemblance to the reaction mechanism of Smith et al. [1991] and Forzatti et al. [1991].

The increase in HA selectivity by the alkali doped catalyst follows the trend shown below:

$$Cs > Li > Na > Rb > K$$

The Cs-doped catalyst is best suited for production of HA since it reveals the highest HA selectivity of all. The isobutanol selectivity for the different alkali metal dopants followed the following order:

$$Li > Cs > Na > Rb > K$$

The Li-impregnated catalyst is best suited for synthesis of isobutanol on our catalyst because of its high STY and selectivity towards the alcohol. The above HA and isobutanol selectivity trends which are not related to the basicity of the

alkali metals in question could be explained by the presence of sodium in the form of sodium chromate. The abnormally high activities and HA selectivities of the Li- and Na-doped catalyst batches are due to the presence of sodium chromate in the parent ISO 63 catalyst. This sodium chromate influences the performances of all our alkali-doped catalysts.

The Cs- and Li-doped catalysts have industrial potential in HAS because they achieved an industrially acceptable methanol/HA ratio of about two. Another favourable aspect of these systems is that they have the lowest methanol/isobutanol ratio. The performance of Li- and Cs-doped catalysts show that our systems are among the best of those operating at a relatively low temperature, pressure and GHSV. The optimal doping quantity for the Cs-doped catalyst batch for HAS was found to be 3.25%. The catalyst batch doped with Li had the highest isobutanol selectivity at about $2.26 * 10^{-4}$ moles Li/ $g_{cat.}$. Quantities above this figure poisoned the catalyst.

Physico-chemical Properties: The ISO 63 catalyst has moderate surface area which was modified by alkali impregnation. Alkali doping of the catalyst caused the blocking of pores by deposition of material (both catalytic material and alkali metal salts) on the pore walls. The effect decreased the catalyst pore area but, it did not change the shape of pores.

Another effect of alkali doping was to decrease the external surface area for the catalyst batches doped with Cs, K and Na salts and increase it in the case of Li and Rb-doped batches. The decrease in external surface area could be attributed to crystallization of the remaining hydrotalcite precursor when it came into contact with water of the impregnating solution. It is believed that the recrystallization process led to restructuring of the catalyst surface with resultant decrease in external surface area.

External surface area increased in the Li- and Rb-doped catalysts because of the

prevailing pH of the impregnating salts. This led to dissolution of catalytic material e.g. CuO and ZnO, which were subsequently re-deposited on the surface. High calcination temperature in the Rb-doped catalyst altered the surface composition by encouraging the decomposition of the catalyst precursor in favour of the Cu and Zn spinels. The change in the composition of the surface was confirmed by both the TPD and XPS methods. It can be concluded that the catalyst bulk was different from the surface in respect of composition. XPS data showed that the catalyst surface was dominated by the presence of Zn.

Catalyst Characterization: It is concluded that the catalyst was predominantly mesoporous. The pores were open-ended and cylindrical in shape. Therefore the catalyst does not suffer mass transfer limitations during the synthesis reaction. It is again concluded that the average CuO crystallite size of the near-optimal catalyst is 78 ± 6 Å in diameter. The catalyst had basic HAS sites in the form of sodium chromate and individual alkali metals. Acidic centres we present too, as shown by production of dimethyl ether in all catalyst batches. The bulk of the catalyst shows the presence of at least CuO, ZnO and the spinels of Cu/Zn phases.

Parameters to be optimized: The pH of the impregnating solution that will result in acceptably high surface area should be determined. Such investigations should be coupled with determinations of the calcination temperature that encourages the formation of high concentrations of active phases. A mathematical model similar to that of Bhasin et al. [1993] has to be adopted in optimizing the effects of different alkali metals and establishing optimum quantities of sodium chromate. A mixture of the alkali metals dopants of Cs and Li could be investigated in the above manner.

6.2 REFERENCES

Bhasin, M.M. and Hendrix, C.D., Alkali Promoter Synergism in Selective Oxidation, In: New Frontiers in Catalysis. Proc. 10th Int. Congr. Catal., Guczi et al., 1431-1439, Elsevier Science Publishers, Budapest, **1993**.

Forzatti, P., Tronconi, E. and Pasquon, I., Higher Alcohol Synthesis. Catal.Rev.-Sci.Eng., **1991**, 33 (1&2), 109-168.

Klier, K., Herman, R.G., Simmons, G.W., Nunan, J.G., Bogdan, C.E. and Himelfarb, P.B., Direct Synthesis of 2-methyl-1-propanol / Methanol Fuels and Feedstocks. Final Technical Report, DOE # DE-AC22-84PC70021. **1988a**.

Smith, K.J., Young, C.-W., Herman, R.G. and Klier, K., Development of a Kinetic Model for Alcohol Synthesis over a Cesium-Promoted Cu/ZnO Catalyst. Ind. Eng. Chem. Res. **1991**, 30, 61-71.

APPENDIX 1

ISOTHERM PLOT OF A BLANK ISO 63 CATALYST

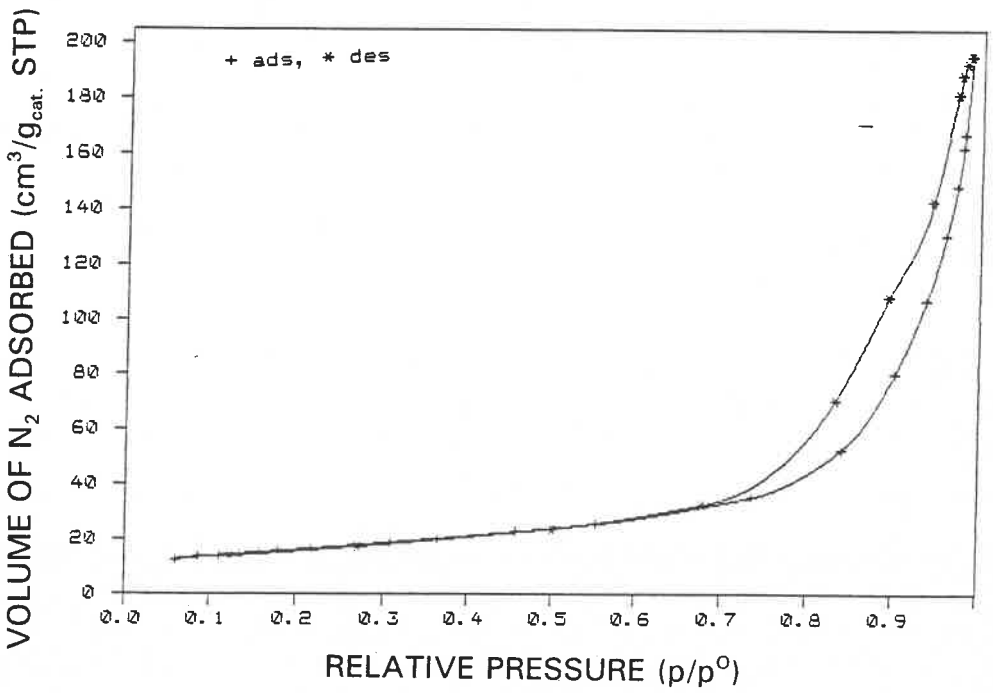

ISOTHERM PLOT OF ISO 63 CATALYST DOPED WITH LITHIUM FORMATE

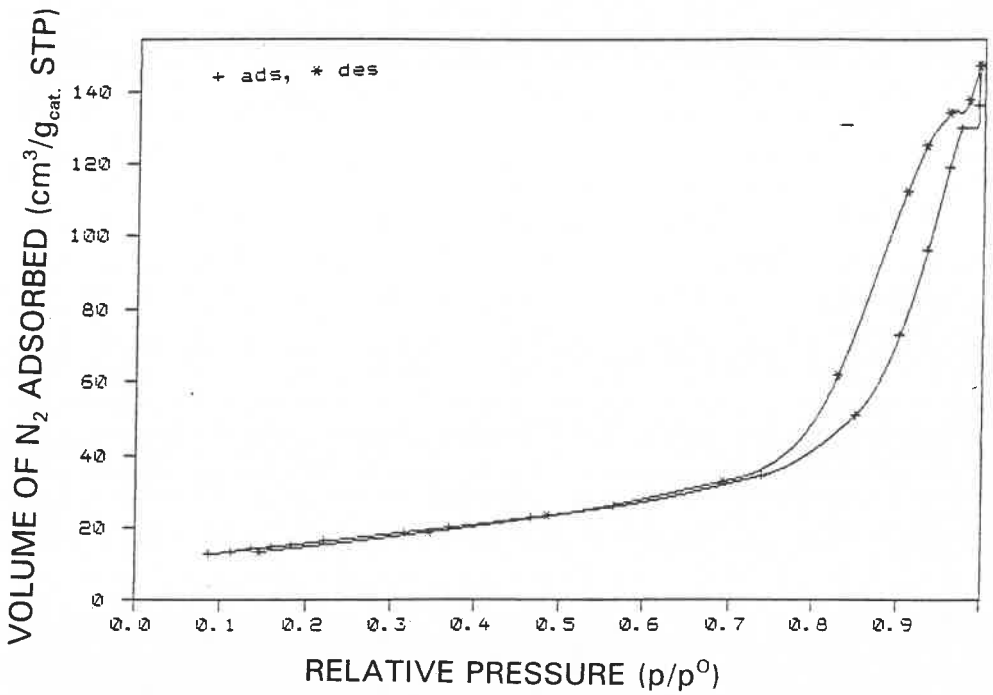

ISOTHERM PLOT OF ISO 63 CATALYST DOPED WITH RUBEDIUM FORMATE

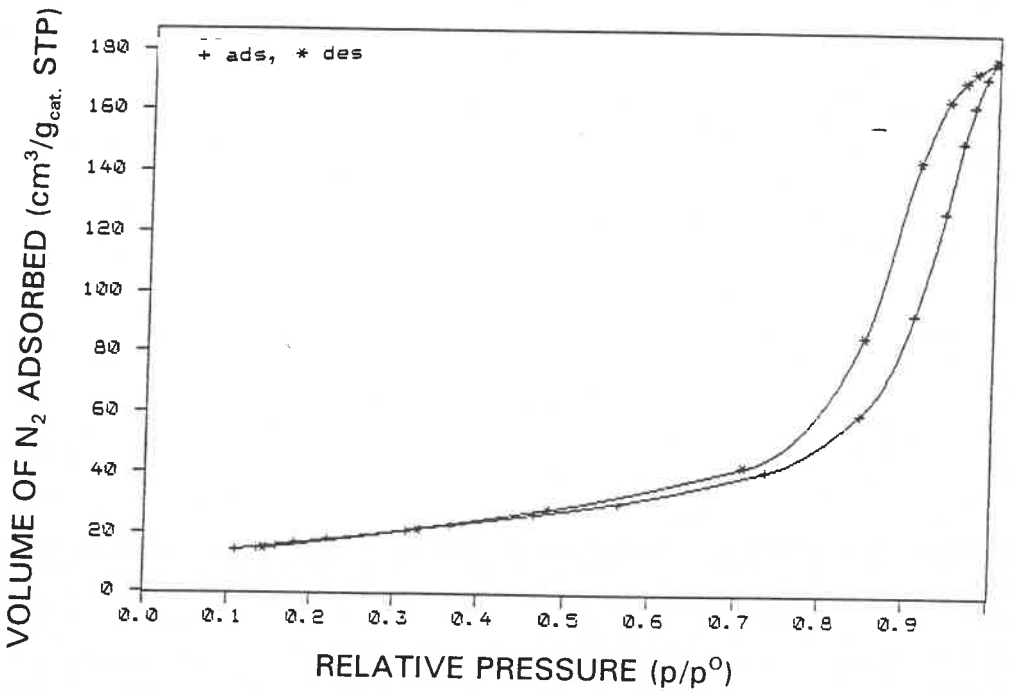

ISOTHERM PLOT OF ISO 63 CATALYST DOPED WITH POTASSIUM FORMATE

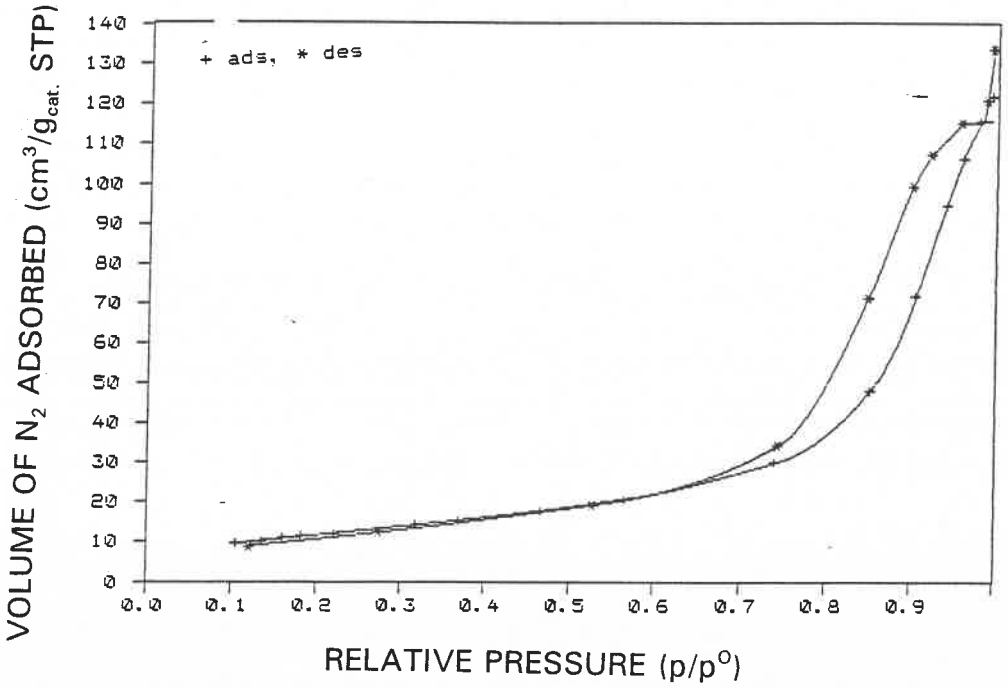

ISOTHERM PLOT OF ISO 63 CATALYST DOPED WITH CESIUM FORMATE

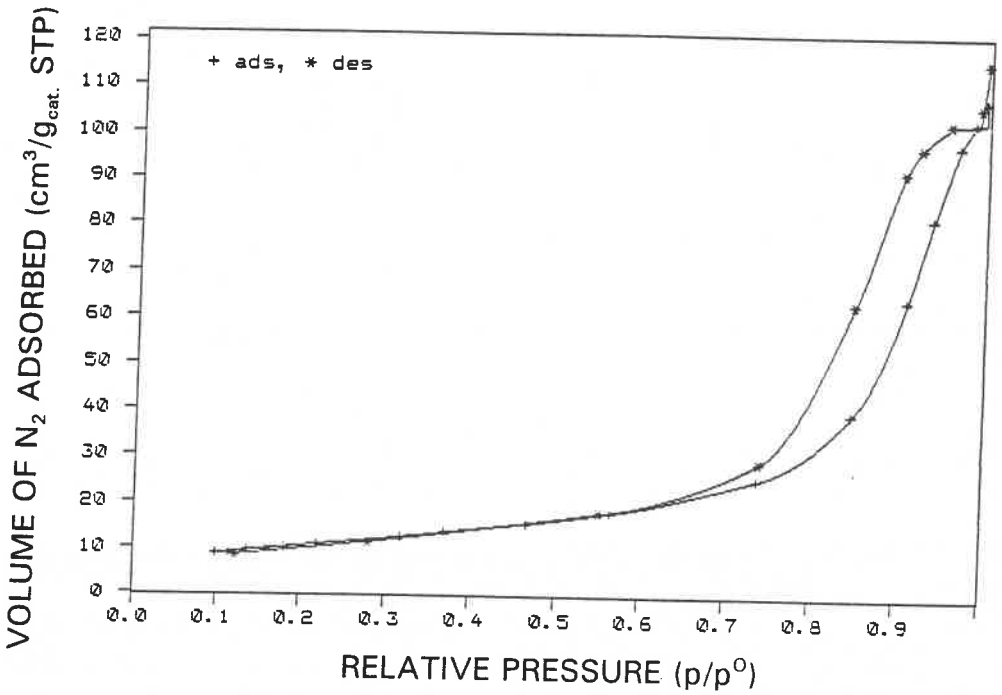

ISOTHERM PLOT OF ISO 63 CATALYST DOPED WITH SODIUM FORMATE

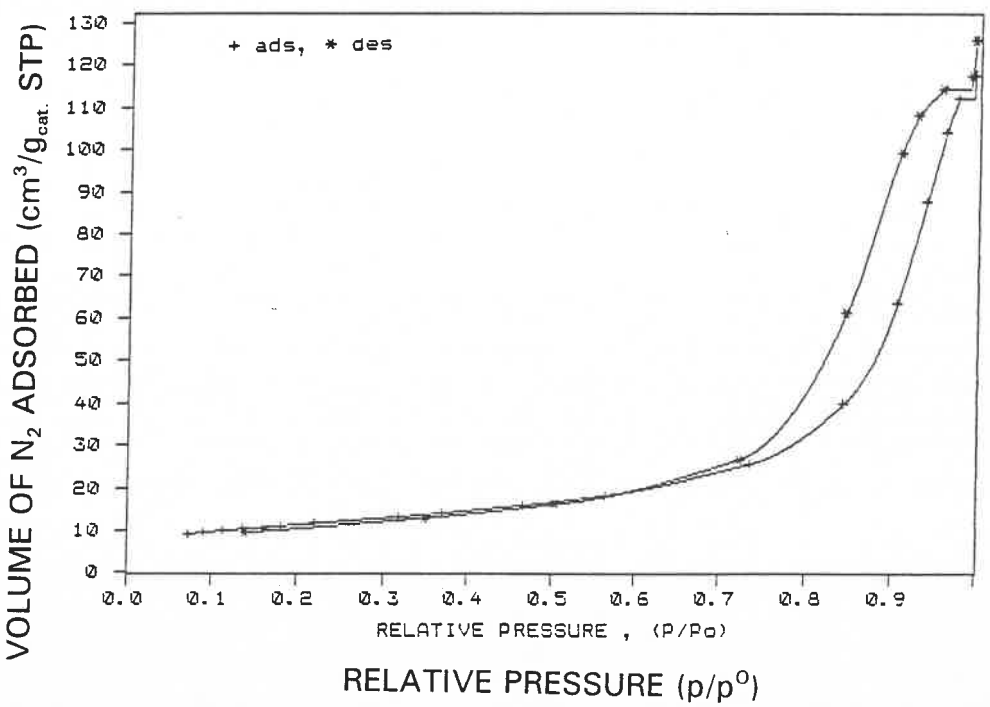

APPENDIX 2

BET SURFACE AREA REPORT AND ITS PLOT

CATALYST BATCH: ISO 63 BLANK

BET Surface Area Report

Relative Pressure	Volume Adsorbed cm^2/g	$1/[VA(p^o/p - 1)]$
0.0605	12.4299	0.005182
0.0867	13.1978	0.007196
0.1338	14.3952	0.010732
0.1792	15.4521	0.014132
0.2170	16.3289	0.16977

BET SURFACE AREA:	57.3559 +/- 0.119 m^2/g
SLOPE:	0.075248 +/- 0.000146
Y-INTERCEPT:	0.000650 +/- 0.000022
C:	116.752068
V_m:	13.175567 cm^3/g STP
CORRELATION COEFFICIENT:	$9.99994 * 10^{-1}$

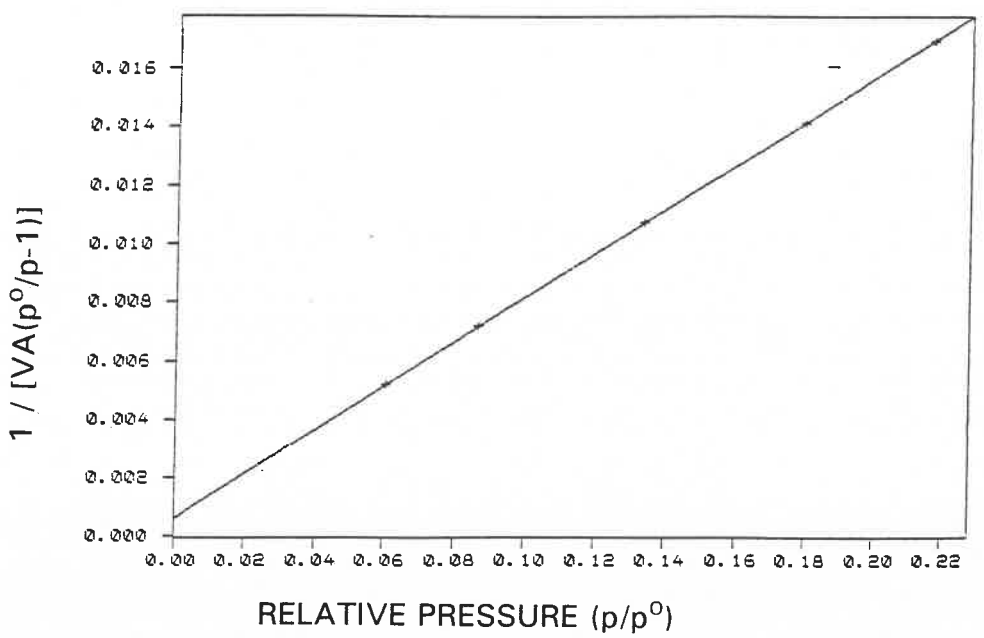

BET SURFACE AREA REPORT AND ITS PLOT

CATALYST BATCH: ISO 63 + Li

BET Surface Area Report

Relative Pressure	Volume Adsorbed cm^2/g	$1/[VA(p^0/p - 1)]$
0.0861	12.5972	0.007479
0.1358	14.0720	0.011162
0.1811	15.2378	0.014514
0.2200	16.2402	0.017370

BET SURFACE AREA:	58.0459 +/- 0.0939 m^2/g
SLOPE:	0.073869 +/- 0.000120
Y-INTERCEPT:	0.001126 +/- 0.000020
C:	66.582901
V_m:	13.334082 cm^3/g STP
CORRELATION COEFFICIENT:	$9.999997 * 10^{-1}$

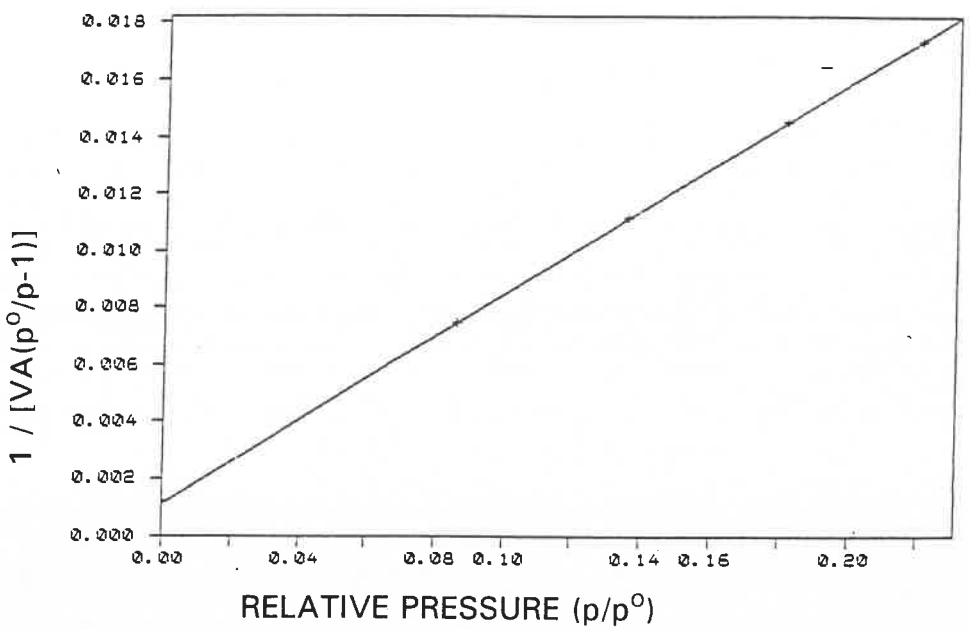

BET SURFACE AREA REPORT AND ITS PLOT

CATALYST BATCH: ISO 63 + Rb

BET Surface Area Report

Relative Pressure	Volume Adsorbed cm^2/g	$1/[VA(p^o/p - 1)]$
0.1097	14.1800	0.008690
0.1354	15.0098	0.010437
0.1807	16.4599	0.013396
0.2195	17.6732	0.015917

BET SURFACE AREA:	64.7699 +/- 0.3785 m^2/g
SLOPE:	0.065700 +/- 0.000387
Y-INTERCEPT:	0.001510 +/- 0.000065
C:	44.508102
V_m:	14.878689 cm^3/g STP
CORRELATION COEFFICIENT:	$9.99965 * 10^{-1}$

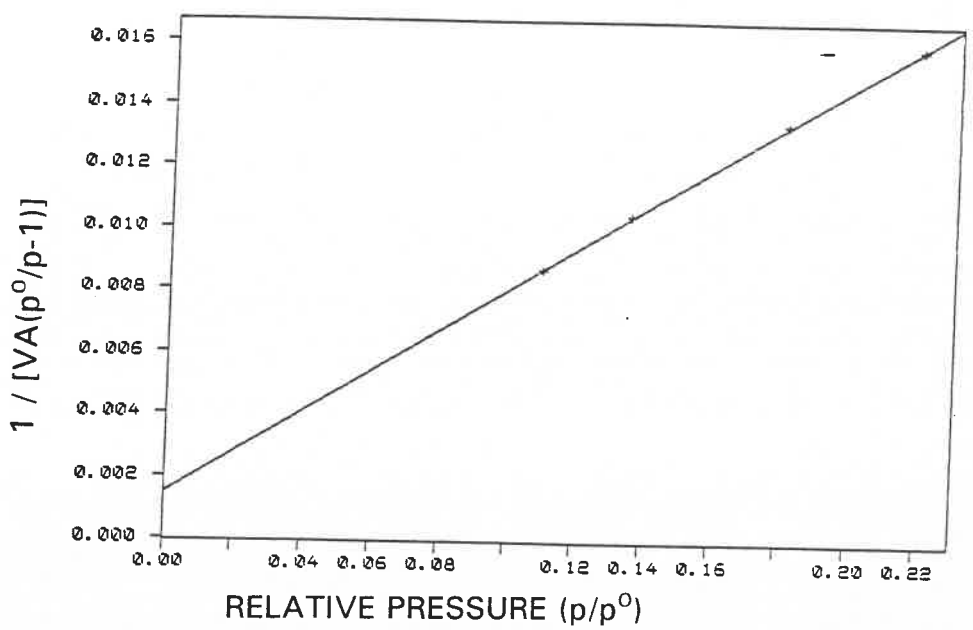

BET SURFACE AREA REPORT AND ITS PLOT

CATALYST BATCH: ISO 63 + K

BET Surface Area Report

Relative Pressure	Volume Adsorbed cm^2/g	$1/[VA(p^o/p - 1)]$
0.1056	9.6899	0.012187
0.1358	10.4074	0.015103
0.1813	11.4076	0.019408
0.2206	12.2616	0.023090

BET SURFACE AREA:	44.8993 +/- 0.1904 m^2/g
SLOPE:	0.094747 +/- 0.000406
Y-INTERCEPT:	0.002208 +/- 0.000068
C:	43.916924
V_m:	10.314085 cm^3/g STP
CORRELATION COEFFICIENT:	$9.99982 * 10^{-1}$

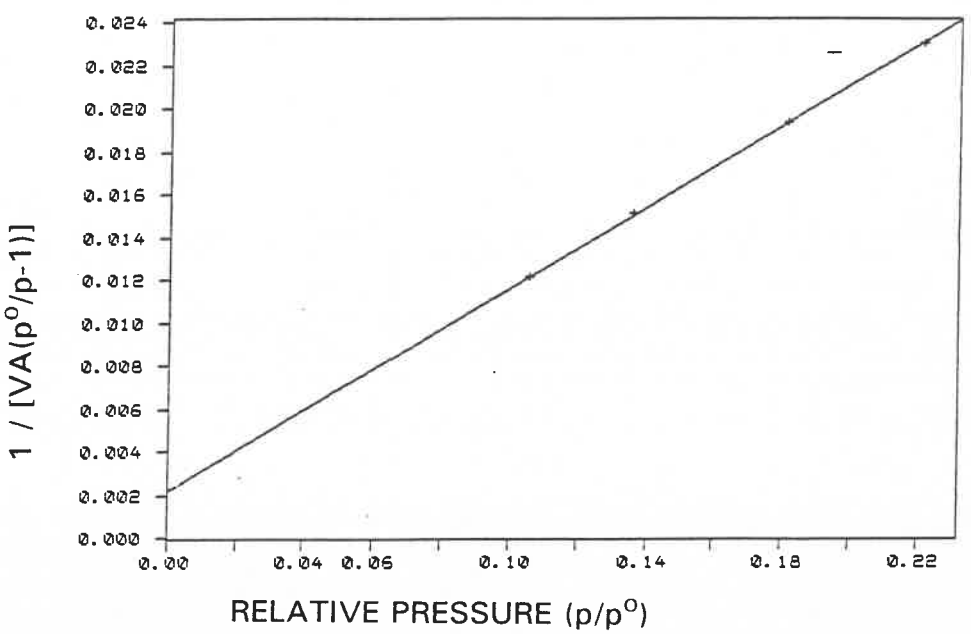

BET SURFACE AREA REPORT AND ITS PLOT

CATALYST BATCH: ISO 63 + Cs

BET Surface Area Report

Relative Pressure	Volume Adsorbed cm^2/g	$1/[VA(p^0/p - 1)]$
0.0989	8.7122	0.012601
0.1361	9.4393	0.016697
0.1813	10.2271	0.021646
0.2203	10.9156	0.025886

BET SURFACE AREA:	39.1267 +/- 0.0768 m^2/g
SLOPE:	0.109475 +/- 0.000215
Y-INTERCEPT:	0.001784 +/- 0.000036
C:	62.375816
V_m:	8.988040 cm^3/g STP
CORRELATION COEFFICIENT:	$9.99996 * 10^{-1}$

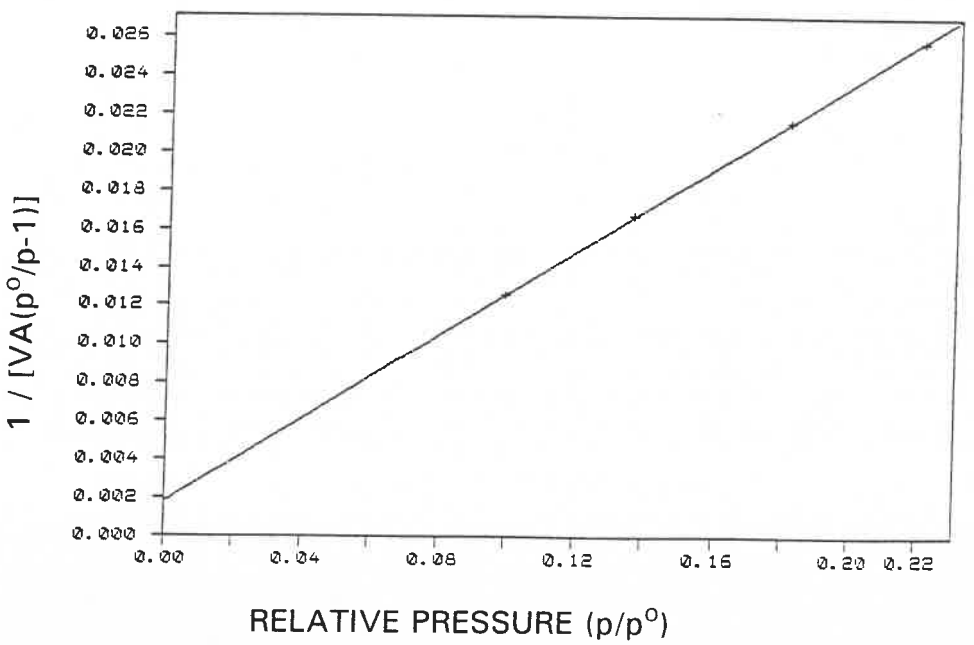

BET SURFACE AREA REPORT AND ITS PLOT

CATALYST BATCH: ISO 63 + Na

BET Surface Area Report

Relative Pressure	Volume Adsorbed cm^2/g	$1/[VA(p^o/p - 1)]$
0.0729	9.2084	0.008542
0.0903	9.5485	0.010400
0.1362	10.3304	0.015266
0.1812	11.0264	0.020066
0.2203	11.6354	0.024279

BET SURFACE AREA:	39.1267 +/- 0.0768 m^2/g
SLOPE:	0.109475 +/- 0.000215
Y-INTERCEPT:	0.001784 +/- 0.000036
C:	62.375816
V_m:	8.988040 cm^3/g STP
CORRELATION COEFFICIENT:	$9.99996 * 10^{-1}$

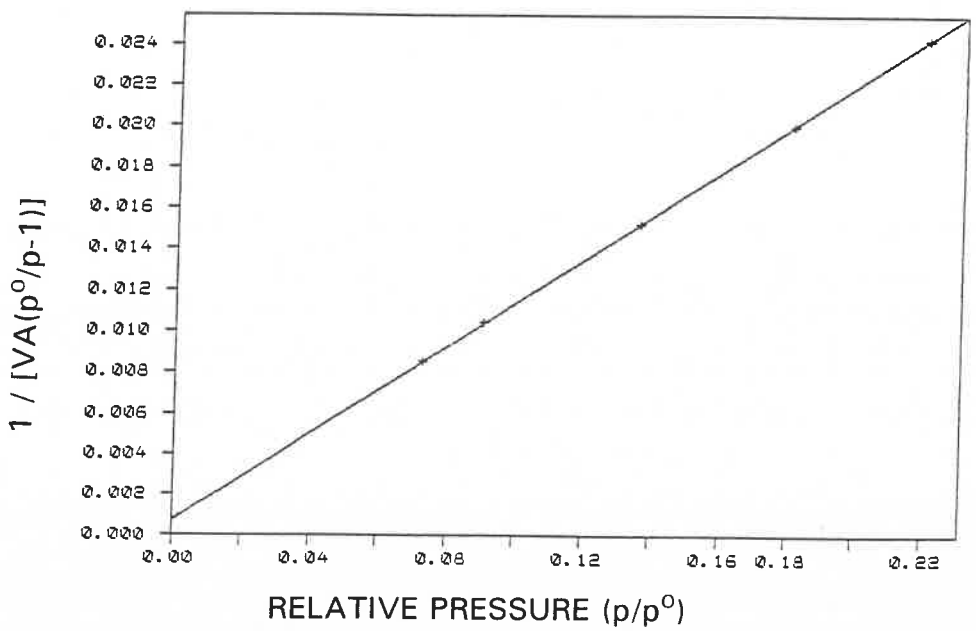

APPENDIX 3

MICROPORE ANALYSIS REPORT AND A V-t PLOT

CATALYST BATCH: ISO 63 (BLANK)

MICROPORE ANALYSIS REPORT

Relative Pressure	Statistical Thickness (Å)	VOLUME ADSORBED cm^3/g
0.0605	3.343	12.4299
0.0867	3.473	13.1978
0.1105	3.758	13.8214
0.1338	3.926	14.3952
0.1569	4.085	14.9348
0.1792	4.233	15.4521
0.2170	4.479	16.3289
0.3187	5.069	18.5021
0.4582	6.109	22.3016
0.5529	6.929	25.1958

NOTE: • THICKNESS VALUES USED IN THE LEAST-SQUARES ANALYSIS WERE BETWEEN 3.500 AND 5.000 Å

• $t = [\ 13.9900/(0.0340 - \log(p/p^0))]^{0.500}$

• SURFACE AREA CORRECTION FACTOR IS 1.000

MICROPORE VOLUME:	0.001317 cm^3/g
MICROPORE AREA:	3.9704 m^2/g
EXTERNAL SURFACE AREA:	53.3855 m^2/g
SLOPE:	3.451351 +/- 0.021170
Y-INTERCEPT:	0.851577 +/- 0.085110
CORRELATION COEFFICIENT:	$9.99925 * 10^{-1}$

V-t PLOT FOR: ISO 63 CATALYST (BLANK)

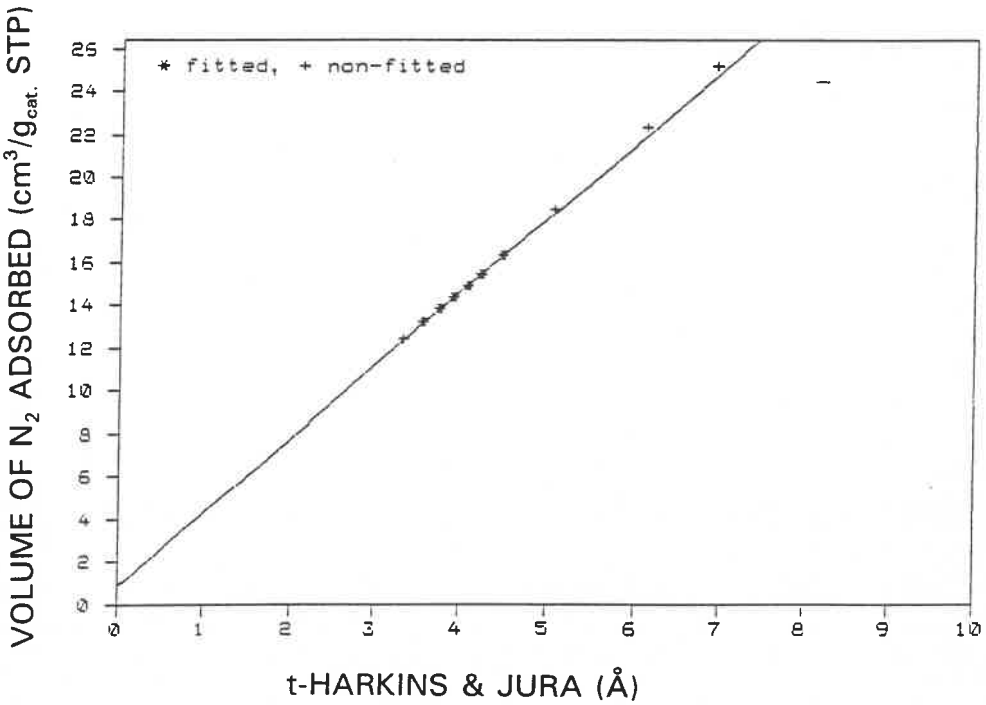

MICROPORE ANALYSIS REPORT AND A V-t PLOT

CATALYST BATCH: ISO 63 + Li

MICROPORE ANALYSIS REPORT

Relative Pressure	Statistical Thickness (Å)	VOLUME ADSORBED cm^3/g
0.0861	3.568	12.5972
0.1125	3.773	13.3923
0.1358	3.940	14.0720
0.1588	4.098	14.6647
0.1811	4.246	15.2378
0.2200	4.498	16.2402
0.3165	5.120	18.6193
0.4653	6.181	22.5398
0.5639	7.034	25.5423

NOTE: • THICKNESS VALUES USED IN THE LEAST-SQUARES ANALYSIS WERE BETWEEN 3.500 AND 5.000 Å

• $t = [\ 13.9900/(0.0340 - \log(p/p^0))]^{0.500}$

• SURFACE AREA CORRECTION FACTOR IS 1.000

MICROPORE VOLUME:	-0.002100 cm^3/g
MICROPORE AREA:	-2.4538 m^2/g
EXTERNAL SURFACE AREA:	60.4997 m^2/g
SLOPE:	3.911283 +/- 0.021170
Y-INTERCEPT:	-1.357487 +/- 0.059503
CORRELATION COEFFICIENT:	$9.99972 * 10^{-1}$

V-t PLOT FOR: ISO 63 + Li

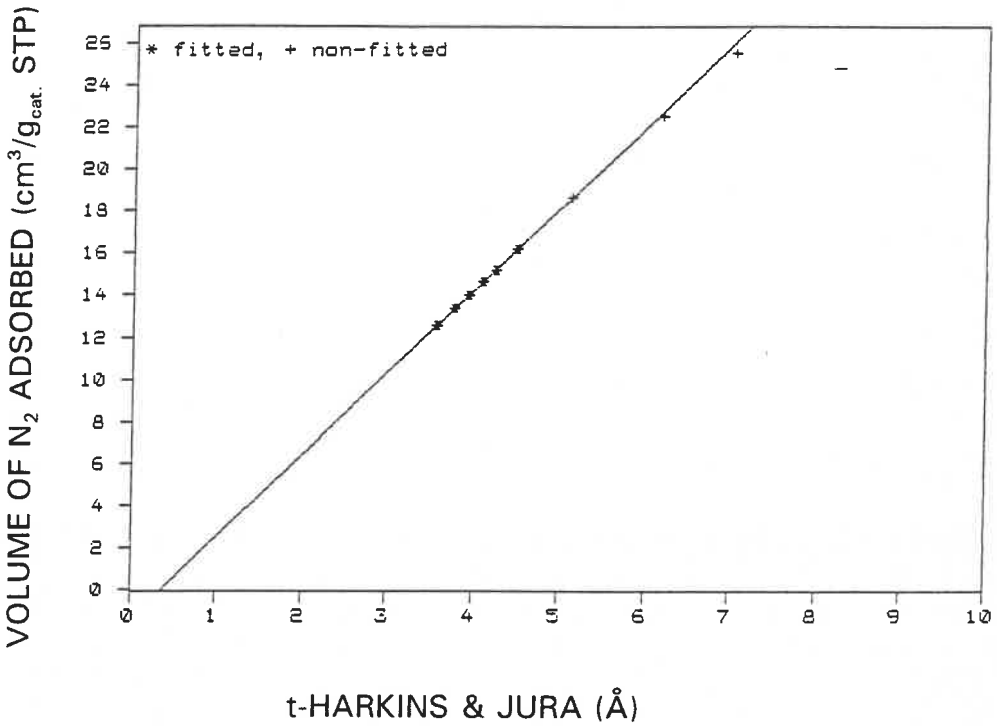

MICROPORE ANALYSIS REPORT AND A V-t PLOT

CATALYST BATCH: ISO 63 + Rb

MICROPORE ANALYSIS REPORT

Relative Pressure	Statistical Thickness (Å)	VOLUME ADSORBED cm^3/g
0.1097	3.752	14.1800
0.1354	3.938	15.0098
0.1588	4.098	15.7372
0.1807	4.242	16.4599
0.2195	4.495	17.6732
0.3154	5.113	20.7597
0.4641	6.171	26.0855
0.5623	7.018	30.2005
0.5639	7.034	25.5423

NOTE: • THICKNESS VALUES USED IN THE LEAST-SQUARES ANALYSIS WERE BETWEEN 3.500 AND 5.000 Å

• $t = [\ 13.9900/(0.0340 - \log(p/p^0))]^{0.500}$

• SURFACE AREA CORRECTION FACTOR IS 1.000

MICROPORE VOLUME:	-0.005483 cm^3/g
MICROPORE AREA:	-8.1684 m^2/g
EXTERNAL SURFACE AREA:	72.9383 m^2/g
SLOPE:	4.715434 +/- 0.057298
Y-INTERCEPT:	-3.545000 +/- 0.236600
CORRELATION COEFFICIENT:	$9.99779 * 10^{-1}$

V-t PLOT FOR: ISO 63 + Rb

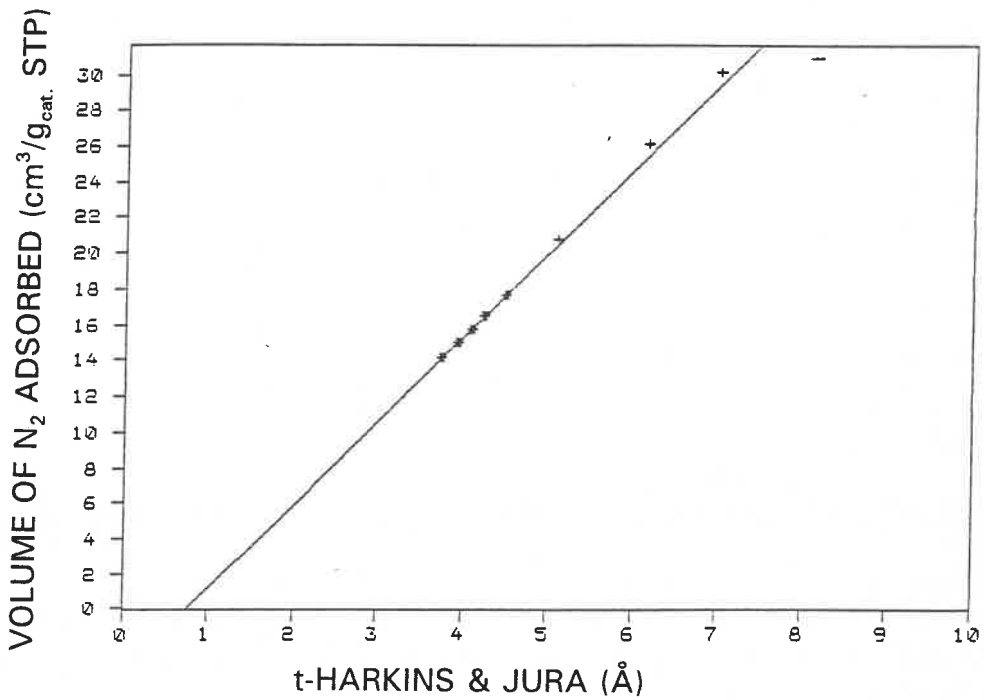

MICROPORE ANALYSIS REPORT AND A V-t PLOT

CATALYST BATCH: ISO 63 + K

MICROPORE ANALYSIS REPORT

Relative Pressure	Statistical Thickness (Å)	VOLUME ADSORBED cm^3/g
0.1056	3.721	9.6899
0.1358	3.940	10.4074
0.1593	4.101	10.9167
0.1813	4.247	11.4076
0.2206	4.502	12.2616
0.3177	5.128	12.2616
0.4665	6.190	17.8970
0.5651	7.045	20.7816

NOTE: • THICKNESS VALUES USED IN THE LEAST-SQUARES ANALYSIS WERE BETWEEN 3.500 AND 5.000 Å

• $t = [\ 13.9900/(0.0340 - \log(p/p^0))]^{0.500}$

• SURFACE AREA CORRECTION FACTOR IS 1.000

MICROPORE VOLUME:	-0.003967 cm^3/g
MICROPORE AREA:	-6.0075 m^2/g
EXTERNAL SURFACE AREA:	50.9068 m^2/g
SLOPE:	3.291104 +/- 0.020968
Y-INTERCEPT:	-2.564351 +/- 0.086168
CORRELATION COEFFICIENT:	$9.99939 * 10^{-1}$

V-t PLOT FOR: ISO 63 + K

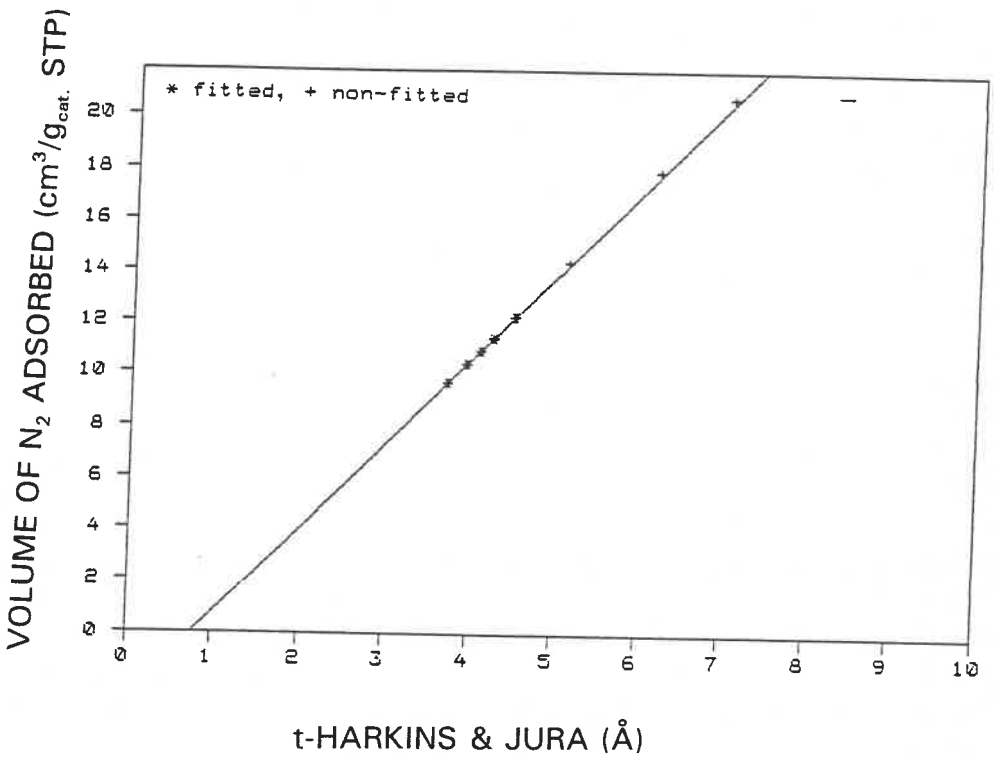

MICROPORE ANALYSIS REPORT AND A V-t PLOT

CATALYST BATCH: ISO 63 + Cs

MICROPORE ANALYSIS REPORT

Relative Pressure	Statistical Thickness (Å)	VOLUME ADSORBED cm^3/g
0.0989	3.670	8.7122
0.1134	3.779	9.0115
0.1361	3.943	9.4393
0.1591	4.100	9.8310
0.1813	4.247	10.2271
0.2203	4.500	10.9156
0.3171	5.124	12.5929
0.4659	6.184	15.5194
0.5642	7.037	17.8857

NOTE: • THICKNESS VALUES USED IN THE LEAST-SQUARES ANALYSIS WERE BETWEEN 3.500 AND 5.000 Å

• $t = [\ 13.9900/(0.0340 - \log(p/p^0))]^{0.500}$

• SURFACE AREA CORRECTION FACTOR IS 1.000

MICROPORE VOLUME:	-0.003967 cm^3/g
MICROPORE AREA:	-6.0075 m^2/g
EXTERNAL SURFACE AREA:	50.9068 m^2/g
SLOPE:	3.291104 +/- 0.020968
Y-INTERCEPT:	-2.564351 +/- 0.086168
CORRELATION COEFFICIENT:	$9.99939 * 10^{-1}$

V-t PLOT FOR: ISO 63 + Cs

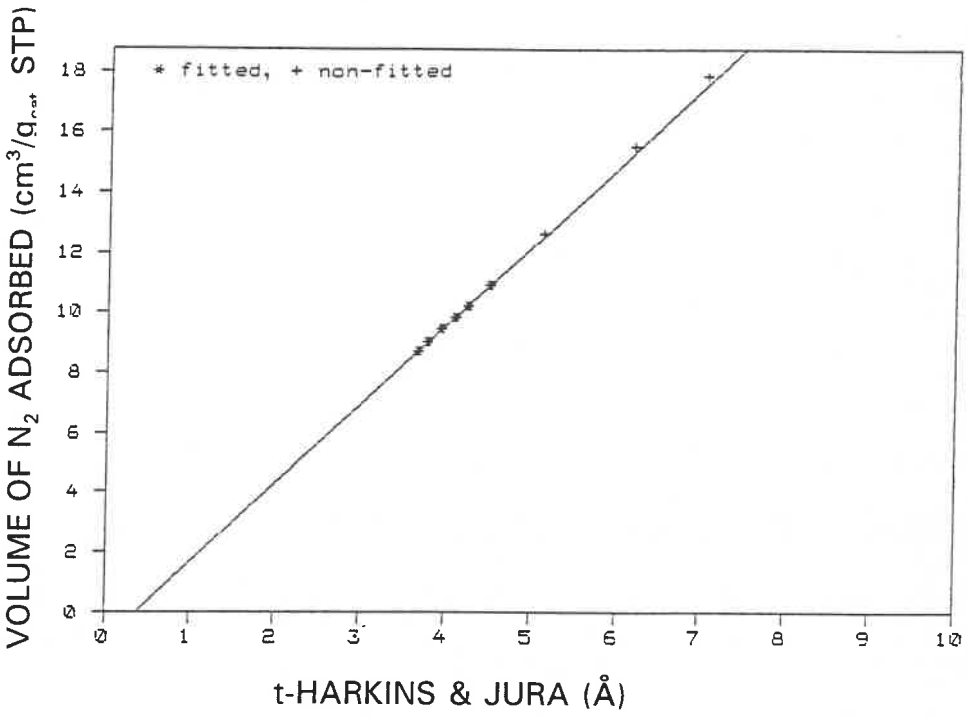

MICROPORE ANALYSIS REPORT AND A V-t PLOT

CATALYST BATCH: ISO 63 + Na

MICROPORE ANALYSIS REPORT

Relative Pressure	Statistical Thickness (Å)	VOLUME ADSORBED cm^3/g
0.0729	3.456	8.2084
0.0903	3.602	9.5485
0.1130	3.777	9.9537
0.1362	3.943	10.3304
0.1593	4.101	10.6838
0.1812	4.246	11.0264
0.2203	4.499	11.6354
0.3171	5.124	13.1708
0.4657	6.184	15.8600
0.5639	7.033	18.1364

NOTE: • THICKNESS VALUES USED IN THE LEAST-SQUARES ANALYSIS WERE BETWEEN 3.500 AND 5.000 Å

• $t = [\ 13.9900/(0.0340 - \log(p/p^0))]^{0.500}$

• SURFACE AREA CORRECTION FACTOR IS 1.000

MICROPORE VOLUME:	0.001854 cm^3/g
MICROPORE AREA:	4.6752 m^2/g
EXTERNAL SURFACE AREA:	35.8323 m^2/g
SLOPE:	2.316543 +/- 0.015129
Y-INTERCEPT:	1.198424 +/- 0.061105
CORRELATION COEFFICIENT:	$9.99915 * 10^{-1}$

V-t PLOT FOR: ISO 63 + Na

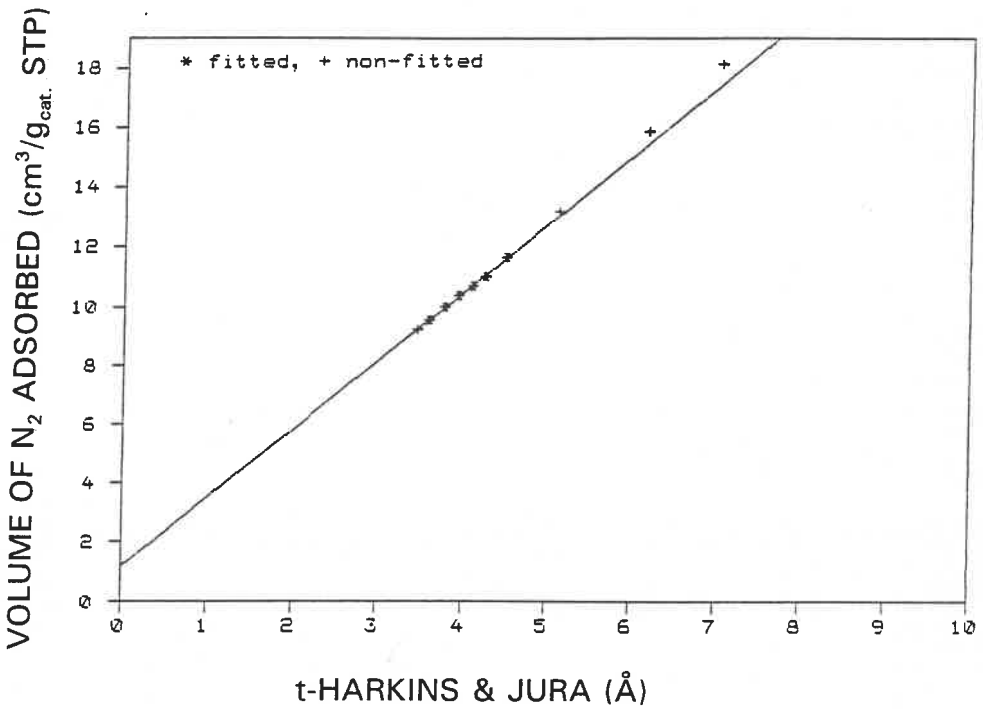

APPENDIX 4

THE BJH DESORPTION PORE DISTRIBUTION REPORT AND CURVE

CATALYST: ISO 63 (BLANK)

BJH DESORPTION PORE DISTRIBUTION REPORT

PORE DIAMETER RANGE (Å)	AVERAGE DIAMETER (Å)	CUMULATIVE PORE VOLUME cm^3/g	CUMULATIVE PORE AREA cm^2/g
1032.2 - 849.8	923.1	0.006909	0.299
849.4 - 700.5	760.5	0.018482	0.908
700.5 - 349.8	417.0	0.086743	7.455
349.8 - 190.3	225.0	0.148546	18.441
190.3 - 120.5	139.6	0.220376	39.026
120.5 - 61.3	72.4	0.293984	79.714
61.3 - 36.7	42.7	0.298895	84.319

THE dV/dlog (D) DESORPTION PORE VOLUME PLOT (DISTRIBUTION CURVES)

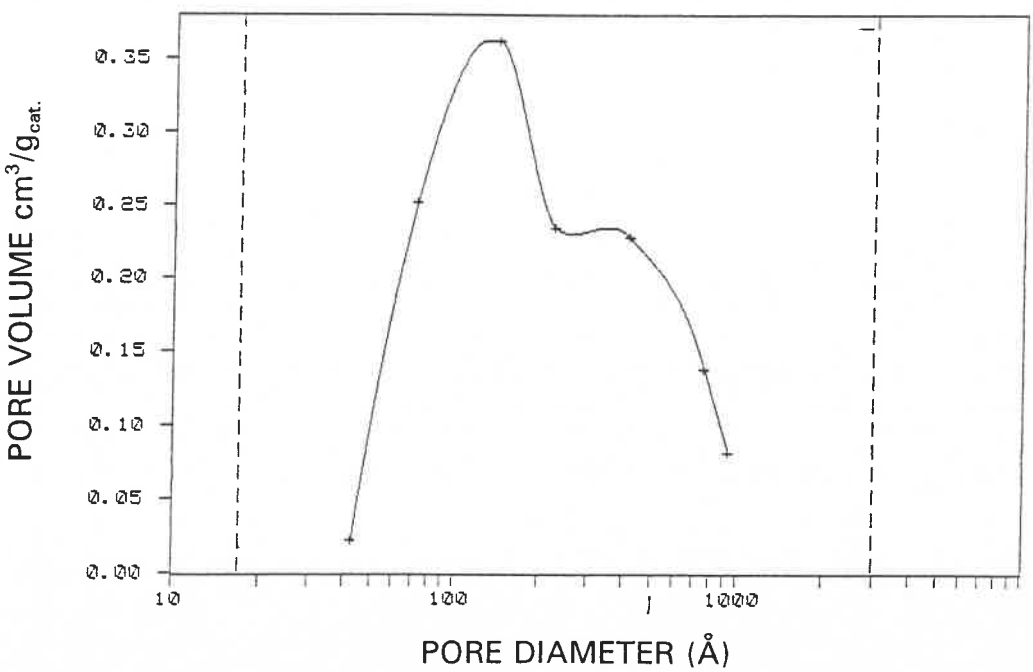

THE BJH DESORPTION PORE DISTRIBUTION REPORT AND CURVE

CATALYST: ISO 63 + Li

BJH DESORPTION PORE DISTRIBUTION REPORT

PORE DIAMETER RANGE (Å)	AVERAGE DIAMETER (Å)	CUMULATIVE PORE VOLUME cm^3/g	CUMULATIVE PORE AREA cm^2/g
1106.7 - 478.1	573.0	0.007135	0.498
478.1 - 294.7	343.7	0.022513	2.288
294.7 - 223.0	248.7	0.046027	6.071
223.0 - 118.2	139.7	0.146070	34.721
118.2 - 64.4	75.7	0.201617	64.060
64.4 - 35.8	41.8	0.209941	72.018
35.8 - 25.7	28.9	0.212648	75.763

THE dV/dlog (D) DESORPTION PORE VOLUME PLOT (DISTRIBUTION CURVE)

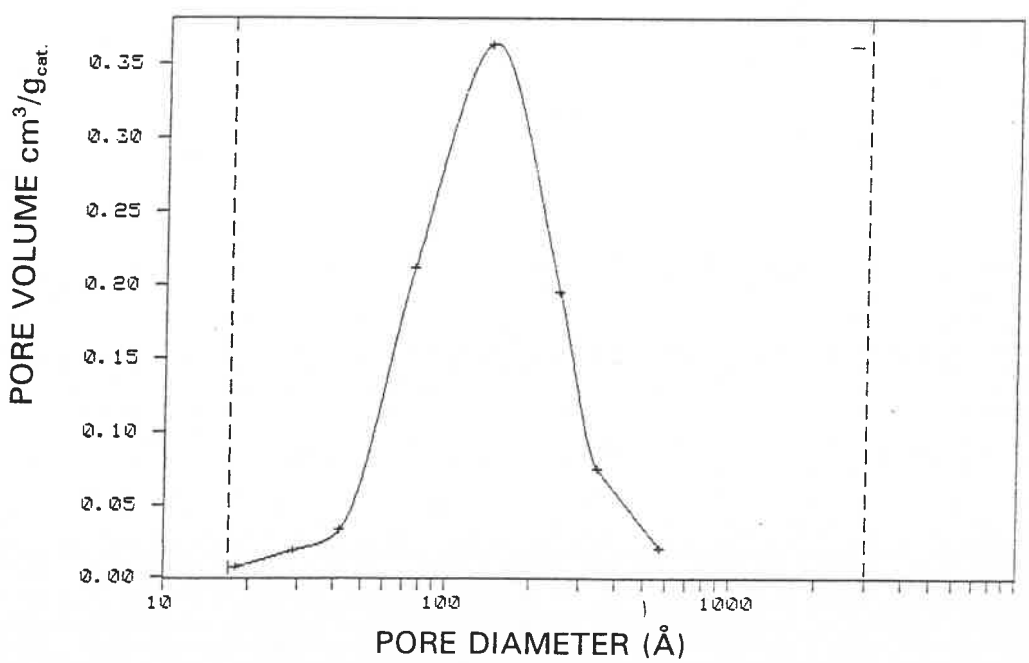

THE BJH DESORPTION PORE DISTRIBUTION REPORT AND CURVE

CATALYST: ISO 63 + Rb

BJH DESORPTION PORE DISTRIBUTION REPORT

PORE DIAMETER RANGE (Å)	AVERAGE DIAMETER (Å)	CUMULATIVE PORE VOLUME cm^3/g	CUMULATIVE PORE AREA cm^2/g
762.1 - 505.2	582.2	0.005570	0.383
505.2 - 352.5	401.6	0.015890	1.411
352.5 - 229.1	264.7	0.053280	7.061
229.1 - 134.0	157.1	0.164621	35.402
134.0 - 67.4	79.7	0.248120	77.307
67.4 - 34.4	40.5	0.262262	91.270
34.4 - 23.7	27.0	0.267446	98.949

THE dV/dlog (D) DESORPTION PORE VOLUME PLOT (DISTRIBUTION CURVE)

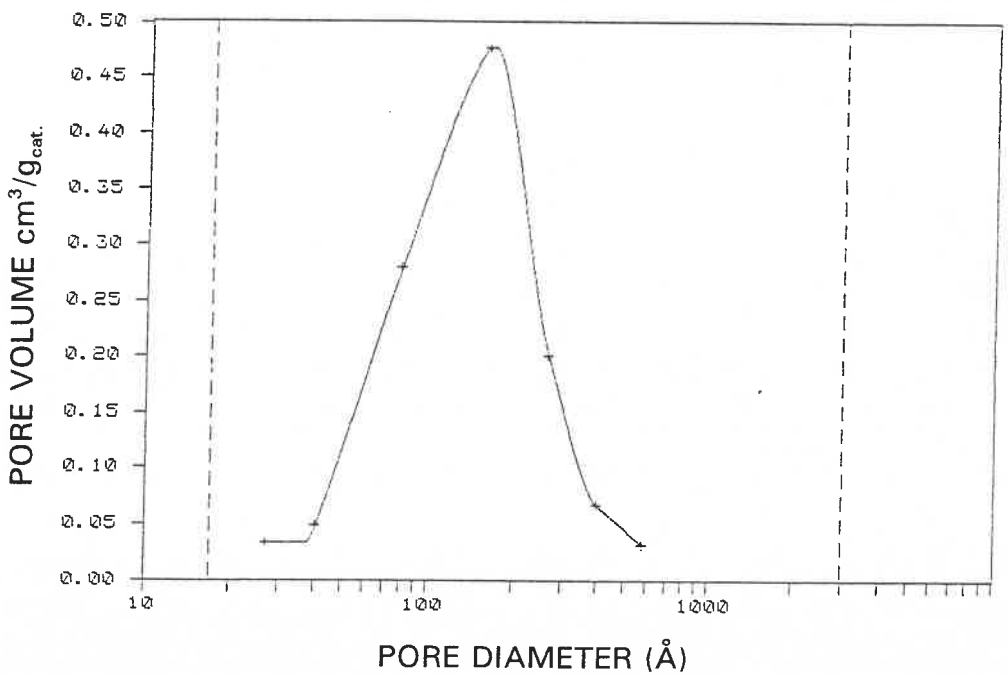

THE BJH DESORPTION PORE DISTRIBUTION REPORT AND CURVE

CATALYST: ISO 63 + K

BJH DESORPTION PORE DISTRIBUTION REPORT

PORE DIAMETER RANGE (Å)	AVERAGE DIAMETER (Å)	CUMULATIVE PORE VOLUME cm^3/g	CUMULATIVE PORE AREA cm^2/g
1442.1 - 457.0	542.5	0.010216	0.754
457.0 - 255.2	301.5	0.024401	2.638
255.2 - 200.3	220.9	0.038831	5.248
200.3 - 132.0	151.9	0.092322	19.330
132.2 - 77.1	90.3	0.165067	51.553
77.1 - 38.4	45.4	0.186024	70.025
38.4 - 20.4	24.0	0.187841	73.049

THE dV/dlog (D) DESORPTION PORE VOLUME PLOT (DISTRIBUTION CURVE)

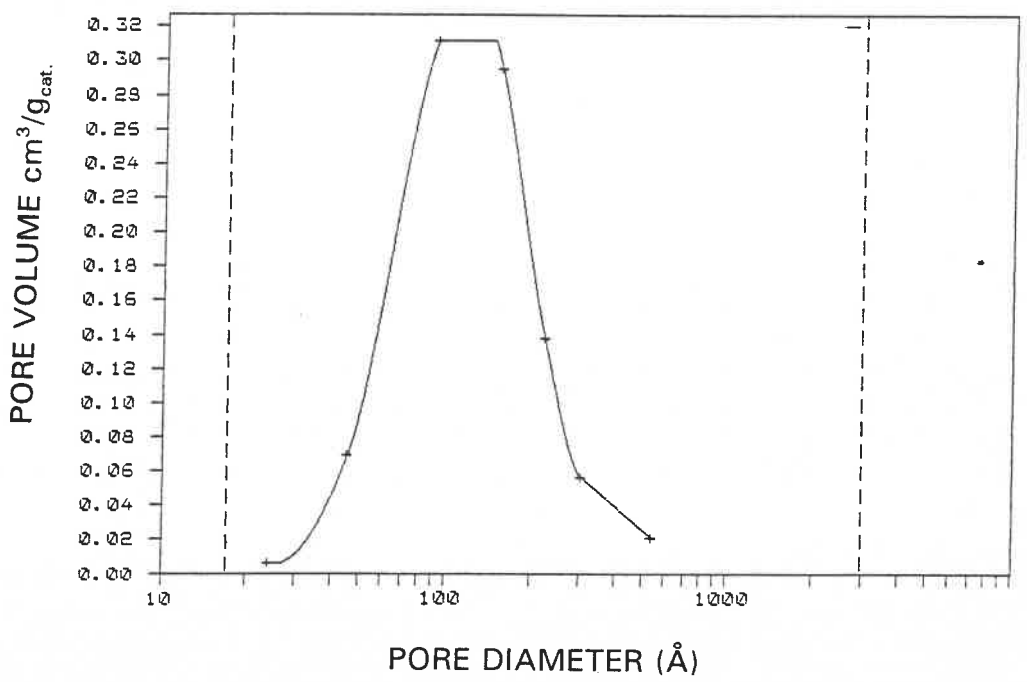

THE BJH DESORPTION PORE DISTRIBUTION REPORT AND CURVE

CATALYST: ISO 63 + Cs

BJH DESORPTION PORE DISTRIBUTION REPORT

PORE DIAMETER RANGE (Å)	AVERAGE DIAMETER (Å)	CUMULATIVE PORE VOLUME cm^3/g	CUMULATIVE PORE AREA cm^2/g
1881.2 - 442.3	512.9	0.006384	0.498
442.3 - 255.5	300.6	0.015691	1.736
255.5 - 207.9	226.6	0.025916	3.541
207.9 - 132.1	153.1	0.080799	17.880
132.1 - 75.9	89.0	0.149211	48.616
75.9 - 41.2	48.4	0.163424	60.353
41.2 - 21.0	24.7	0.164945	62.812

THE dV/dlog (D) DESORPTION PORE VOLUME PLOT (DISTRIBUTION CURVE)

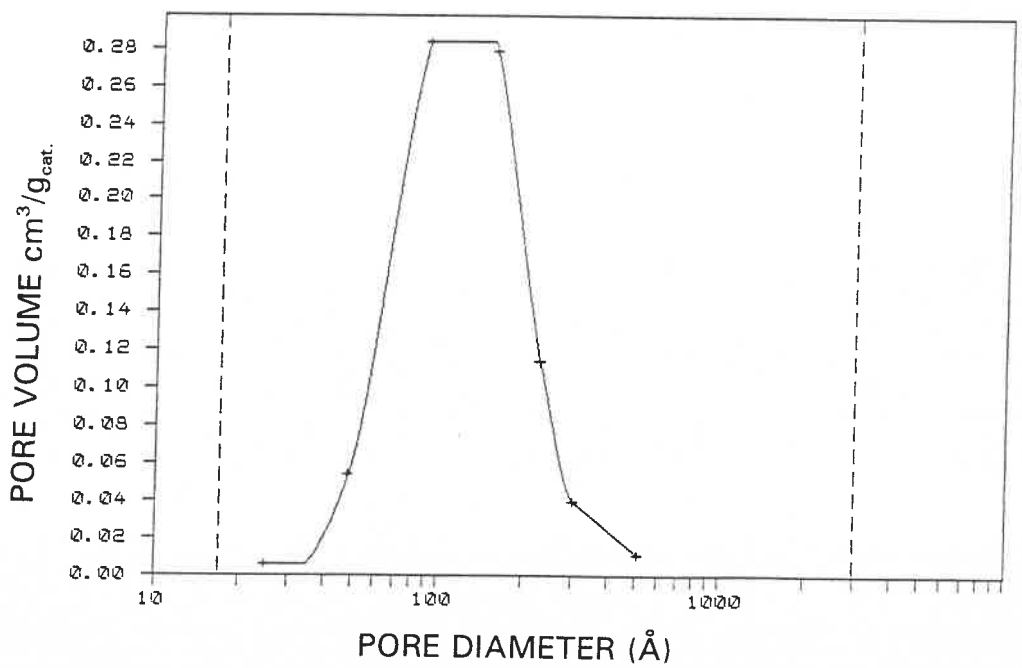

THE BJH DESORPTION PORE DISTRIBUTION REPORT AND CURVE

CATALYST: ISO 63 + Na

BJH DESORPTION PORE DISTRIBUTION REPORT

PORE DIAMETER RANGE (Å)	AVERAGE DIAMETER (Å)	CUMULATIVE PORE VOLUME cm^3/g	CUMULATIVE PORE AREA cm^2/g
1887.4 - 465.8	542.2	0.005415	0.400
465.8 - 282.4	330.3	0.017065	1.810
282.4 - 220.8	243.9	0.032707	4.376
220.8 - 130.5	152.8	0.105764	23.500
130.5 - 71.0	83.7	0.172166	55.242
71.0 - 36.1	42.6	0.182470	64.912

THE dV/dlog (D) DESORPTION PORE VOLUME PLOT (DISTRIBUTION CURVE)